

NORTHWESTERN UNIVERSITY

A Multi-Modal Investigation into Titanium Dioxide Degradation of Oil Paints: Shedding Light on
the Effect of Environmental Factors

A DISSERTATION

SUBMITTED TO THE GRADUATE SCHOOL

IN PARTIAL FULFILLMENT OF THE REQUIREMENTS

for the degree

Doctor of Philosophy

Field of Materials Science and Engineering

By

Thomas Schmitt

Evanston, IL

December, 2022

© Copyright by Thomas Schmitt, 2022

All Rights Reserved

A Multi-Modal Investigation into Titanium Dioxide Degradation of Oil Paints: Shedding Light on
the Effect of Environmental Factors

Thomas Schmitt

Since its introduction as an artist's pigment in the early 20th century, titanium white has become one of the most common white pigments. The early formulations of titanium white contained anatase, which has been studied to facilitate degradation of oil paint under UV illumination. Around the 1940s production shifted to a less photocatalytically active form, rutile. Although these pigments are not traditionally seen as active under visible light illumination, interactions within the paint mixture may result in increased photocatalytic activity. In this thesis, we present findings from a series of works painted by Jackson Pollock in the 1940s investigating the pigments used in white paints. Raman spectra from different locations on each of four paintings identify the phase of titanium dioxide present as well as some other pigments present. We further probed one painting, *Eyes in the Heat*, using reflection FT-IR (r-FT-IR) to interrogate the binder and other pigments in 4 distinct white paints. We identified signs of degradation in anatase and rutile containing white paint areas, suggesting TiO_2 facilitated degradation has taken place. Further, we expand on the existing understanding of TiO_2 facilitated degradation of linseed oil, by examining the effect of visible light and crystallographic phase (either anatase or rutile) on the reactivity of TiO_2 . We combine experimental chemical characterization via FT-IR with computational calculation through Density Functional Theory (DFT) modeling of the TiO_2 -oil system. Under visible and UV light illumination, samples containing rutile or anatase (but not BaSO_4 or pure linseed oil) based paint

showed signs of degradation products when probed with FT-IR. Density Functional Theory (DFT) modeling of interactions between anatase TiO_2 and oleic acid, a fatty acid component of linseed oil, showed the formation of a charge transfer complex, providing one possible mechanism for the visible light activity observed in artificial aging. Finally, we observed mass changes under UV aging at moderate (50 % RH) and high (80 % RH) humidity conditions through the use of the Quartz Crystal Microbalance (QCM) as a high frequency rheometer. We observed a significant increase in mass loss in high humidity UV irradiated samples, and were able to measure a corresponding change in mechanical properties. These results suggest that both anatase and rutile based paints are more active under UV and visible light than originally thought due to complex interactions within the paint film.

Acknowledgments

I have been incredibly privileged and fortunate during my Ph.D. and I could not have completed it without the support of so many people. I thank the many people who have supported my research by contributing time, training, ideas, and feedback. I also, and more importantly, want to thank the people and cats who have supported me as a person, offering mentorship, guidance, and emotional support through this process.

First, I would like to thank my adviser Dr. Kenneth Shull. You have been a supportive and helpful presence throughout my whole Ph.D., and you were always there to help when I needed you. The patience and kindness you offer every student each day inspire me. When I struggled early in the program, you offered me nothing but support and encouragement. You have seen me not just as a researcher, but as a whole person, and encouraged me to grow as one. Each time I worked closely with you, I felt myself learning and deepening my love for material science. I strongly believe that choosing you as my adviser was the best decision of my Ph.D.

I would like to thank my mentors in Italy, Costanza Miliani, Francesca Rosi, and Simona Fantacci. The time I spent in Perugia was transformative for my research, my career, and my character. Costanza, I am ever thankful for the opportunity to work with you at the Peggy Guggenheim Collection in Venice. I think back on that as one of the best moments of my Ph.D. Your expertise and experience in the field of cultural heritage science inspire me. I hope that one day, I can once again work in a museum studying a painting. Francesca, your dedication and knowledge in the lab helped immensely when understanding FT-IR spectra and degradation mechanisms. Simona, I have learned so much about computational chemistry from you. When I was first exposed to Quantum Espresso and computational methods, I struggled greatly, but under your guidance, I was able to more fully understand what we were doing.

I would like to thank my committee members, Professor John Torkelson, Professor James Rondinelli, and Professor Marc Walton. Professor Torkelson, you provided useful feedback during

my qualifying exam and helped shape the project. Professor Rondinelli, I learned so much when I TA'd for you. Professor Walton, I want to thank you for all the support and help you gave me during my first few years. I will always remember our early morning coffee chats.

I thank the staff of the Peggy Guggenheim Collection (Venice, Italy), especially Luciano Pensabene, for their generous assistance and access to Eyes in the Heat, as well as other early 20th century works.

I would also like to thank Professor Gray. Your expertise and high standard of excellence pushed me to be a better researcher, writer, presenter, and global citizen. Under your supervision, I learned to temper my confidence, not overstate my conclusions, and admit when I don't know something. These skills will improve my work, both in and outside the lab.

To Edoardo Mosconi, who taught me so much about DFT, you are an incredible computational chemist and person. Thank you so much for everything you have done to help me.

To Gwen dePolo, you have been my partner in (art) crime since the GRC 2018. You have never ceased to impress me with your dedication, knowledge, and willingness to help others. I am excited to see all the ways you will shape the art conservation science community. You have helped shape my research and my personality. I would not be where I am today without you.

To Kazi and Yaoyao, your guidance and fun in the office during my early years helped make me feel welcome and included in the Shull group.

To David Delgado, thank you for helping get me set up and oriented in the lab. You taught me so much both in the lab and outside.

To Qifeng, you are the backbone of the Shull group. Thank you for everything you have done to help me, from comments on presentations to helping debug QCM issues.

To Anthony, Qihua, and Yuling, I love to see the fun and happiness you bring to the lab and office. The Shull office has never been a dull place. I wish you all luck in your last years.

To Waldemar and Nadege, Thank you both for all the beers, bowling, computational help, laughs and smiles. I hope we can all have drinks in the square in Perugia again.

To Diamiano, Eros, Bea, Danielle, Arup, and Costanza, I had so much fun at lunchtime in the lab with you all. I wish you all the best!

To Katya, your support during the PIRE grant has helped me in so many ways. You have helped me process concerns, feel heard, and regain motivation. You bring an immeasurable value to the PIRE team.

To Professor Gary Rubloff, thank you for encouraging me during my undergrad. Without your support, I wouldn't have pursued a Ph.D.

To Steve Roush, my high school wrestling coach, you were the reason I found and fell in love with Materials Science. I will always thank you for encouraging me to apply to SEAP and mentoring me on and off the mat.

To James, Tyler, Louis, and Broderick, living with you guys has been the highlight of grad school. I am so happy I met you guys and I thank you for all the support you have given over the years, you know it would be way too much to list.

To Jennie, Dalton, and Elise, you are some of the best friends a grad student could ask for. I can't wait for all the dinner parties to come.

To River, thanks for keeping my lap warm and letting me pet you when I was stressed.

To Pooja, each day is easier with you believing in and supporting me. You have taught me so much and inspired so much change in my life; I am forever grateful.

To my mom and dad, I know I would not be here without all the sacrifices you've made for me and the opportunities I have because of you. You have always believed in me, encouraging me to achieve my best. I see you both as models for wonderful and dedicated parents.

Finally, I would like to acknowledge the National Science Foundation (NSF) for funding this work

through Partnerships for International Research and Education (PIRE) program under Grant number 1743748. The FT-IR work was performed in the Keck II facility of the NUANCE center at Northwestern University, which has received support from the SHyNE Resource (NSF ECCS-2025633), the International Institute for Nanotechnology (IIN), and Northwestern's MRSEC program (NSF DMR-1720139). The SEM work was done at the LUNA laboratory of the University.

Contents

1 Background: Titanium White and Characterization techniques	16
1.1 Introduction	16
1.2 Background	16
1.2.1 History of Use and Development	16
1.2.2 The Problem of TiO ₂ activity	19
1.3 Research Objectives	24
2 Identification of TiO₂ paints in Jackson Pollock Paintings	27
2.1 Introduction and Background	27
2.2 Materials and Methods	29
2.2.1 Twentieth Century Paintings	29
2.2.2 Portable Raman Measurements	30
2.2.3 Portable reflection FT-IR	30
2.2.4 Portable XRF	30
2.2.5 Reference Samples	31
2.3 Results and Discussion	31
2.4 Conclusions	40
3 New Insights into the deterioration of TiO₂ based oil paints: The effects of illumination conditions and surface interactions	41
3.1 Introduction	41
3.2 Experimental Materials and Methods	43
3.3 Results	45
3.4 Discussion	54
3.5 Conclusion	58

	10
4 Computational Modeling of Fatty Acids' Interaction with Anatase TiO₂	61
4.1 Introduction and Background	61
4.1.1 Role of Paint Materials	66
4.2 Computational Details and Models	66
4.3 Computational Results and Discussion	71
4.4 Conclusions	79
5 Study of Mass and Mechanical Property Changes During TiO₂ Facilitated Degradation Using the Quartz Crystal Microbalance	82
5.1 Introduction and Background	82
5.2 Materials and Methods	86
5.3 Results	90
5.4 Conclusions	97
6 Outlook, Future Work, and Summary	98
6.1 Outlook	98
6.1.1 Identification of TiO ₂ Based Paints in Jackson Pollock Paintings	98
6.1.2 New Insights into TiO ₂ Facilitated Degradation Under Visible Light	98
6.1.3 Computational Modeling of Interactions in Art Materials	99
6.1.4 Study of Mass and Mechanical Property Changes during TiO ₂ facilitated degradation using the QCM	100
6.2 Future Work	101
6.2.1 Identification of TiO ₂ based paints in Jackson Pollock Paintings	101
6.2.2 New Insights into TiO ₂ Facilitated Degradation Under Visible Light	101
6.2.3 Computational Modeling of Interactions in Art Materials	102
6.2.4 Study of Mass and Mechanical Property Changes during TiO ₂ facilitated degradation using the QCM	103
6.3 Summary	104

	11
References	108
Apendix	120

List of Tables

3.1	Assignment of the main spectral changes observed in linseed oil aging and summary of the observed changes.	59
4.1	Frontier energy levels and HOMO-LUMO gap for linseed oil component acids calculated with B3YLP and PBE functionals.	75
4.2	Frontier energy levels and effective band gap for bare TiO ₂ and oleic acid-TiO ₂ system.	78
5.1	Sample Names and Conditions	89

List of Figures

1.1	Crystal structure of anatase and rutile TiO ₂	18
1.2	Schematic representation of photoinduced excitation in a semiconductor.	19
1.3	Effect of reactive oxygen species on fatty acid chains of linseed oil.	22
1.4	Proposed degradation of linseed oil facilitated by TiO ₂ reprinted from Van Driel. [39]	23
1.5	Multi-modal approach for characterizing degradation in model paint films using FT-IR, SEM, and QCM	25
2.1	Paintings Studied at the Peggy Guggenheim collection and featured in this study. .	29
2.2	<i>The Moon Woman</i> (1942) with (b) Raman of selected points and anatase reference	32
2.3	(a) <i>Two</i> (1943-1945) with (b) Raman of selected points and anatase reference . . .	33
2.4	(a) <i>Croaking Movement</i> (1946) with (b) Raman of selected points and anatase and rutile references	34
2.5	(a) <i>Eyes in the Heat</i> (1946) with zoomed area and (b) Raman of selected points and anatase and rutile references (c) microscope image of anatase based paint and (d) microscope image of rutile based paint	35
2.6	FT-IR spectra of upper layer of <i>Eyes in the Heat</i> (1946) showing (a) more signs of degradation, and (b) less signs of degradation. Characteristic markers are indicated with arrows.	36
2.7	FT-IR of lower white layer measured on the edge of the painting, characteristic markers are indicated with arrows.	38
2.8	MIR of lower ground layer probed via the canvas border	39
3.1	(a) Section of <i>Eyes in the Heat</i> (1946) painted by Jackson Pollock. Inserts show an area of (b) rutile based paint and (c) an area of anatase based paint, inset shows the Raman spectra used to confirm the presence of rutile in point (b) and anatase in point (c).	42
3.2	Setup of Aging Chamber	44
3.3	Linseed oil aged in (a) vis, and (b) UV-vis conditions. Characteristic markers of degradation are marked with dotted lines and functional groups.	46
3.4	Linseed oil only, anatase, and rutile based paint aged in (a) vis and (b) UV-vis light with a total exposure of 269 kJ cm ⁻² . Characteristic markers of degradation are marked with dotted lines and functional groups.	48
3.5	Anatase based paint aged in (a) vis, and (b) UV-vis conditions, and rutile based paint aged in (c) vis, and (d) UV-vis conditions. Characteristic markers of degradation are marked with dotted lines and functional groups.	49
3.6	Change in the intensity for the 1710 cm ⁻¹ peak, the 1670-1610 cm ⁻¹ region measured at 1640 cm ⁻¹ , and the 1168 cm ⁻¹ peak in (a, c, e) visible light and in (b, d, f) UV-vis light. The considered bands are normalized to the 1736 cm ⁻¹ ester peak.	50
3.7	SEM images at 36 days aged in various lighting conditions for (a) anatase, (b) rutile, and (c) BaSO ₄ oil paints.	53
3.8	FT-IR spectra of samples aged in < 30 % RH environment under UV light with (a) linseed oil only and (b) anatase TiO ₂	55

4.1	Processes of formation of reactive oxygen species in (a) bare photocatalyst such as TiO_2 , (b) a photocatalyst sensitized by a material whose LUMO lies close to the photocatalysts conduction band, and (c) a photocatalyst sensitized by a material whose LUMO lies far above the photocatalysts conduction band.	62
4.2	Structure of alizarin carmine	68
4.3	Structure of (a) linseed oil and (b) its component fatty acids.	69
4.4	Absorption spectra for Alizarin carmine and alizarin	70
4.5	Effect of sulfonate composition on absorption spectrum for alizarin carmine	72
4.6	Visualization of frontier orbitals for alizarin carmine in different forms.	72
4.7	Alizarin Carmine attached to TiO_2 slab in a bidentate bridging configuration.	73
4.8	Visualized highest occupied electronic states (right) and lowest unoccupied electronic states (left) for the alizarin carmine TiO_2 complex	74
4.9	Density of States for both bare anatase TiO_2 slab and the same slab with alizarin carmine attached in a bidentate bridging mode	75
4.10	Structures and frontier orbitals for the component acids of linseed oil. Positive spin polarization of the frontier orbitals is represented as blue and negative spin polarization is represented as red.	76
4.11	Binding modes and optimized geometry for oleic acid on the 101 surface of anatase TiO_2 ; (a) monodentate and (b) bidentate.	77
4.12	Density of States of the oleic acid- TiO_2 complex, and the partial density of states separated contributions showing the orbital origin of the intra-band state are reported. The intra-band state is denoted by an arrow.	78
4.13	Band alignment diagram for TiO_2 and oleic acid showing a possible pathway and associated reactions for ROS generation.	80
4.14	Pathway of oleic acid degradation due to electron transfer from the oleic acid to TiO_2	81
5.1	Frequency shift resulting from depositing an oil film.	84
5.2	(a) Peak fitting of the frequency versus conductance (G_p) and susceptance (B_p); and (b) the fit and relationship between conductance (G_p) and susceptance (B_p).	85
5.3	Coating Procedure showing (a) mixing the paint on a glass plate with a palette knife, (b) placing the parafilm over the unused vacuum holes, (c) the coating in action, and (d) the finished cured crystal.	87
5.4	Schematic of aging setup showing how humidity and wavelength dependency was achieved and monitored.	88
5.5	Spectra of aging lamp for UV-vis (orange) and vis (blue) aging conditions; the inset shows the zoomed area denoted by the box.	90
5.6	Measured properties as a function of the total light exposure dose for the Ana-Vis-50 sample (Anatase TiO_2 , visible light exposure, 55 % relative humidity).	91

5.7	Comparison of the experimentally measured values of $\Delta\Gamma_n$ and Δf_n to the values that are calculated from Eqs. 5.2-5.6, using the properties shown in Figure 5.6. These properties were obtained from a 3.5.5 calculation which means that the equations were solved to force agreement of the calculated and measured values of Δf_3 , Δf_5 and $\Delta\Gamma_5$.	92
5.8	Measured properties as a function of the total light exposure dose for the Rut-50-Vis sample as calculated with a 3.5.5 calculation.	93
5.9	Comparison of the experimentally measured values of $\Delta\Gamma_n$ and Δf_n to the values that are calculated from Eqs. 5.2-5.6, using the properties shown in Figure 5.8. These properties were obtained from a 3.5.5 calculation which means that the equations were solved to force agreement of the calculated and measured values of Δf_3 , Δf_5 and $\Delta\Gamma_5$.	94
5.10	Measured values of the modulus-density product and phase angle as a function of the total light exposure dose for four different anatase samples.	95
5.11	Measured values of the modulus-density product and phase angle as a function of the total light exposure dose for similarly behaving anatase samples.	96
5.12	Film mass as a function of light exposure dose for films containing anatase TiO_2 .	97
.1	(a)Vis and (b) UV-vis aging of BaSO_4 based paints	121
.2	Dark aged (a) anatase, (b) rutile, (c) BaSO_4 , and (d) linseed oil films	121
.3	DOS comparison between the calculation carried out at Γ point with 10A of vacuum, with 20A of vacuum and with a k-point grid of 2x2x1 and 10A of vacuum	122
.4	Comparison of the experimentally measured values of $\Delta\Gamma_n$ and Δf_n to the values that are calculated from Eqs. 5.2-5.6, using the properties for Ana-Vis-80 shown in Figure 5.10. These properties were obtained from a 3.5.5 calculation which means that the equations were solved to force agreement of the calculated and measured values of Δf_3 , Δf_5 and $\Delta\Gamma_5$.	123
.5	Comparison of the experimentally measured values of $\Delta\Gamma_n$ and Δf_n to the values that are calculated from Eqs. 5.2-5.6, using the properties for Ana-UV-50 shown in Figure 5.10. These properties were obtained from a 3.5.5 calculation which means that the equations were solved to force agreement of the calculated and measured values of Δf_3 , Δf_5 and $\Delta\Gamma_5$.	124
.6	Comparison of the experimentally measured values of $\Delta\Gamma_n$ and Δf_n to the values that are calculated from Eqs. 5.2-5.6, using the properties for Ana-UV-80 shown in Figure 5.10. These properties were obtained from a 3.5.5 calculation which means that the equations were solved to force agreement of the calculated and measured values of Δf_3 , Δf_5 and $\Delta\Gamma_5$.	125

Chapter 1

Background: Titanium White and Characterization techniques

1.1 Introduction

This thesis addresses the concern of TiO_2 based paints first identified by Birgit Van Driel in her thesis “Titanium Dioxide: Friend or Foe”. This work extends the body of research and understanding around titanium white oil paints through non-invasive investigation into the white paints used by Jackson Pollock presented in Chapter 2, characterization of the effect of visible light on anatase and rutile pigments via FT-IR presented in Chapter 3, development and validation of a computational model to describe visible light sensitization of TiO_2 in oil paints presented in Chapter 4, and characterization of mass and mechanical property changes during photo aging of anatase based films with QCM presented in Chapter 5. Finally, outlook, future work, and summary are presented in Chapter 6.

1.2 Background

1.2.1 History of Use and Development

Since the early 20th century, titanium dioxide (TiO_2) has become the most common white pigment for both artist and commercial paint applications, as well as a popular photocatalytic material for chemical and environmental science. [1, 2] TiO_2 is well studied for chemical and environmental applications due to the ability to generate electron hole pairs from the absorption of UV light and create radical species. Much research has been done to enhance the photoactivity of TiO_2 . [1, 3, 4] In conservation science, where the goal is to limit, not promote photocatalytic activity, TiO_2 is

not seen as a problematic pigment in museum environment. This is because the higher activity crystal structure, anatase, is believed to be relatively rare in paintings and only active in UV light, which is restricted in museums. The less active and more common structure, rutile, is believed to be inactive due to a high electron hole recombination rate. [2, 5] These beliefs may not hold as wisdom taken from fields of conservation science, catalysis engineering, and dye sensitized solar cells suggest that when complex mixtures are present, many factors can alter the standard model of TiO_2 activity.

Formulations of titanium white oil paint produced in the first half of the 20th century primarily contained TiO_2 in the anatase crystal structure, which is characterized by a tetragonal lattice ($P4_2/mmm$) with four TiO_2 units per unit cell. [6, 7] Difficulty purifying a synthetic rutile pigment delayed its widespread commercialization until after 1950. [2] Rutile is also tetragonal lattice in the $P4_2/mmm$ space group, but the degree of distortion of the octahedral differs as can be seen in Figure 1.1.

In anatase this distortion allows for octahedrals to share 4 edges creating a long octahedral chain. In rutile, the octahedrals share at most one edge. [8] This small difference in structure is one of the factors behind the difference in photocatalytic activity.

TiO_2 was first manufactured for pigment purposes in 1914 after an investigation into the potential uses of the ore ilmenite (FeTiO_3) yielded a process to remove iron with sulfuric acid. [2] Initial formulations involved precipitating TiO_2 onto barium sulfate particles already used as filler in oil paints produced composite pigments with “the color of India ivory”. [2] Other processes were developed soon after resulting in mixtures rather than composites of anatase and fillers. In 1922, pure anatase pigment began to be commercially available, but wide ranges of formulations and qualities were present in the market. [2]

Rutile was known to have better hiding power and weathering properties than anatase. However, commercial processes for creating synthetic rutile yielded coarse sintered material that was not

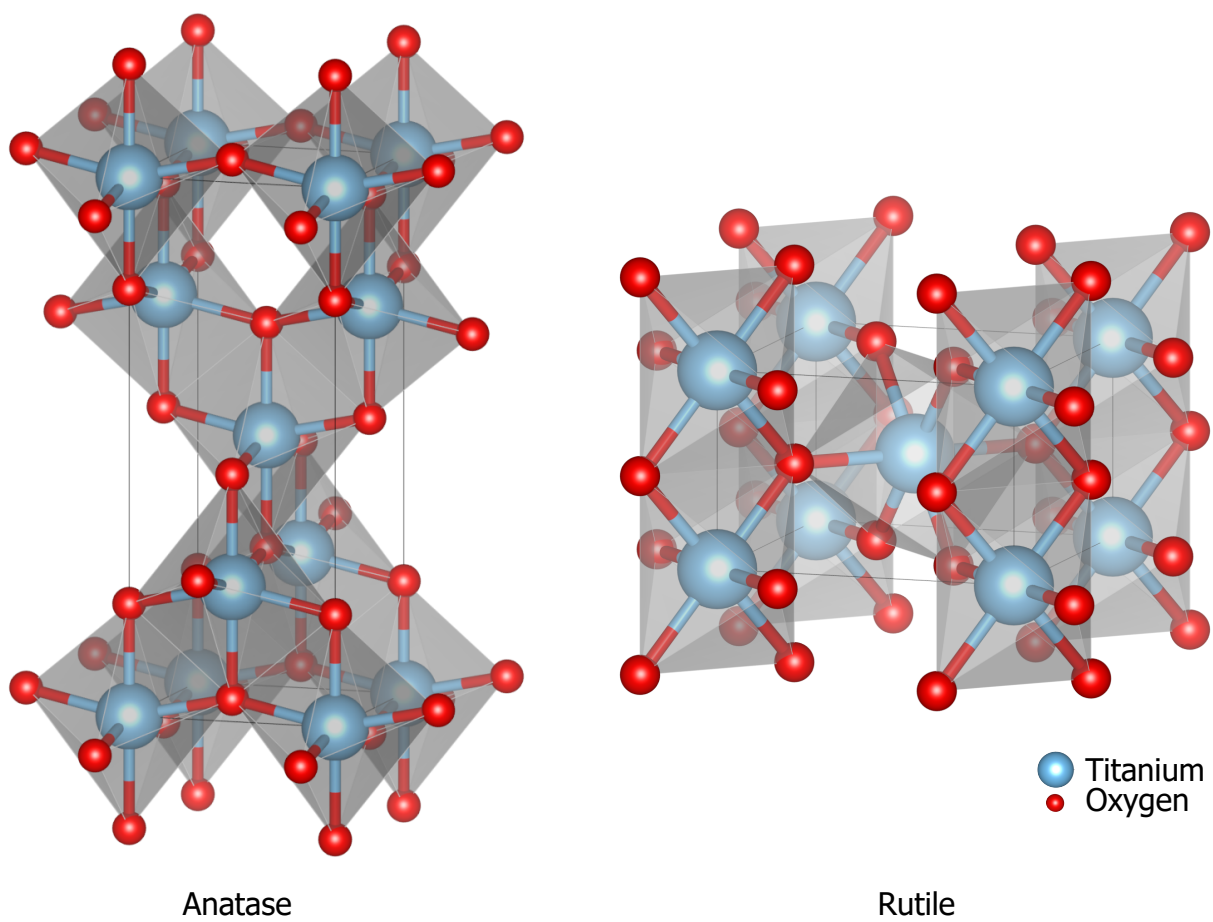


Figure 1.1: Crystal structure of anatase and rutile TiO₂

suitable for artist's pigments. [2] After becoming first available as a viable pigment in the early 1940s in the United States, rutile was sold as a more weather resistant white and often mixed with anatase to lower the cost. [2] Although rutile was available beginning in the 1940s, artists continued to use anatase based paints. Paintings well into the 1940s contain anatase phases due to a combination of, reduced cost, more desirable color, or simply availability. [9–11]

Titanium white has been found in many modern works produced in the first half of the 20th century including Piet Mondriaan's *Broadway Boogie Woogie* (1942-1943) and *Victory Boogie Woogie* (1944) and many works by Jackson Pollock including his 1947 drip masterpiece *Alchemy*. [9, 10, 12, 13] Formulations of titanium white containing anatase, rutile, composite heterostructures of anatase and rutile, and mixtures with additives such as zinc oxide and barium sulfate were all available during the creation of these paintings. [2, 12] Although the presence of titanium has been identified, many surveys stop short of identifying the crystallographic phase, composite nature, and degradation condition.

1.2.2 The Problem of TiO₂ activity

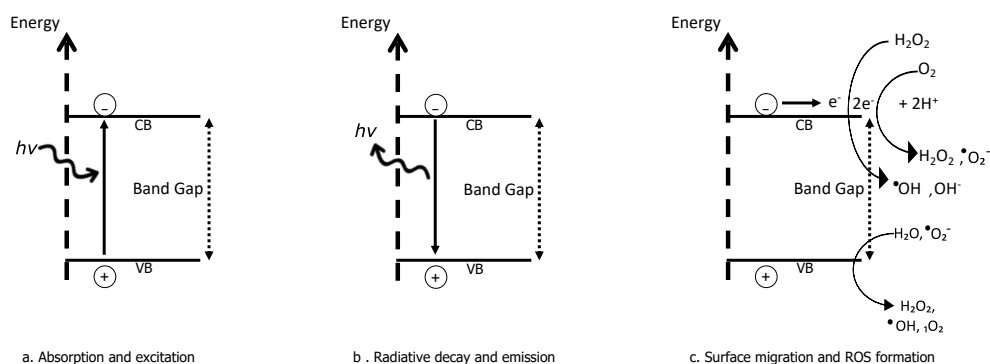


Figure 1.2: Schematic representation of photoinduced excitation in a semiconductor.

The electronic structure of TiO₂ is characterized by an energetic gap in permitted states between the highest occupied states (valence band) and lowest unoccupied states (conduction band) of 3.2 eV for anatase and 3.0 eV for rutile. [6, 14] When TiO₂ is irradiated with a photon of ultra-band

gap energy, the photon transfers its momentum to an electron in the valence band. This extra momentum facilitates an excitation from the valence band into the conduction band as can be seen in Figure 1.2a. This excitation leaves behind an electron vacancy, often called a hole. In most cases, the excited electron will go through radiative decay, returning to the valence band shown in Figure 1.2b. The excited electron can also migrate to the surface and interact with bound and free floating molecules as shown in Figure 1.2c. This interaction can lead to the formation of Reactive Oxygen Species (ROS). ROS, such as O_2^- and H_2O_2 at the conduction band and $\cdot OH$, singlet oxygen, and H_2O_2 formed at the valence band. Although each of these products forms from water and oxygen at their respective bands, inter-conversion between products allows for most to be generated at either band.

The electronic structure of TiO_2 and the rate of generation of ROS can be affected by surface conditions, particle size, and interactions with anchoring molecules. [15–21] Etacheri *et al.* 2011 have shown that excess oxygen at the surface of the particles in the form of H_2O_2 can decrease the band gap of anatase TiO_2 , allowing for excitation of an electron into the conduction band with visible light. [22] Zhang and Yates summarize the effect of many surface interactions such as OH and $1H^+$ on the band edges. They show that an increase in band bending at the TiO_2 complex interface, increases charge separation thus decreasing recombination. [23] Schneider *et al.* summarize how when attached non-metallic molecules act as electron donors it often facilitated hydrogen abstraction or decomposition. [24] In the case of small attached molecules, such as water, this introduces a new pathway for ROS formation.

Using Density Functional Theory (DFT) and time-dependent DFT (TD-DFT) methods, Auvinen *et al.* showed that the band gap initially narrows for nanoparticle-anatase compared to bulk anatase. However, when the nanoparticles are sufficiently small, the band gap widens compared to bulk which would decrease activity. [25] Almquist and Biswas report that at smaller particle size, charge recombination is increased due to less space for charge separation which would increase recombination and decrease activity. [26] However, a theoretical investigation performed by Gerischer

showed that although fewer electron-hole pairs are generated, the small particle size leads to a higher percentage of generated electron-hole pairs participating in surface reactions. [27] Experimentally this has been shown by Xu *et al.* who showed that particles of TiO₂ less than 30 nm in diameter degrade methylene blue in aqueous solution at an elevated rate compared to larger particles. They found a positive correlation between surface area and initial reaction rate. [28]

Anatase and rutile crystals may also interact resulting in defect rich regions and the creation of electronic trapped states. [29, 30] These kinds of hetero-structured materials such as the commercially produced Degussa P-25 have been engineered to increase photoactivity for chemical and environmental applications. [1, 4, 31] The mechanism of the increased photoactivity lies in the disorder of the interfacial region and in 4 coordinated titanium atoms. [32] Furthermore, it has been shown that simple mixtures of anatase and rutile, when exposed to water and subsequently dried, can form heterostructured regions and exhibit greatly increased photoactivity. [33] This research suggests that even in pigments which were originally created by a mechanical mixture of anatase and rutile, a heterostructured and therefore highly photoactive product can occur if there is significant hydration and dehydration. Additionally, previous work has found that the addition of rutile extends the electron promoting ability of mixed phase TiO₂ to wavelengths as high as 410 nm. [34] ROS may also form in pure oil films, especially under illumination and drives normal curing. [35] However, when TiO₂ and light are present, the concentration of ROS is greatly increased, in turn facilitating degradation in the paint film through similar, but much accelerated reactions presented by Lazzari and Chiantore and shown in Figure 1.3. [36–38] Initial hydrogen abstraction leads to the delocalization of the unsaturated bonds of linoleic and linolenic acid. Following delocalization, reaction with ambient oxygen leads to the formation of conjugated double bonds and a oxygen crosslinking group. The oxygen radical side chain can then react with water to form hydroperoxide, and facilitate scission leading to a β -unsaturated carbonyl compound and a short carbon chain.

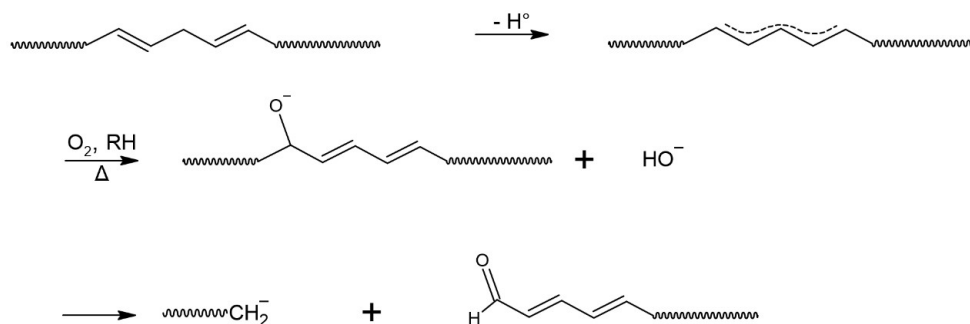


Figure 1.3: Effect of reactive oxygen species on fatty acid chains of linseed oil.

Previous research has thoroughly studied the effect of UV light on anatase and rutile containing linseed oil based paints. Dr. Van Driel has pioneered most of the initial work in this area. She has studied anatase TiO_2 based oil paint under UV lighting conditions and found that an increase in surface roughness can be measured through AFM and gloss measurements. Using X-ray Photoelectron Spectroscopy (XPS), she showed that UV exposure of anatase based paint leads to a surfacing of titanium particles. [39] This inspired the creation of a schematic representation of the degradation process similar to Figure 1.4 and is consistent with proposed UV degradation of semiconductor pigments presented by Anaf *et al.* [40] In another investigation, Morsch *et al.* has probed the chemical reactions that drive the surface roughening and chalking effect seen in Van Driel 2017. [5] By employing AFM-IR and traditional ATR-IR methods, Morsch *et al.* identified spectral markers of compounds characteristic of TiO_2 facilitated UV degradation and proposed a series of reactions which would produce these observed compounds. [5] Van Driel *et al.* 2018 studied the effect of other paint components on photocatalytic activity as measured by change in gloss under UV illumination. They revealed that the crystal structure and presence of protective coatings played a large role in preventing degradation. They also noted that the effect of other fillers and pigments such as ZnO and aluminum stearate is complex and may be significant. [41] They showed that high additions of ZnO can decrease chalking as measured by gloss number in anatase based paints. However, when aluminum stearate is added, ZnO increases the chalking

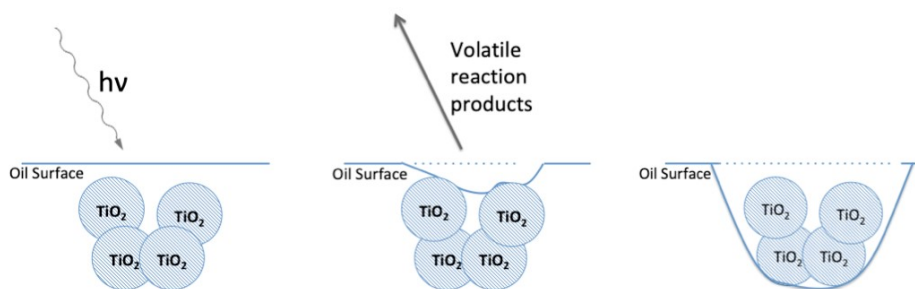


Figure 1.4: Proposed degradation of linseed oil facilitated by TiO₂ reprinted from Van Driel. [39]

effect. Finally, the effect of UV light intensity, and system scale were investigated by Van Driel 2016 by dispersing flakes of TiO₂ based paint into a beaker with acid blue 9 as a degradation indicator. This demonstrated that the UV intensity and system scale had direct effects on the rate of degradation. [42]

The state of research on the activity of TiO₂ based paints leaves certain questions open for investigation. Previous research has identified the presence of titanium white paint in a number of paintings from the first half of the 20th century. However, as discussed above, the condition and formulation (anatase vs rutile) of the titanium white paint identified in these studies has not been consistently noted. There is a need to investigate areas of paintings which may have undergone TiO₂ facilitated degradation to identify the presence of other components and the nature of the degradation. Previous studies have identified the effect of UV light on TiO₂ based paints, however in museums UV light is often filtered out. Based on previous research, many effects could lead to the visible light activity of TiO₂ based paints. Therefore, the effect of visible light on anatase and rutile based paints is a major gap in the current understanding. Previous research has investigated the effect of other pigments and inorganic components on the photocatalytic activity of titanium white. However, the effect of linseed oil on TiO₂ has not been fully investigated and is present in every titanium white paint. This interaction may introduce new modes of degradation, sensitize the TiO₂ to visible light, or increase the activity of the less photocatalytically active phase: rutile. Based

on an understanding of the role of water in TiO_2 band structure, high humidity may introduce band bending which could influence the paint's photocatalytic activity. [23] Additionally, higher humidity would provide more water for conversion to reactive oxygen species, which degrade the oil binder. It is therefore important to explore the effect of humidity on the degradation of TiO_2 based oil paints especially under visible light.

1.3 Research Objectives

This project uses a multi-modal approach using chemical, morphological, and gravimetric characterization methods and computational calculations to:

1. Identify the phases of TiO_2 present in a survey of oil paintings in the early 20th century and use non invasive methods to identify signs of chemical or physical changes consistent with TiO_2 facilitated degradation in these works.
2. Characterize the chemical changes in model systems due to the exposure of TiO_2 based oil paints to both UV and visible light in aging experiments.
3. Use computational methods to study the interaction of organic components commonly used in paintings with TiO_2 and the effect on the electronic and optical properties.
4. Probe the effect of humidity using the QCM to quantify the mass loss of model paint films pigmented with different TiO_2 polymorphs under UV and visible lighting conditions.

Specific projects were undertaken to address these goals. First, in order to best inform model systems, we non-invasively studied a number of 20th century oil paintings of Jackson Pollock focusing on the presence and form of TiO_2 . We employed X-ray Fluorescence Spectroscopy (XRF) to identify areas of paint containing titanium, then used Raman spectroscopy to identify the phase

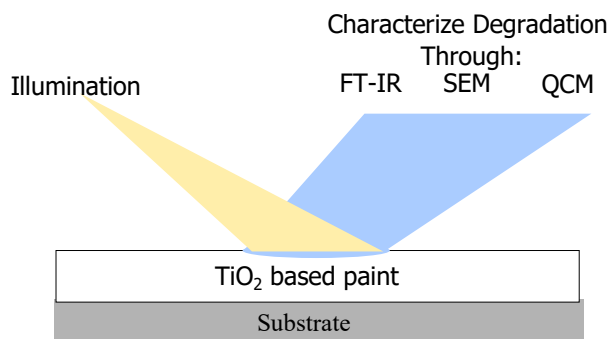


Figure 1.5: Multi-modal approach for characterizing degradation in model paint films using FT-IR, SEM, and QCM

of TiO₂ present. In one painting, *Eyes in the Heat*, all areas of white paint were also studied with reflection IR and visible microscopy to more thoroughly characterize the complex nature of these paint mixtures.

Second, based on the knowledge gained from non-invasive measurements, the multi-modal approach was applied to model paint films aged under museum-like conditions as seen in Figure 1.5. This experiment was aimed at investigating the effect of visible light on the degradation of anatase and rutile based paints. The chemical changes in the paint films were characterized with Attenuated Total Reflectance (ATR) Fourier Transform Infra-red Spectroscopy, and characteristic markers of degradation were noted and tracked. The surface morphology of the aged paint films was probed using Scanning Electron Microscopy (SEM), revealing significant cratering and pitting in TiO₂ containing samples under illumination.

Third, because the environment of titanium dioxide particles in oil paint is complex, experimental approaches aimed at reproducing exact historical conditions are impractical or impossible. The use of computational modeling allows us to answer specific questions by isolating certain components, such as the effect of the oil media on the band structure of TiO₂. We paired the experimental approach described above with a computational investigation into the effect of oil components, such as oleic acid, on the electronic structure of anatase TiO₂. We modeled all three fatty acid

components of linseed oil, oleic acid, linoleic acid, and linolenic acid, as well as an anatase TiO_2 slab. We optimized the structures of each component individually, then attached each fatty acid component to the surface of the anatase TiO_2 and studied the resulting complex. The results of this study, paired with the experimental results, strongly suggest that LO fragments form charge transfer complexes and sensitize anatase TiO_2 for visible light activity. We propose 2 mechanisms by which this interaction results in LO degradation and suggest that these results are likely true for rutile as well.

Finally, we have studied the effect of humidity on the degradation of TiO_2 based paints as measured with the Quartz Crystal Microbalance (QCM). We have used the mass and mechanical property information gathered by the QCM to show the rates of degradation in anatase TiO_2 based paints in moderate (50% RH), and high (RH > 80%) humidity. Additionally we discuss the QCM results with note of the FT-IR results from Chapter 3, providing a more complete picture of TiO_2 facilitated degradation of oil paint.

This set of objectives will add value to the cultural heritage science and materials science field by expanding the knowledge and risk surrounding TiO_2 based artist's paints.

Chapter 2

Identification of TiO₂ paints in Jackson Pollock Paintings

2.1 Introduction and Background

Titanium white was first developed in the early 20th century and has been used in many paintings and sculptures. [10, 43, 44] It has been recently documented that titanium dioxide may drive degradation of the oil binder under UV light. [3, 5, 12, 39, 41, 42] We also present in Chapter 4 a mechanism that would facilitate degradation under visible light. This mechanism involves interactions of titanium dioxide with other components of paint. It is therefore important to survey paintings that may contain titanium dioxide and investigate the other components of the paint to best understand the complex mixture.

A multi-technique approach has been developed by Miliani *et al.* allowing for the non-invasive identification of pigments, binders, and materials of art objects. [45] This approach includes the use of portable X-Ray Fluorescence spectroscopy (XRF) to identify component elements, portable Raman spectroscopy to identify phases of inorganic pigments and characteristic signals of many organic pigments, and reflection Fourier Transform Infrared Spectroscopy (r-FT-IR) to help identify the binder and other IR active pigments. [9, 45–47] Each of these characterization techniques has limitations and, therefore, is alone not sufficient to definitively identify pigments. [45] However, when used together, complementing information from different methods can create a more complete picture.

XRF operates by illuminating a material with x-rays, which then interact with the sample. The interactions of the x-rays with the material produce three main signals, Rayleigh scattering, Compton scattering, and fluorescence. XRF, as the name implies, uses the fluorescence signal. When an x-ray photon with sufficient energy, interacts with an electron in the material, it may facilitate

the ejection of that electron. In order to fill the recently created vacancy, an electron in a higher orbital will transfer which emits another photon with energy corresponding to the difference in the electrons initial and final orbitals. [48] Because the characteristic energies derive from the electronic structure of the atoms, it is unique to each element and can be considered a fingerprint with specific naming conventions describing transitions.

Raman operates by measuring the inelastic scattering of light caused by molecules and lattices. [49] It is often employed with XRF to provide complementary information on crystallographic phase or organic molecule identification. However, it can only detect Raman active materials. Luckily, TiO_2 is Raman active and the crystallographic phase can be determined via Raman spectroscopy.

Reflection-FT-IR measures the vibration response of samples created from the illumination of broad IR radiation. Based on the specific energy of the resulting vibration, bond characteristics can be determined and the resulting chemistry can be inferred. [50] We use this technique to identify the chemistry of the binder, and any conservation coatings applied.

There are 11 Jackson Pollock paintings at the Peggy Guggenheim Collection in Venice, Italy all painted between 1942 and 1947. These paintings were purchased from Jackson Pollock by Marguerite “Peggy” Guggenheim, an American art collector who eventually settled with her large art collection in Venice, Italy. In 1976, her Venice home became a museum and the permanent home to this collection. Prior to the conversion to a public collection, the paintings on display were subjected to uncontrolled humidity, light exposure, and exposure to other substances such as dirt and dust. [51, 52] As discussed in Chapter 1, these substances may have drastically affected the photocatalytic activity of titanium white paints in these paintings. Based on initial XRF screening of paintings containing titanium, four paintings spanning 1942 to 1946 were selected as shown in Figure 2.1. XRF was used as an initial screening to identify paintings that may contain titanium white. After the initial selection, Raman was used to confirm the presence of titanium white and identify the phase. In addition, one painting, *Eyes in the Heat*, was selected for further study and

all white paints were characterized with FT-IR.



Figure 2.1: Paintings Studied at the Peggy Guggenheim collection and featured in this study.

2.2 Materials and Methods

2.2.1 Twentieth Century Paintings

The selected paintings were studied by a multi-technique, non-invasive approach within the MOLAB activity at the Peggy Guggenheim Collection in Venice, Italy. For *The Moon Woman* (1942), *Two* (1943-1945), *Croaking Movement* (1946), certain points were selected based on preliminary screening using XRF results from a previous trip to the Peggy Guggenheim Collection by the MOLAB team. Points containing titanium signal in XRF plots were selected for further study using Raman. For *Eyes in the Heat* (1946), points were selected instead in all areas of white paint focusing mostly on areas with signs of degradation. These areas were investigated with Raman,

reflection FT-IR, and video microscopy. Spectra were taken directly on the painting surface in the museum.

2.2.2 Portable Raman Measurements

In-situ Raman analysis was performed with the portable Xantus- 2 by Rigaku. It is equipped with a double laser excitation at 785 and 1064 nm. In both cases, the laser power at the sample can be software modulated thus avoiding any sample damage. The spectral resolution with the 785 nm excitation is 7–10 cm^{-1} and it works with a cooled charged-coupled device (CCD) detector (Peltier cooled). An InGaAs detector is employed for the 1064 nm excitation working with a spectral resolution of 15–18 cm^{-1} . In both configurations the spatial resolution is about 4 mm^2 . The laser power at the sample was kept between 1 and 30 mW with an exposure time of 1000 ms for each spot collecting 1 to 5 accumulations.

2.2.3 Portable reflection FT-IR

Reflection FT-IR spectra were taken using the reflection mode of the Alpha spectrometer (Bruker Optics). The spectra were recorded from 350 to 7500 cm^{-1} at a resolution of 4 cm^{-1} and 128 scans. The spacial resolution is about 28 mm^2 and the probe head-to-surface distance is larger than 1 cm.

2.2.4 Portable XRF

XRF measurements were carried out by means of the ELIO spectrometer (XGLab). It consists of a Silicon Drift Detector cooled by a Peltier system with an active area of 25 mm^2 and a resolution of 135 eV to the Mn $K\alpha$ line. It has a Rhodium source with a maximum power of 50 kV and maximum current of 200 μA . The spatial resolution is of about 1 mm^2 .

2.2.5 Reference Samples

Reference samples were created in the lab on chemical grade TiO_2 powders. Raman reference spectra were collected using a Bruker Senterra system with a thermoelectrically CCD detector. Raman spectra were recorded by focusing a 1064 nm laser beam through a 50 \times and 100 \times Olympus objectives. 400 lines/mm gratings and 1200 lines/mm gratings were used. The laser power at the sample was 50 mW with an exposure time of 1000 ms for each sample collecting 1 to 5 accumulations.

2.3 Results and Discussion

Seven different points were sampled from pink, cyan, and white areas of Pollock's *The Moon Woman* ('42) as shown in Figure 2.2. XRF results from each point confirmed the presence of Ti, suggesting the use of titanium white. To interrogate the crystallographic phase, we performed Raman spectra on the points. As can be seen in Figure 2.2b, all points exhibit medium strength peaks at 400, and 518 cm^{-1} , and a strong peak at 638 cm^{-1} , exactly matching the reference anatase TiO_2 . In addition, all points exhibited a peak at 992 cm^{-1} which is closely associated with to BaSO_4 , commonly used as a filler. [11] Interestingly, three of the studied areas contained colored paint, namely cyan in two points and pink in a third. The XRF spectra of the pink areas show the presence of Zn, Ba, and Ti, all common components of white pigments. The light blue areas show similar elements present suggesting that the color derives from an organic dye which would not register with XRF. Instead, other methods such as UV-vis reflection and fluorescence spectroscopy are necessary to identify these components. Through these techniques it can be deduced that these areas likely used phthalo blue for the light blue, and an organic red dye which has a characteristic UV-vis fluorescence emission at 650 nm such as an alizarin type dye. Pigments such as phthalo blue or alizarin which may have been used in these areas may interact with anatase

TiO₂ to create complexes with increased photoactivity such as those discussed in Chapter 4. [51,52] This could lead to combined effects increasing photoactivity and accelerating degradation. The paint in these areas have visible areas of white that look discolored. However, it is not clear if this is due to degradation or Pollock's original intent. A more thorough study could be done with special attention paid to gloss, condition, and identification of other components. This study was aimed at getting an initial survey of the materials used by Pollock.

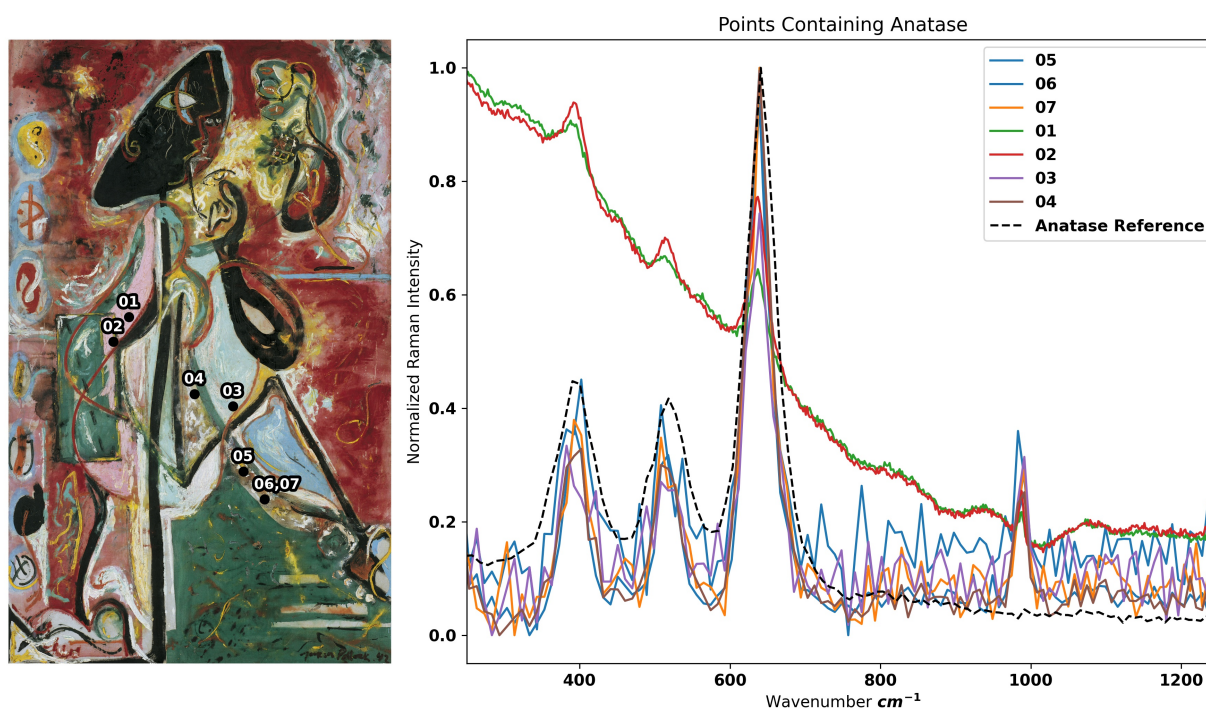


Figure 2.2: *The Moon Woman* (1942) with (b) Raman of selected points and anatase reference

In *Two* ('43-'45), only 3 points were studied, all in the same white area, as can be seen in Figure 2.3a. Similar to *Moon Woman*, all areas exhibited characteristic anatase TiO₂ peaks and match the reference spectra.

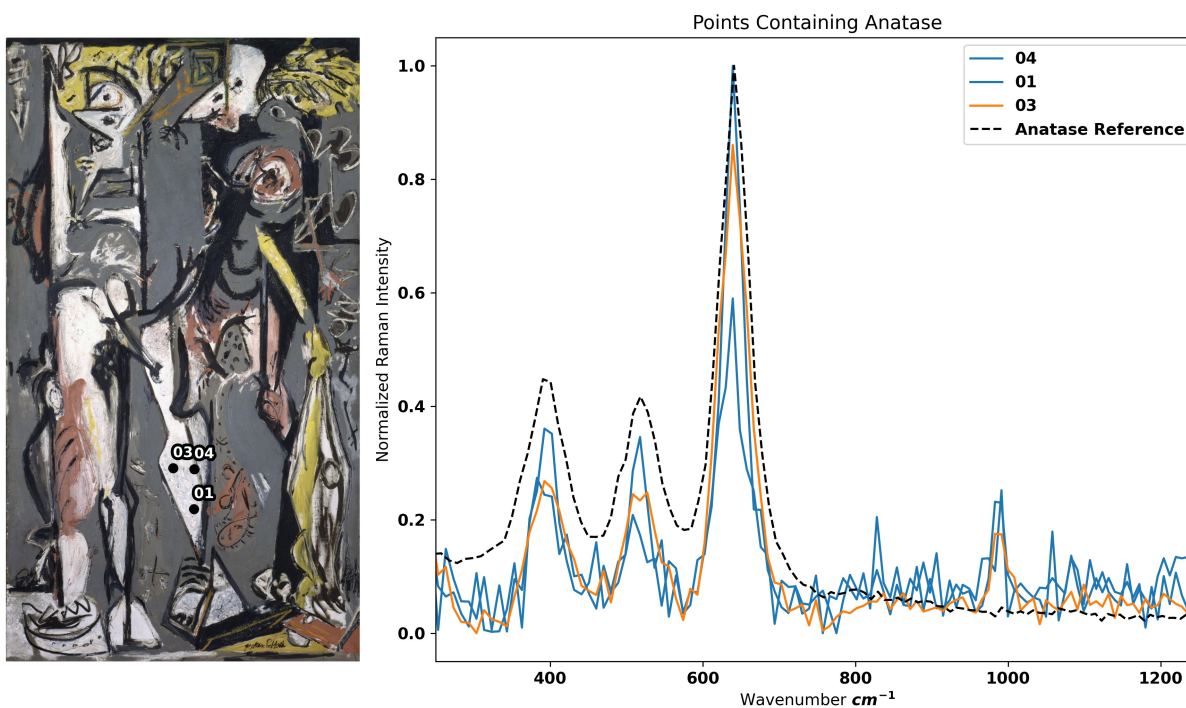


Figure 2.3: (a) *Two* (1943-1945) with (b) Raman of selected points and anatase reference

Croaking Movement was painted in 1946 and represents a different style of Pollock's paintings characterized by an even more abstract nature. As such, for *croaking movement*, locations were chosen for study within distinct brush strokes. Eight points were chosen from across a 55 cm x 70 cm section of the painting as can be seen in Figure 2.4a. Despite similar use in the painting, Raman analysis revealed both anatase and rutile phases of TiO_2 present. Not all brush strokes were studied, so the relative use of anatase and rutile based whites cannot be commented. There was a slight noticeable difference in appearance between the anatase and rutile paints. Rutile areas had a glossier look where anatase had a more matte look. This may be due to degradation or the original look of the paint. Of the points studied, three points contained rutile phase and five contained anatase phase. This painting suggests a transition to using rutile based paint.

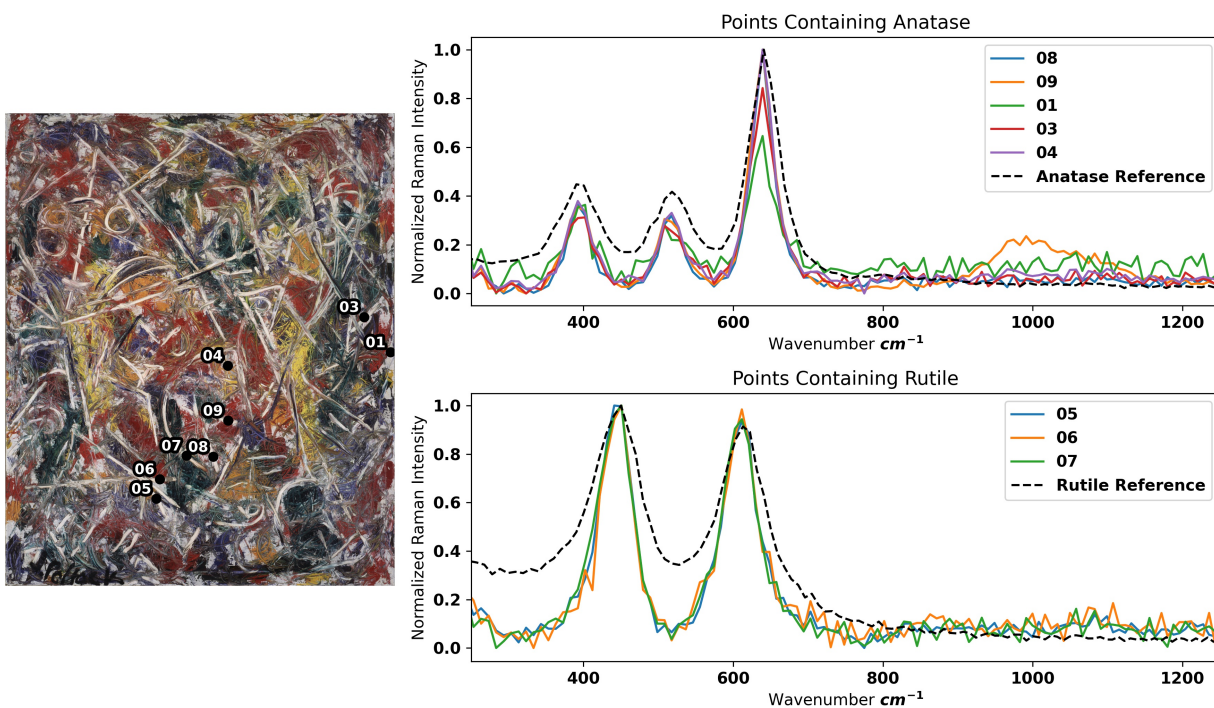


Figure 2.4: (a) *Croaking Movement* (1946) with (b) Raman of selected points and anatase and rutile references

Finally, also painted in 1946 by Pollock, *Eyes in the Heat* also displays Pollock's drip style. Like *Croaking Movement*, *Eyes in the Heat* shows the use of both anatase and rutile phases of titanium white as can be seen in Figure 2.5b. The zoomed area shows point 26, which contains rutile, and point 23, which contains anatase. It is therefore very interesting to note that areas containing anatase show signs of degradation such as yellowing, and cracking as can be seen in Figure 2.5c where as rutile shows a more pristine white surface. The proximity of these points suggests similar or nearly identical aging conditions, leaving the different pigment to account for the different conditions.

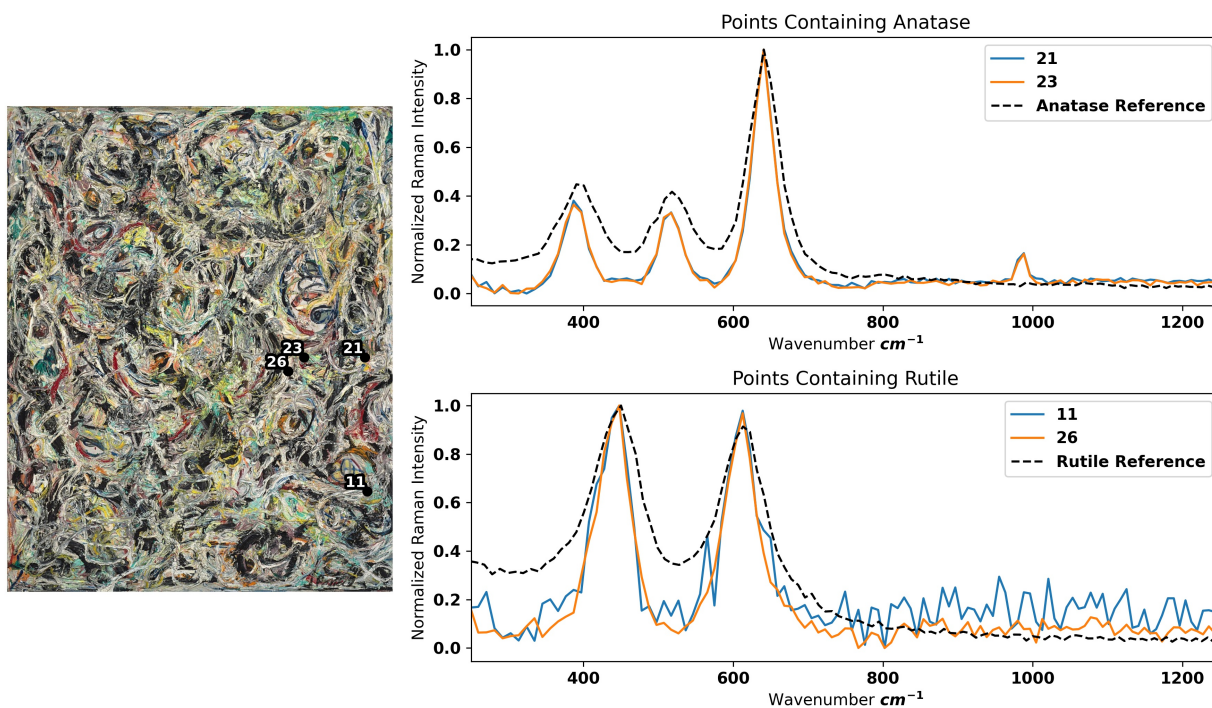


Figure 2.5: (a) *Eyes in the Heat* (1946) with zoomed area and (b) Raman of selected points and anatase and rutile references (c) microscope image of anatase based paint and (d) microscope image of rutile based paint

To probe in more detail the use of titanium white in *Eyes in the Heat*, distinct types of white paint were identified based on position, texture, color, and condition. One such paint identified on the top surface exhibited significant cracking, yellowing, and chalking as can be seen in Figure 2.6a. Raman spectra of this area exhibited characteristic signal of anatase and barium sulfate similar to those presented in Figure 2.5b. The FT-IR of this area presented in Figure 2.6 Point A shows a more complex picture. Based on work by Rosi *et al.* we used the shape of the carbonyl asymmetric stretching band around 1740 cm^{-1} to distinguish between different binders. In Figure 2.6 Point A, this band appears as a derivative shape and there are characteristic $\delta(\text{CH})$ peaks at 1400 and 1470 cm^{-1} suggesting an acrylic binder. The $\delta + \nu(\text{CH})$ between 4250 and 4260 cm^{-1} is characteristic of an oil binder. These seemingly contradicting identifications provide spacial information about the binder. Higher wavenumber signal can travel from deeper in the film. The presence of an acrylic

binder at lower wavenumbers and oil binder at higher wavenumbers suggest that a conservation coating was applied with the more modern acrylic. The combination of the anatase pigment and the condition suggests that this paint has undergone TiO₂ facilitated degradation. The IR spectra for point a also shows strong sulfate contributions as seen around 2060 and 1150 cm⁻¹ suggesting the use of a calcium or barium sulfate filler. As discussed in Chapter 1, mixtures of anatase and BaSO₄ are common and may interact in unintended ways.

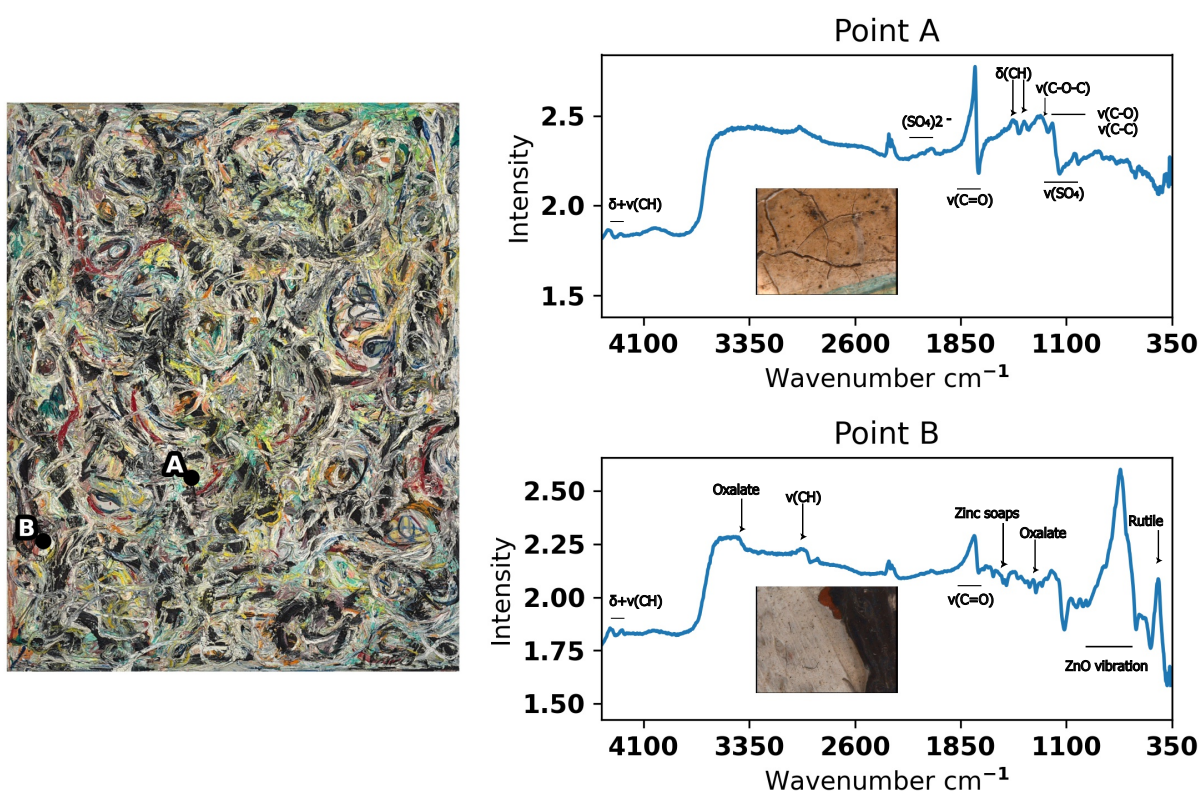


Figure 2.6: FT-IR spectra of upper layer of *Eyes in the Heat* (1946) showing (a) more signs of degradation, and (b) less signs of degradation. Characteristic markers are indicated with arrows.

Another upper area of *Eyes in the Heat* was found with distinctly different condition. The area shown in Figure 2.6 Point B displays very little cracking or yellowing. The appearance is still bright white with high gloss. The image does show some discoloration and speckles forming which may indicate some initial degradation. The FT-IR spectra reveals a broad carbonyl asym-

metric stretch around 1740 cm^{-1} and small doublet peaks corresponding to (CH) bending and stretching around 4370 cm^{-1} characteristic of a linseed oil binder. [47, 53] The presence of rutile TiO_2 can be observed in the FT-IR spectra as a peak at 435 cm^{-1} as well as through Raman spectra. The large broad peak at 842 cm^{-1} indicates the presence of zinc oxide, another common white pigment which has shown instability in linseed oil. [54–56]. Zinc oxide undergoes a different degradation process than TiO_2 . ZnO pigments undergo ionization and mobile zinc ions react with fatty acid components to form metal soaps. [57–59] As discussed in Chapter 1, the presence of other inorganic materials can greatly affect the photocatalytic activity of TiO_2 based paints and mobile zinc ions may attach to the TiO_2 surface leading to a heterostructure. [60] Although this sample does not exhibit signs of significant TiO_2 facilitated degradation, the FT-IR spectra reveal that the zinc oxide pigment may have undergone degradation. Signal from oxalates around 3500 and 1300 cm^{-1} and the markers around 1530 cm^{-1} shown in Figure 2.6 Point B are consistent with formation of such zinc soaps. [11, 55, 57, 59, 61, 62] It is also possible that mobile zinc ions absorbed onto the TiO_2 surface are slowed the formation of metal soaps. In this way, TiO_2 may decrease the rate of metal soap formations in mixtures of zinc or lead white and TiO_2 .

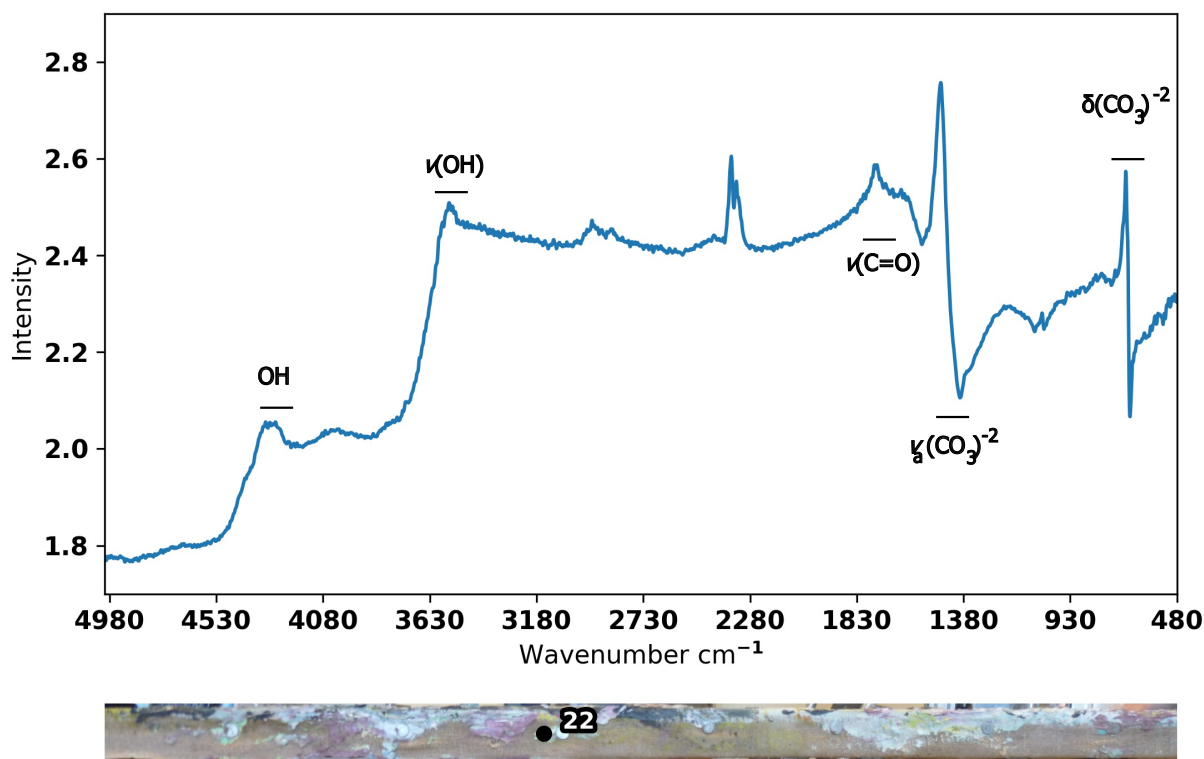


Figure 2.7: FT-IR of lower white layer measured on the edge of the painting, characteristic markers are indicated with arrows.

A lower layer was identified on the edge of the painting which exhibited bright white and no signs of degradation. The FT-IR spectra in Figure 2.7 show CO_3 vibration and bending around 1460 and 700 cm^{-1} , and OH stretching at 3560 cm^{-1} indicative of lead white. [47, 63] The lead white signal covers many other bands used for binder identification, but the asymmetric carbonyl stretch is still visible around 1740 cm^{-1} and shows a broad peak indicative of an oil based binder. [53, 64] Because this area is on the edge of the canvas, it was likely not exposed to as much light and therefore the condition may not be a good indication of the pigment photo-activity.

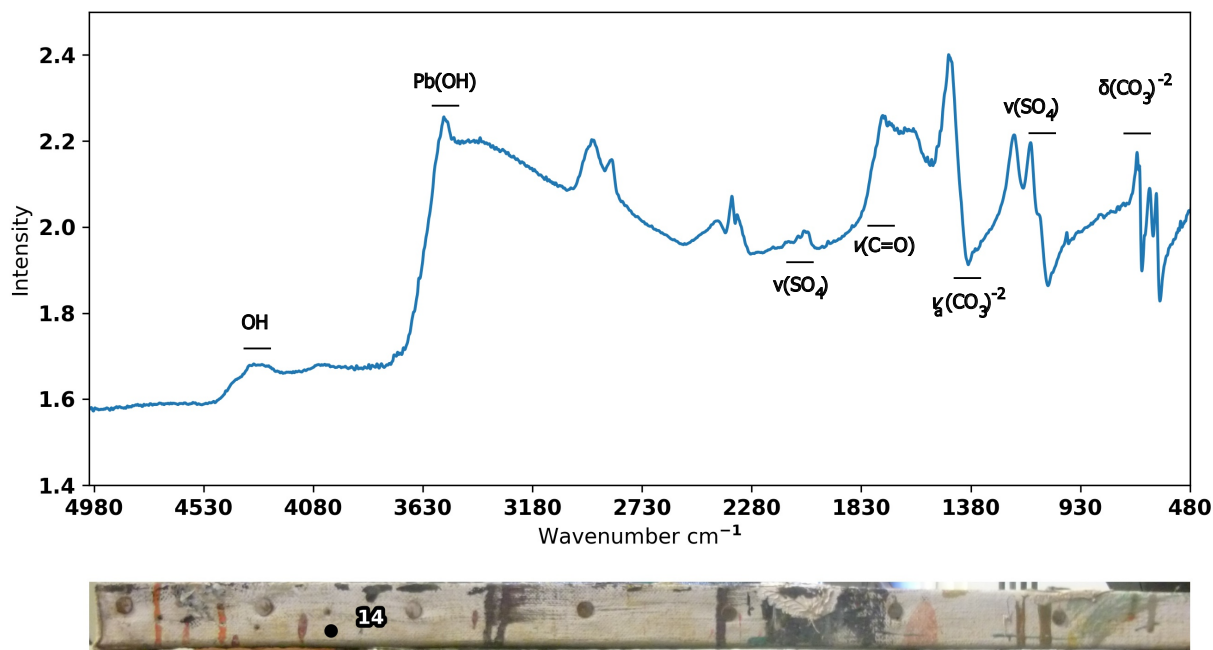


Figure 2.8: MIR of lower ground layer probed via the canvas border

Lead signal was found using XRF in many areas of the painting, suggesting the use of a lead white ground. On the edge of the canvas, an area was identified where the ground layer was exposed. Similar to Figure 2.7, signal of CO_3 vibration and bending around 1460 and 700 cm^{-1} , and OH stretching at 3560 cm^{-1} can be seen in Figure 2.8. However, in the ground layer SO_4 vibrations can be seen around 2050 and 1130 cm^{-1} suggesting a barium or calcium based filler. XRF was performed on a similar area on the painting border, showing strong signal of lead, zinc, and barium. This suggests that the sulfate filler seen in the IR spectrum is BaSO_4 . Although the XRF spectra shows the presence of zinc, the IR spectra does not show the strong zinc vibration around 842 cm^{-1} seen in Figure 2.6 point B. This may suggest the use of another zinc compound such as ZnS , which was often mixed with barium sulfate to create lithopone.

2.4 Conclusions

This work has shown that both anatase and rutile forms of titanium dioxide have been identified in works painted by Jackson Pollock in the 1940s. We have shown that areas containing anatase based paints are in various states of degradation, yet areas of rutile based paint show significantly less degradation. Additionally, we have identified four distinct white paints used in the painting *Eyes in the Heat* including, anatase/barium sulfate and rutile/zinc oxide based paints in the upper layers and lead white based paints in the lower and ground layers. We have discussed evidence of degradation and noted one occurrence of conservation action. Finally, in all paints measured, we have identified the primary binder as oil and we discuss in further detail the possibility of interactions with TiO_2 in Chapter 4. This work demonstrates the need for further study into the activity of anatase and rutile in complex mixtures such as oil paint.

Chapter 3

New Insights into the deterioration of TiO₂ based oil paints: The effects of illumination conditions and surface interactions

3.1 Introduction

Since the early 20th century, titanium dioxide (TiO₂) has become the most common white pigment for both artist and commercial paints due to its high hiding power, non-toxic nature, and reasonable cost. [1, 2] TiO₂ is found in many modern works, including Piet Mondrian's *Broadway Boogie Woogie* (1942-1943) and *Victory Boogie Woogie* (1944), and many works by Jackson Pollock, including his 1947 drip masterpiece *Alchemy*. [9, 10, 12] A recent analysis of Pollock's *Eyes in the Heat* (1946), shown in Figure 3.1, revealed areas containing TiO₂ which showed signs of degradation. The degradation presents as yellowing, cracking, and a chalked appearance, similar to that identified in previously published research. [5, 39, 42]

TiO₂ is present in paintings primarily as one of two crystalline structures: anatase or rutile. Both phases were found in *Eyes in the Heat* by in-situ measurements through a portable Raman system and shown in the insert of Figure 3.1. Anatase was first produced in 1914 and is the more photo-reactive phase. Over time, the production of TiO₂ based white paints switched to the less photocatalytically active rutile phase. [2] In addition to being a pigment, TiO₂ is a semiconductor and facilitates the formation of radical oxygen species (ROS) under ultra-band gap illumination. [8] For anatase, the ultra-band gap illumination is limited to near UV light ($\lambda < 385$ nm), whereas rutile has a tail that extends the response into visible light ($\lambda < 410$ nm). [8] While it is widely reported that anatase has lower rates of recombination and hence, higher photo-reactivity than rutile, these differences may be diminished under certain conditions and both materials may generate radical products that promote degradation of the oil binder. [30, 65–68] Furthermore, the behavior of semi-

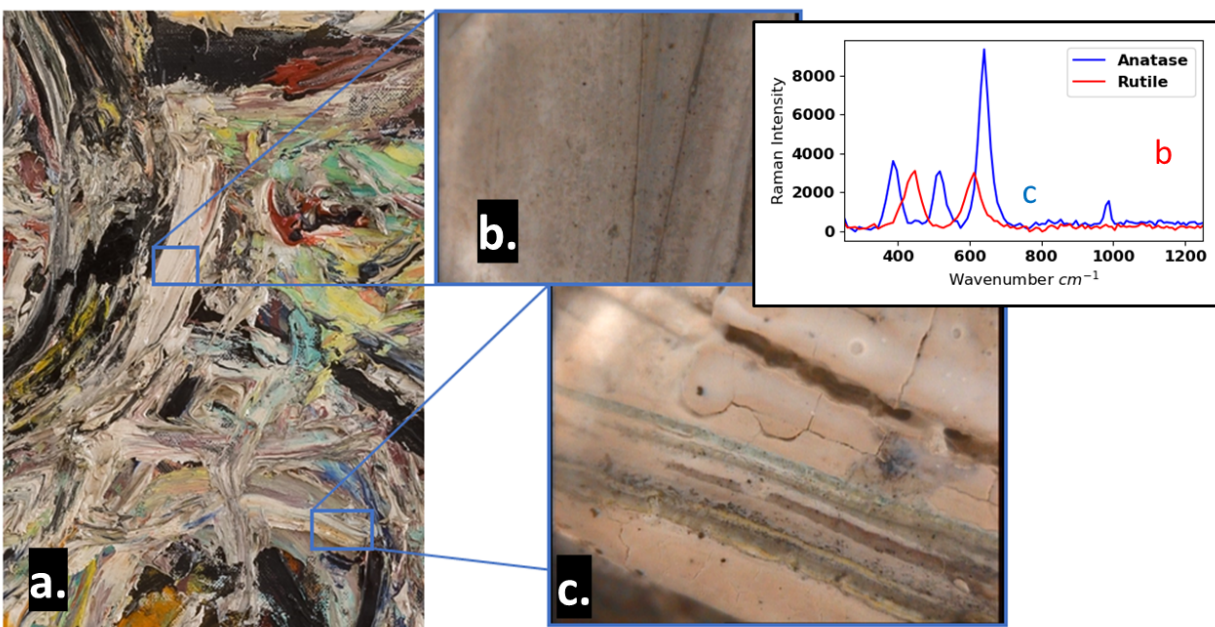


Figure 3.1: (a) Section of *Eyes in the Heat* (1946) painted by Jackson Pollock. Inserts show an area of (b) rutile based paint and (c) an area of anatase based paint, inset shows the Raman spectra used to confirm the presence of rutile in point (b) and anatase in point (c).

conductor pigments such as TiO_2 is influenced by interactions with other components present in the complex matrix of a paint film, such as inorganic and organic compounds. These interactions can result in charge transfer complexes such as those studied in solar cell applications and are well documented to extend the response of TiO_2 into visible light. [20, 30, 65–73]

In order to probe the pathway of paint deterioration under various illumination conditions, we monitored chemical and morphological changes using FT-IR spectroscopy and electron microscopy to investigate the effects of aging anatase and rutile pigments in linseed oil based model systems under three lighting conditions: UV and visible light (UV-vis, $\lambda > 350$ nm), visible light (vis, $\lambda > 400$ nm) and dark. Control experiments with both pure linseed oil and BaSO_4 based paints were also conducted.

3.2 Experimental Materials and Methods

Model paint-outs were created by mixing the selected pigment with linseed oil (Sigma-Aldrich CAS 8001-26-1) using a palette knife on a glass plate. Pigments were mixed at pigment weight concentrations of 25% for rutile TiO_2 (Strem Chemicals CAS 13463-67-7) and anatase TiO_2 (J.T. Baker Material No. 4162-01) and 30% for BaSO_4 (Sigma-Aldrich CAS 7727-43-7). The paint mixture was blade coated onto 2 cm x 2 cm Lexan polycarbonate squares at a nominal thickness of 250 μm . The coated paint-outs were left to cure for 1 month in the ambient lab environment (~50% RH and 22 °C). Following the methods outlined in de Viguerie *et al*, polymerization was confirmed after 1 month by monitoring the absence of the =C-H cis stretch peak at 3010 cm^{-1} with Fourier Transform Infrared Spectroscopy in Attenuated Total Reflection mode (ATR-FT-IR). [74]

Samples were aged for a total of 2 months in a custom designed illumination apparatus constructed of polycarbonate chambers, shown in Figure 3.2. The chambers were controlled and monitored to be at 25 ± 1 °C and $50 \pm 5\%$ RH. Lighting conditions were fixed through a single mounted 400 W



Figure 3.2: Setup of Aging Chamber

metal halide lamp (Sylvania M400/U), with either a Pyrex filter to remove wavelengths below 350 nm for UV-vis light, or a UV blocking filter (Edmund optics UV filter sheet) to remove wavelengths below 400 nm for visible light aging. The intensities of the UV ($350 < \lambda < 400$ nm) and visible ($\lambda > 400$ nm) portions of the spectra were $232 \mu\text{Wcm}^{-2}$, and $6.33 \times 10^4 \mu\text{Wcm}^{-2}$ respectively. The spectra for the UV-vis and visible lighting conditions are illustrated in Figure 5.5. One chamber was covered with blackout optics cloth to achieve dark conditions.

All samples were characterized every ~8 days through micro ATR-FT-IR using a Bruker LUMOS II equipped with a $100 \mu\text{m}$ germanium crystal. Spectra consisted of an average of 32 scans from 4000 cm^{-1} to 600 cm^{-1} with a resolution of 4.0 cm^{-1} and low ATR pressure. Surface spectra were obtained from 6 positions across the sample and once the spectral reproducibility was verified, they were averaged. Spectra were then baseline corrected and normalized to the 1736 cm^{-1} carbonyl peak.

SEM images were taken with Hitachi S-4800. Before imaging with the SEM, samples were coated with 5 nm of osmium to prevent charging due to the low electrical conductivity of linseed oil.

3.3 Results

For all samples and aging conditions, explicit attention was paid to the characteristic markers of oxidation products in FT-IR spectra: the formation of a spectral feature at 1710 cm^{-1} assigned to C=O stretching of carboxylic acids and aldehydes, the formation of a broad shoulder centered around 1776 cm^{-1} attributed to the C=O stretching of peracids, peresters, γ -lactones, and anhydrides, the formation of a broad shoulder between $1670\text{-}1610\text{ cm}^{-1}$ assigned to $\nu(\text{C}=\text{C})$ of conjugated dienes, and changes to peaks in the region around 1168 cm^{-1} associated with the triglyceride ester linkages. [5,53,75] These spectral markers were associated with the degradation of linseed oil through β -scission reactions and γ -lactones formation reactions proposed by Van Driel. [12] The broad region between 1670 and 1610 cm^{-1} contains multiple peaks including $\nu(\text{C}=\text{C})$ of conjugated diene compounds which has been previously attributed to the degradation of linseed oil. [50,75–80] For the purposes of comparing peak intensity, the region $1670\text{-}1610\text{ cm}^{-1}$ is measured at 1640 cm^{-1} .

For the linseed oil only samples (Figure 3.3a and b) and the samples made with non-photoreactive BaSO_4 (Figure .1)), the FT-IR spectra show changes consistent with hydrolysis and direct photolysis as reported in previous research. [81] Hydrolysis and direct photolysis generate free fatty acids through auto-oxidation and β -scission reactions which can be observed as slight shoulders forming at 1710 cm^{-1} and 1776 cm^{-1} in Figure 3.3a and b. In the oil paint samples, very small changes were observed in the 1168 cm^{-1} peak associated with tri-glyceride ester linkages. Under visible illumination (Figure 3.3a) the 1168 cm^{-1} peak is stable until the last exposure point where the intensity decreases slightly. Under UV-vis illumination (Figure 3.3b) the 1168 cm^{-1} peak increases slightly for the first three exposure amounts and then decreases for the last exposure. In the BaSO_4 pigmented samples shown in Figure .1, the tri-glyceride ester linkage peaks are obscured by the contribution of the sulfate peaks and therefore no conclusions can be made about the changes of the tri-glyceride ester linkages with aging in these samples.

The linseed oil sample illuminated with visible light (Figure 3.3a) shows the slight formation of a

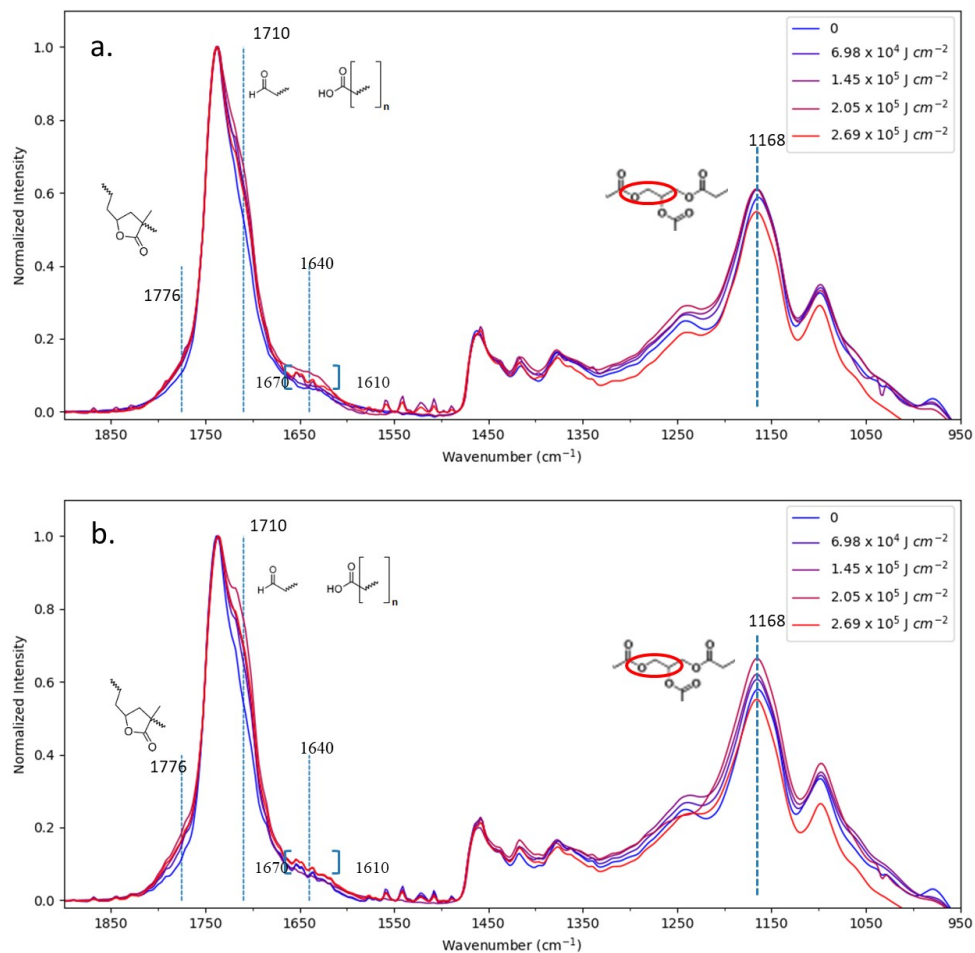


Figure 3.3: Linseed oil aged in (a) vis, and (b) UV-vis conditions. Characteristic markers of degradation are marked with dotted lines and functional groups.

broad shoulder between 1670 and 1610 cm^{-1} . Interpretation of this region's degradation products is not trivial because of overlapping spectral features. Hayati *et al.* has attributed some features in this region to reaction products of the polyunsaturated fatty acid components of linseed oil such as the $\nu(\text{C}=\text{C})$ of conjugated diene compounds formed by processes similar to autooxidation. [82] Meilunas *et al.* attributes this more specifically to β -unsaturated carbonyl compounds. [75] Both compounds could form through allylic hydrogen abstraction as mediated by OH radicals and subsequent oxygen mediated conversion from an unconjugated to conjugated structure. [50,82,83] However, the UV-vis illuminated linseed oil sample (Figure 3.3b), and both UV-vis and visible illuminated BaSO_4 samples (Figure .1) show no appreciable changes in this region. This suggests, as expected, that the conversion of unconjugated to conjugated carbon bonds is not significant in the control samples of pure linseed oil and BaSO_4 .

A number of interesting results were observed when comparing linseed oil with TiO_2 containing samples (Figure 3.4a and b). First, evidence of degradation was observed both in samples exposed to visible light (Figure 3.4a) and samples exposed to UV-vis and visible conditions (Figure 3.4b) after 269 kJ cm^{-2} of aging. Second, the telltale signs of degradation were observed for both anatase and rutile based paints. As shown in Figure 3.5, under visible and UV-vis illumination both rutile and anatase based paints showed the formation of a shoulder at 1710 cm^{-1} which evolved to a strong peak with increasing exposure, suggesting that both anatase and rutile promote the formation of free fatty acids. The degradation of the TiO_2 pigmented oil is also evident in Figure 3.5 by observing the growth of peaks in the 1670-1610 cm^{-1} region due to auto-oxidation as described above. The growth of peaks in this region observed in Figure 3.5 suggests that anatase and rutile based paints promote the degradation of oil through the acceleration of OH radical generation under both visible and UV-vis light conditions driving the conversion of unconjugated carbon bonds to conjugated bonds in polyunsaturated fatty acids. The linseed oil only sample (Figure 3.3a and b) shows little to no growth in this region. Also seen in Figure 3.5, as opposed to pure linseed oil, anatase and rutile based samples showed a marked decrease in the main peak at 1168 cm^{-1} for

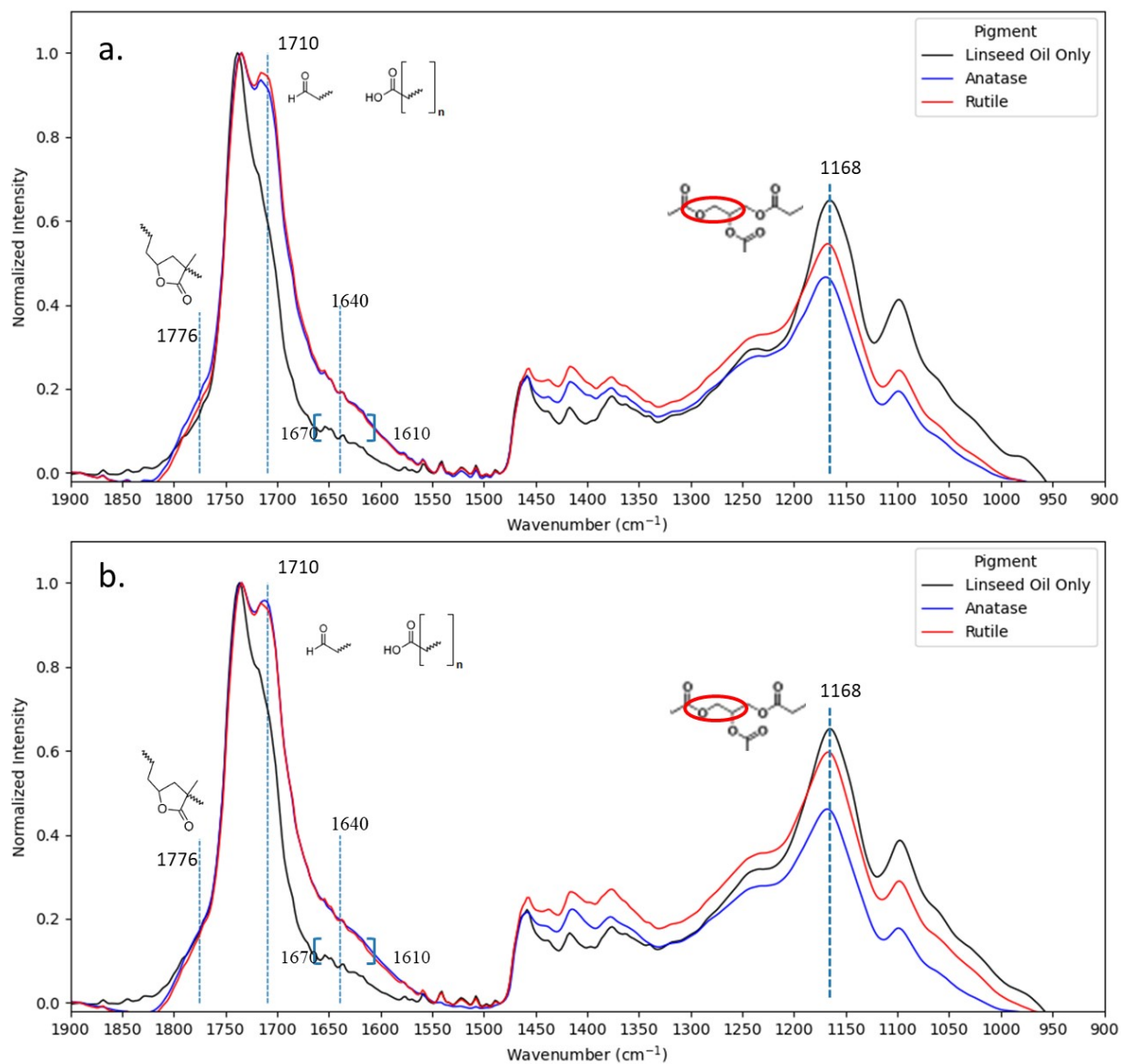


Figure 3.4: Linseed oil only, anatase, and rutile based paint aged in (a) vis and (b) UV-vis light with a total exposure of 269 kJ cm^{-2} . Characteristic markers of degradation are marked with dotted lines and functional groups.

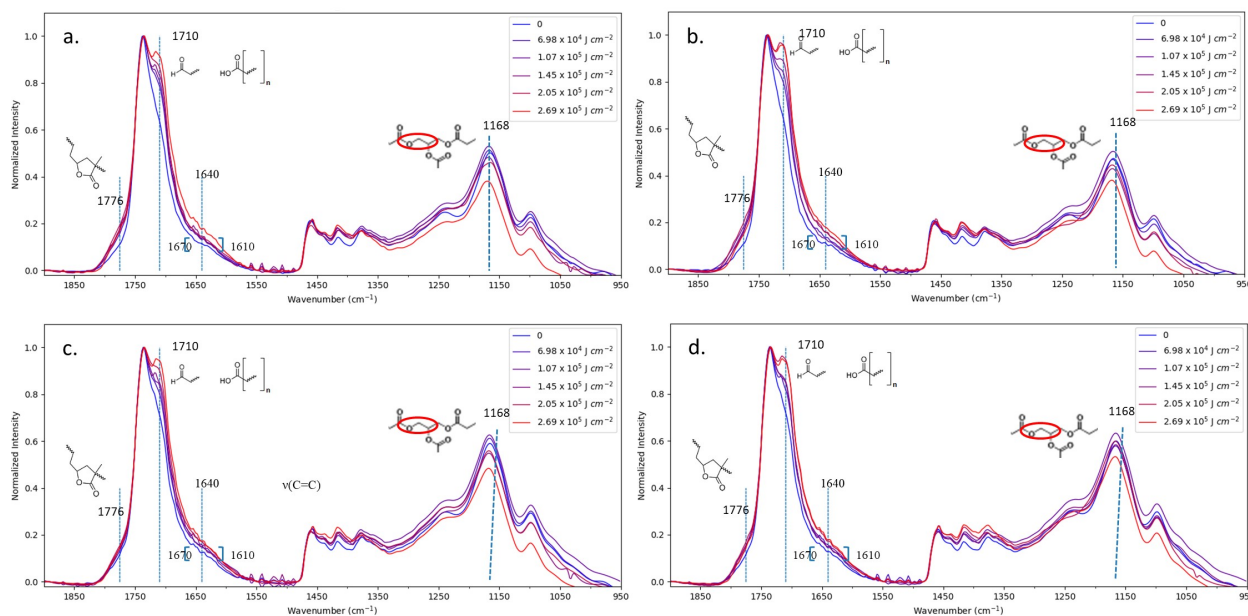


Figure 3.5: Anatase based paint aged in (a) vis, and (b) UV-vis conditions, and rutile based paint aged in (c) vis, and (d) UV-vis conditions. Characteristic markers of degradation are marked with dotted lines and functional groups.

both UV-vis and visible light exposed samples indicating a degradation of the tri-glyceride ester linkage bond as a function of exposure. Dark aged samples showed minimal changes over the same aging period as seen in the SI (Figure .2).

The rate of degradation can be evaluated by plotting the intensity of the 1710 cm^{-1} peak and $1670\text{-}1610\text{ cm}^{-1}$ region (as measured at 1640 cm^{-1}). These plots, shown in Figure 3.6a-d, clearly demonstrate that both rutile and anatase TiO_2 based pigments facilitate oil degradation in both the visible and UV-vis light conditions.

There are two noteworthy differences between the spectral trends for linseed oil only samples and those with TiO_2 . First, TiO_2 based paints demonstrated a higher initial peak intensity for both spectral features compared to linseed oil. This may indicate adsorption of fatty acids to the TiO_2 surface prior to light exposure. Second, the rate of degradation, as measured by the change in the 1710 cm^{-1} free fatty acid peak intensity, is higher for TiO_2 pigmented samples than pure linseed oil for both light aging conditions (Figure 3.6a and c). Additionally, the peaks formed more rapidly

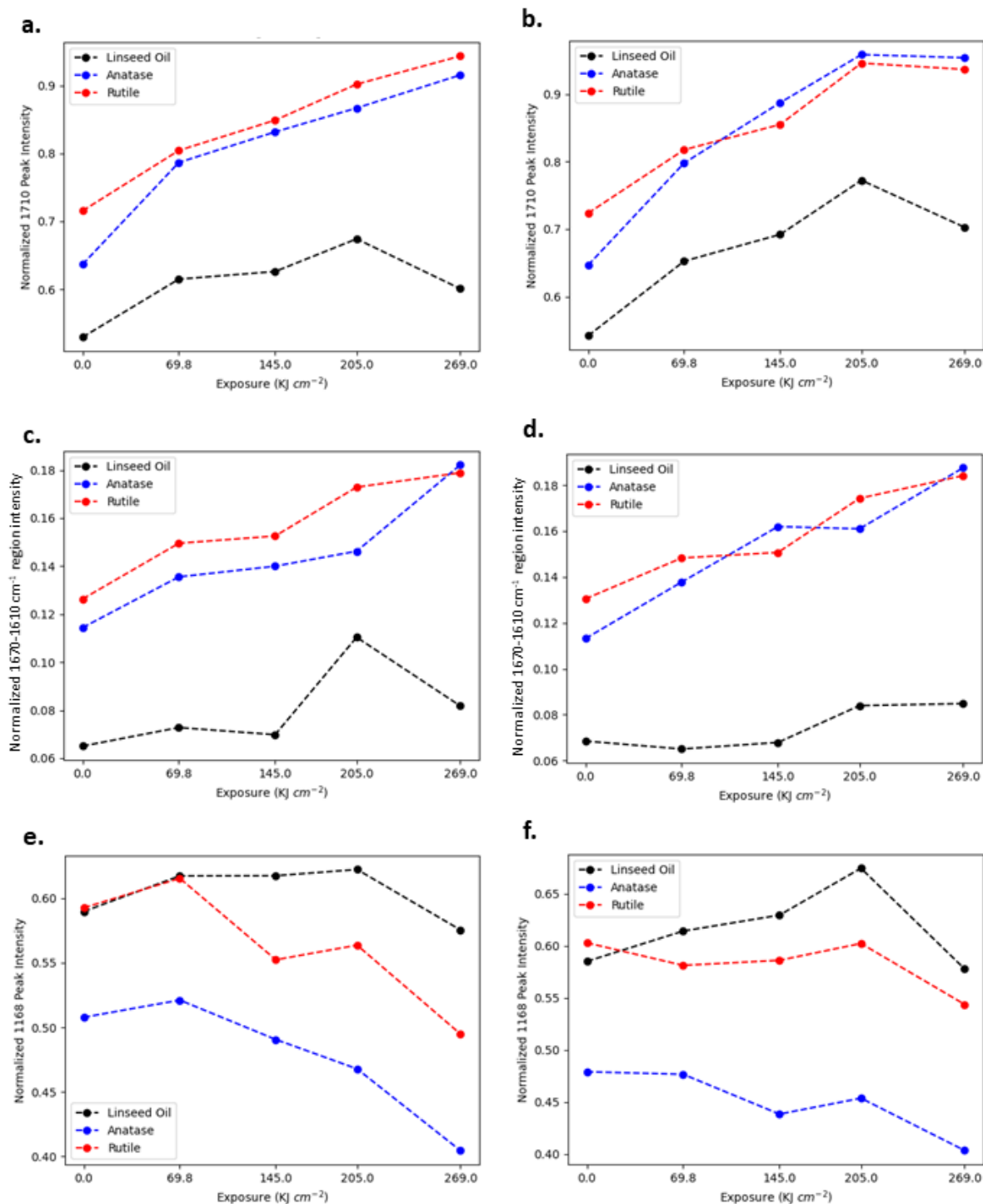


Figure 3.6: Change in the intensity for the 1710 cm⁻¹ peak, the 1670-1610 cm⁻¹ region measured at 1640 cm⁻¹, and the 1168 cm⁻¹ peak in (a, c, e) visible light and in (b, d, f) UV-vis light. The considered bands are normalized to the 1736 cm⁻¹ ester peak.

in UV-vis exposed samples shown in Figure 3.6b, resulting in a steeper slope when fitted with a linear regression than Figure 3.6a. Linseed oil had approximately double the slope under UV-vis light (Figure 3.6b) compared to visible (Figure 3.6a). Anatase's slope showed an increase of about 1.2 times from visible exposure to UV-vis exposure. Interestingly, rutile shows nearly identical slopes under visible exposure and UV-vis exposure according to the linear regression, indicating that the UV component of the light does not have a strong effect on the formation of these free fatty acids by rutile.

The spectral region from $1670\text{-}1610\text{ cm}^{-1}$ as seen in Figure 3.6c and d exhibits similar trends. Both anatase and rutile based paints show strong increases in intensity for this region as a function of exposure of both visible (Figure 3.6c) and UV-vis light (Figure 3.6d) similar to the 1710 cm^{-1} peak. As a contrast to the 1710 cm^{-1} peak, the slope of the 1640 cm^{-1} peak height versus exposure for both UV-vis exposed TiO_2 based paints is approximately double that of the visibly exposed samples indicating that UV-vis light plays a larger role in the generation of the degradation products attributed to this region. Linseed oil only samples show a moderate increase followed by a decrease in this $1670\text{-}1610\text{ cm}^{-1}$ region for visibly aged samples (Figure 3.6c) and a slight increase for UV-vis aged samples (Figure 3.6d). Small sinusoidal noise in the FT-IR spectra for the 205 kJ cm^{-2} and 269 kJ cm^{-2} exposed linseed oil samples made the peak heights difficult to measure resulting in a more variable linear regression between samples. As a result, we are treating the trend as linear. BaSO_4 based samples, showed no increase in intensity for the $1670\text{-}1610\text{ cm}^{-1}$ region and slight increase in 1710 cm^{-1} peak height in UV-vis illuminated samples as can be seen in the SI (Figure .1). We have observed free fatty acid formation as evidenced by the slight increase in 1710 cm^{-1} peak intensity for linseed oil in Figure 3.6b, and the increase in the same peak for UV-vis illuminated BaSO_4 samples in Figure .1. This suggests that direct photolysis of linseed oil also facilitates the formation of free fatty acids. However, the more than two fold difference in rate of formation of the free fatty acids and the formation of conjugated dienes distinguishes TiO_2 facilitated degradation from direct photolysis of linseed oil.

The region corresponding to the tri-glyceride ester linkages ($1300 - 1000 \text{ cm}^{-1}$) shows different behavior for each condition as seen in Figure 3.6. Interpreting the peaks in this region is difficult because this region contains peaks corresponding to multiple structures and competing processes; however, some clear trends appear. Both anatase and rutile TiO_2 pigmented samples show a decrease in the intensity of the 1168 cm^{-1} peak over exposure to both visible (Figure 3.6e) and UV-vis light (Figure 3.6f). Interestingly, the change in peak intensity is greater for both TiO_2 polymorphs samples illuminated with visible light. The rate of diminishment of this band is similar for anatase and rutile based paints, indicating that, especially under visible illumination where the slope is greatest, the primary driver of degradation is not the inherent activity of the TiO_2 polymorph, but instead some other mechanism such as the formation of a charge transfer complex as will be discussed in Chapter 4. Pure linseed oil shows no significant change in visible light as shown in Figure 3.6e. Under UV-vis illumination pure linseed oil shows slight peak growth then rapid decline. These data show that the scission of this linkage is unique to TiO_2 facilitated degradation.

Under all conditions, when observed optically, the surface of the aged paint was relatively smooth with no visible cracks, craters, or particles. However, when observed under SEM, both anatase and rutile TiO_2 oil samples, aged under both UV-vis and visible light, show signs of degradation. A significant oil loss is visible as small clusters of pigment (Figure 3.7a.) in the UV-vis light aged anatase samples characterized also by large cracks and voids in agreement with previously reported results. [42] Notably we also observed in rutile based samples (Figure 3.7b), larger pigment particle clusters and small voids when exposed to UV-vis light. This is consistent with the FT-IR results which show that rutile based paint shows degradation similar to anatase. SEM images also demonstrate that visible light influences the surface of the paint independently from the TiO_2 polymorph showing for both anatase and rutile oil paints early signs of oil loss in visibly illuminated samples. Due to the lack of particles, linseed oil films were difficult to observe under electron microscopy. Instead, paints pigmented with the photocatalytically inert BaSO_4 (Figure 3.7c) show unchanged

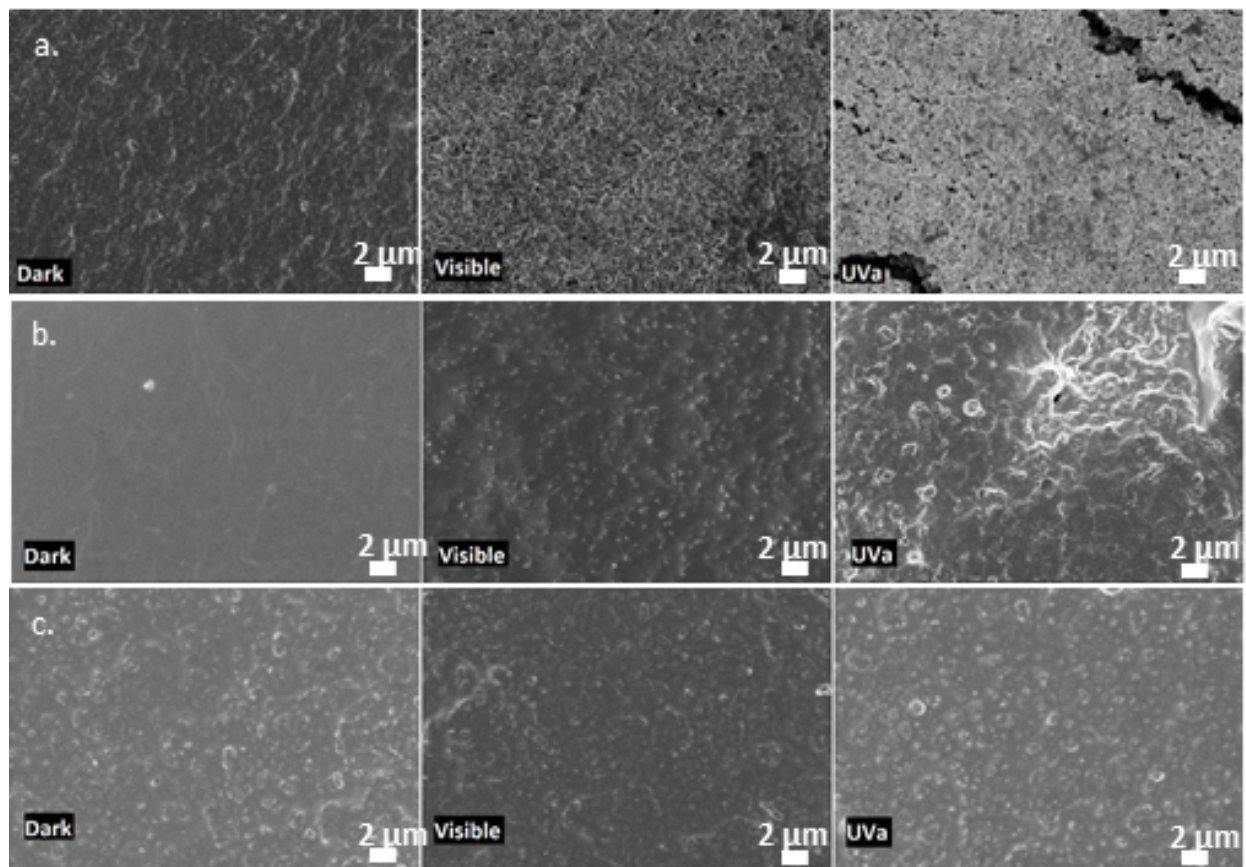


Figure 3.7: SEM images at 36 days aged in various lighting conditions for (a) anatase, (b) rutile, and (c) BaSO₄ oil paints.

surfaces with few signs of degradation and no clear effects due to differing lighting conditions indicating that direct photolysis of linseed oil does not account for the oil degradation and loss seen in TiO₂ pigmented samples.

During a previous experiment, the ambient lab humidity dropped below 30% RH. By comparing the changes in the FT-IR spectra over the course of the UV light aging of linseed oil and TiO₂ based paints we can see how the lowered humidity drastically reduced the photocatalytic degradation of the oil binder driven by TiO₂. In both Figure 3.8 (a) for linseed oil at 50% RH and (b) for anatase based paint at 30% RH, we can see the formation of small shoulders at 1776 cm⁻¹ and 1710 cm⁻¹ corresponding to γ -lactones and free fatty acids/aldehydes respectively. There is

increase with exposure of a shoulder around 1670 cm^{-1} in the anatase based sample, perhaps an indication of TiO_2 mediated degradation. The relationship between TiO_2 activity and humidity is not surprising. As discussed in Chapter 1 of this thesis, water is a reactant in the TiO_2 mediated creation of reactive oxygen species. Water also facilitates hydrolysis of the oil leading to free fatty acids, so a low RH reduces additional modes of linseed oil degradation. However, because art objects contain such complex mixtures and combinations of materials, removing all humidity may be more damaging to the painting. The data collected in this study does not show a humidity “cutoff” for TiO_2 activity, but it does suggest that visible light and moderate ($\sim 30\%$ RH) may significantly limit TiO_2 facilitated degradation of linseed oil.

3.4 Discussion

Previous results have shown that UV light degrades both linseed oil alone, and paint films containing anatase TiO_2 . [81,84–86] This research refines the understanding of photocatalytic degradation of paint pigments presented in previous literature in a number of ways. First, we have demonstrated that anatase based paint films degrade not only under UV-vis illumination, but also under the visible light conditions employed in this study. Second, although the activity of anatase based paint under UV illumination has been well documented, the more common and more modern rutile pigment is believed to be photocatalytically inactive. [42,67] We have presented evidence of the photocatalytic activity of rutile based paint films in both visible and UV light under our experimental conditions that revises this thinking. Third, by investigating computationally the complex interactions between the pigment and binder we simulate a possible mechanism of the visible light activity observed experimentally in anatase based paints and suggest that a similar mechanism may explain the visible light activity seen in rutile based paints. Fourth, the lighting conditions used in this study have a much lower intensity than the conditions used in previous studies. [5,41,42,66] These milder lighting conditions allowed us to probe, in greater detail, the degradation of linseed

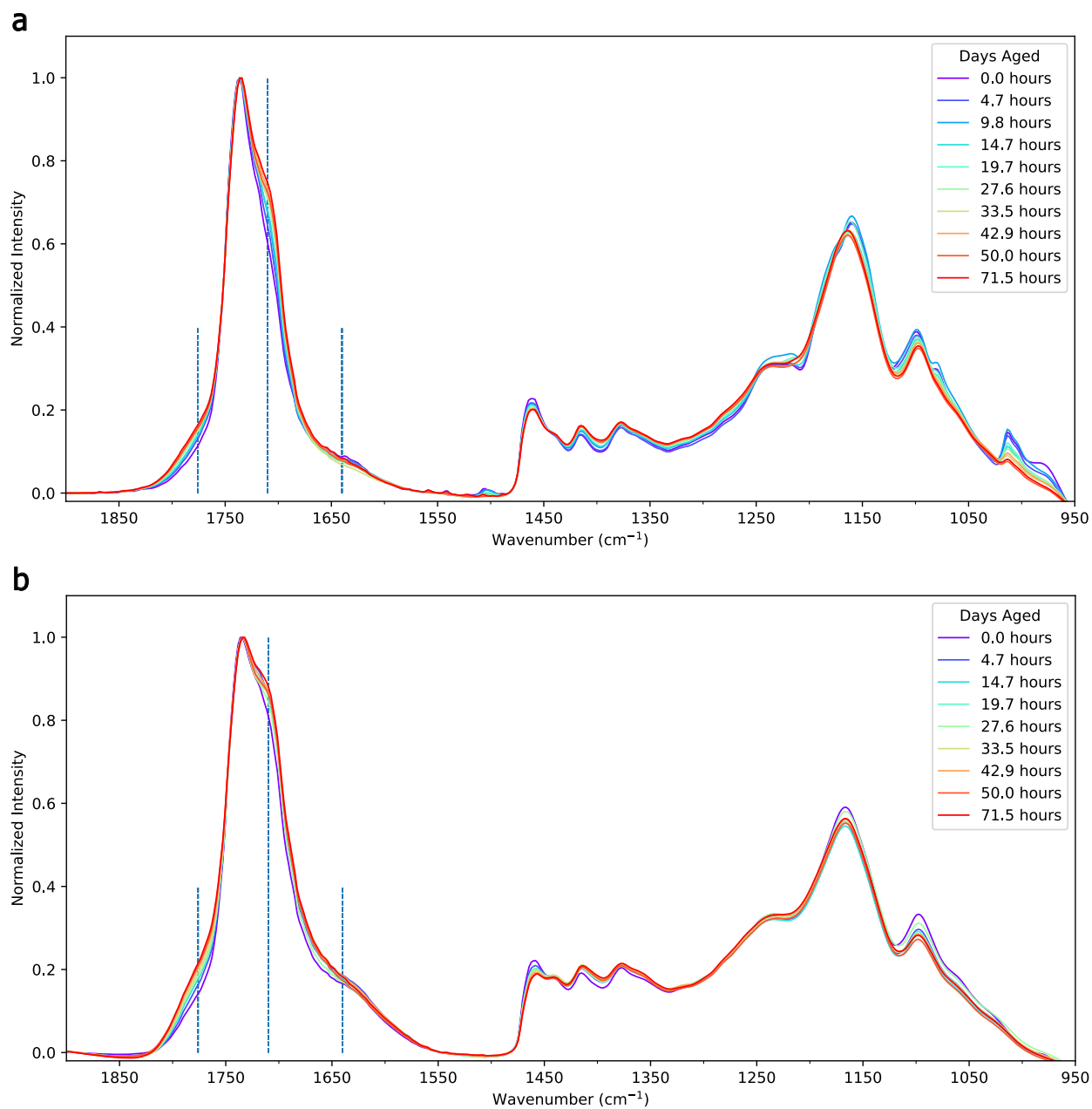


Figure 3.8: FT-IR spectra of samples aged in < 30 % RH environment under UV light with (a) linseed oil only and (b) anatase TiO₂

oil in the presence of TiO₂ by diminishing the contribution of direct photolysis allowing the effect of TiO₂ to dominate, and by slowing the rates of reactions to allow us to follow initial photochemical transformations. As a result, we have gained more insight into the kinds of reactions that may unfold over long exposure times to low intensity interior lighting.

Our experiments explicitly probed photochemical reactions under visible light, whereas this has not been considered previously in the context of TiO₂ paint photocatalysis. The activity we observed for TiO₂ (both anatase and rutile) based paints under visible light is noteworthy for several reasons. The ΔE_{BG} for anatase is 3.2 eV, which corresponds to UV light of wavelengths less than 385 nm. [8] The mechanism of TiO₂ facilitated paint degradation published by Van Driel *et al.* and others suggest that anatase would not be active in visible light due to a lack of ultra-band gap illumination. [26, 41, 87–89] The same proposed mechanism suggests that although rutile may absorb visible light below 410 nm, rutile's photocatalytic activity is less than anatase's due to a lower degree of band bending at the surface resulting in higher rate of charge recombination. [23] However, the experimental evidence presented in this study indicates that the two components that are individually inactive in visible light become active when combined with linseed oil suggesting that other mechanisms are at play.

In addition to the visible light activity of TiO₂ based paints, it was also interesting that rutile, one of the most common white pigments today, exhibited rates of degradation similar to anatase. [7] The lower photo-reactivity of rutile is attributed to higher charge recombination rates relative to anatase. [66] This has led many conservators and scientists to dismiss rutile based paints as degradation risks. [5, 41, 42, 76] However, an interaction between rutile and oil fragments, similar to the one shown in Scheme 1a, may sensitize it to visible light by forming a charge transfer complex resulting in similar photocatalytic activity as anatase. Although the interaction of rutile and oil fragments was not investigated computationally in this study, previous results on the interaction of rutile and other carboxylic acids have shown the formation of complexes similar to those demonstrated with anatase in this study. [90] The similarity observed between rutile and anatase's visible and UV-

vis light activity suggests that the sensitization of the TiO_2 may be a dominant factor for both polymorphs.

The difference in illumination conditions between the experiments of this study and previous studies provides another explanation for the photoactivity observed in the rutile based paint. Research has shown that high light intensity accelerates charge recombination. [91] Using a light ($232 \mu\text{W cm}^{-2}$) only 3% as intense as the UVA illumination employed by Morsch *et al.* (8 mW cm^{-2}), we achieved lower recombination rates and slower rates of reaction for both rutile and anatase based paint. [5, 92] These lower recombination rates provide another possible explanation for the increased photocatalytic activity of the rutile pigment compared to previous studies. The lower light intensities, and slower rates of reaction in comparison to other reported work allowed us to observe initial reaction phenomena that was not evident under much stronger radiation conditions. This study implemented a total UV exposure of $0.986 \times 10^3 \text{ J cm}^{-2}$ over 49 days, significantly lower than the total exposure ($7.3 \times 10^3 \text{ J cm}^{-2}$) and even less than the first exposure ($2.1 \times 10^3 \text{ J cm}^{-2}$) in the work by Morsch *et al.* [5] The low amount of total UV exposure used in this study suggests that the chemical and physical changes presented reflect early degradation phenomena that could not be observed in studies using much greater illumination flux. The lower intensity light also resulted in less direct photolysis of linseed oil. This allowed the distinction to be made between TiO_2 facilitated degradation of linseed oil and direct photolysis.

Previous studies have discussed that it is difficult to distinguish between hydrolysis and photocatalytic degradation through FT-IR methods alone. [5] However, the presence of unique spectral changes in TiO_2 containing samples reveals a spectroscopic differentiation between hydrolysis and photocatalytic degradation. The FT-IR differences between photo-oxidized linseed oil and TiO_2 facilitated degradation of linseed oil are summarized in Table 3.1. The clearest difference between TiO_2 facilitated degradation and direct photolysis of linseed oil is evident by examining the peak associated with the tri-glyceride ester linkage. The decrease in peak intensity indicates that, unlike direct photolysis, TiO_2 facilitated degradation breaks the C-C(O)-O ester linkage. This is a

unique spectral feature that allows for the detection of TiO₂ facilitated degradation through FT-IR methods.

Anatase TiO₂ facilitated degradation is often characterized by a “chalked” surface. [93, 94] Previous studies have attributed this description to an increase in surface roughness associated with loss of oil and surfacing of pigment particles. [5, 39, 42] The SEM micrographs in this study provide more information to confirm the phenomena of oil loss and pitting. Additionally, the SEM micrographs show surface degradation of rutile based pigments, confirming its activity in both visible and UV-vis light. The presence of large cracks in the micrographs of anatase based paint suggests that microcracking of the paint may occur before large scale degradation is visible. Finally, the SEM micrographs were taken from samples with total UV-vis exposure of $7.50 \times 10^2 \text{ J cm}^{-2}$. This is about 75% light exposure (750 J cm^{-2} vs 1050 J cm^{-2}) than has been previously studied for TiO₂ activity, indicating that damage from TiO₂ facilitated degradation occurs earlier than others have shown. [42] For these reasons, both anatase and rutile TiO₂ based pigments should be considered active in low UV and visible light environments due to surface interactions with fatty acid oil fragments. These results show that degradation of the paint film and loss of binding media may be occurring at early stages before chalking is visible to the naked eye.

3.5 Conclusion

We performed artificial aging of TiO₂ and linseed oil based systems to investigate the mechanisms of degradation under visible and UV light. We used FT-IR to identify characteristic markers of degradation: formation of free fatty acids visible at 1710 cm^{-1} , an increase in the spectral region $1670 - 1610 \text{ cm}^{-1}$ associated with $\nu(\text{C}=\text{C})$ of conjugated dienes and changes in the tri-glyceride ester linkage region centered at 1168 cm^{-1} . Both anatase and rutile TiO₂ based samples showed these characteristic markers of degradation under the visible and UV-vis light conditions used in these experiments. By measuring the change in intensity of characteristic degradation FT-IR peaks,

Table 3.1: Assignment of the main spectral changes observed in linseed oil aging and summary of the observed changes.

Functional Group	Peak position	Assignment	Observed Changes
C=O stretch	1776	Peracids, perester, γ -lactones, and anhydrides	Small increase in visible and UV light and all pigments
	1736	Ester	
	1720-1710	saturated ketones, COOH acid, and aldehydes	Minimal increase in unpigmented and BaSO ₄ samples in UV and visible light; large increase in TiO ₂ containing samples in UV and visible light; no changes in dark
	1640	ν (C=C) in conjugated ketones	Small increase in linseed oil only samples in visible and UV light; strong increase in anatase and rutile pigmented samples in visible and UV light
C=C	1100-1210	ν (C-C-O-) alcohols and hydroperoxides	No change in linseed oil only samples in visible and UV light; Decrease in anatase and rutile pigmented samples in visible and UV light.
ν (C-O) Triglyceride ester linkage	1178	-C(O)-OCH ₂ -	
	1168 (1170 after aging)	ν (C-O) in triglyceride ester linkage + ν as (C-O) of C-C(O)-O of higher aliphatic esters	Decrease in TiO ₂ containing samples in UV and visible light. No change in linseed oil only samples

we showed that anatase and rutile based paints facilitate similar rates of linseed oil degradation. The surface alteration of the paint film was monitored by SEM, highlighting surfacing of pigment particles due to oil loss and confirming the activity of rutile based paints. Through this combination of methods, we have developed a better understanding of the risk that both anatase and rutile TiO_2 containing paints face under low intensity illumination conditions.

Chapter 4

Computational Modeling of Fatty Acids' Interaction with Anatase TiO₂

4.1 Introduction and Background

It is difficult to experimentally probe the effect mixtures have on the overall activity of the resulting paint as every combination must be done. Instead, computation modeling simulations can effectively and in many cases more quickly lend insight into the structural, chemical, and electronic effect of these mixtures. These methods have been employed extensively in other branches of materials science and chemistry such as dye sensitization of TiO₂ for solar cell applications. [95] However, they have only recently begun to be applied to cultural heritage, in part because to the scarce knowledge of the constituent's materials composition. [96]

These computational methods have been employed to study alizarin, which is both an artists's dye and a common dye used in solar cells. [73] Previous research in solar cell development revealed that through the addition of dyes like alizarin, TiO₂ can be sensitized to absorb visible light extending the activity into higher wavelength regions of light. The fundamental concept involves a lower band-gap material such as an organic dye, absorbing light that could not be absorbed by TiO₂ alone, and then injecting the excited electron into the conduction band of the semiconductor as can be visualized in Figure 4.1b. [97–99] Larger band gap materials may also facilitate electron injection similar to as outlined in Figure 4.1c. Once the electron is in the conduction band of the TiO₂, radical formation reactions can take place creating reactive oxygen species and degradation as described elsewhere in this thesis. We propose that the interaction between oil molecules ever-present in the paint mixture and anatase TiO₂ can enhance the photocatalytic activity of the anatase pigment and extend its response to visible light. We also present a novel mode of degradation due

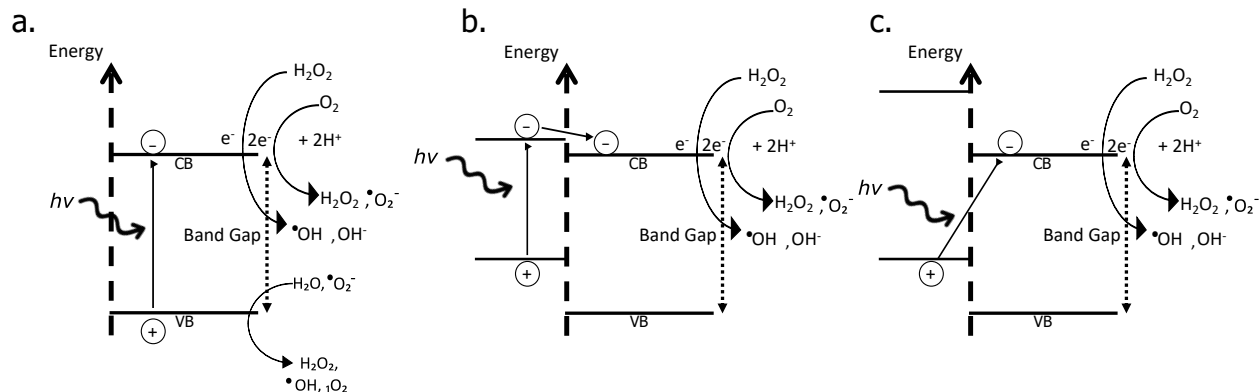


Figure 4.1: Processes of formation of reactive oxygen species in (a) bare photocatalyst such as TiO_2 , (b) a photocatalyst sensitized by a material whose LUMO lies close to the photocatalysts conduction band, and (c) a photocatalyst sensitized by a material whose LUMO lies far above the photocatalysts conduction band.

to the interaction of the fatty acids of linseed oil and anatase TiO_2 .

To model the structure, both chemical and electronic, of materials of interest, computational methods stem from the desire to solve the Schrödinger equation (4.1). For any system greater than hydrogen, directly solving the Schrödinger equation is impossible. Instead, computational scientists have developed *ab-initio* methods which aim to solve the Schrödinger equation by approximating the wavefunction or a set of wavefunctions. One of these approximations, the Born-Oppenheimer approximation, neglects the interaction of the electrons on the nucleus, allowing the motion of electrons and nuclei to be separated. The resulting many electron time independent Schrödinger equation shown in equation 4.2 depends only parametrically on the nuclear geometry and the system size. This equation can be solved computationally via many methods, all of which become computationally expensive at large system sizes due to the electron-electron interaction term.

$$\hat{H}\Psi_n = E_n\Psi_n \quad (4.1)$$

$$H_{el}\Psi_{el} = \left[-\sum_{i=1}^N \frac{\hbar^2}{2m} \nabla_i^2 - \sum_{i=1}^N \sum_{\alpha=1}^M \frac{Z_\alpha}{r_{i\alpha}} + \sum_{i=1}^N \sum_{j>i}^N \frac{1}{r_{ij}} \right] \Psi_{el} = E_{el}\Psi_{el}; \quad (4.2)$$

Many *ab-initio* methods attempt to better solve this equation. DFT simplifies the computation by replacing the electron-electron interaction with electron density. The idea is to express the total energy of a system as a function of its total electron density decreasing the computational expense of large systems. Hohenberg and Kohn showed that the ground state density alone is sufficient to determine every observable quantity of a stationary quantum mechanical system and the exact ground state density of a system can be found by minimizing the energy functional. [100]

The use of electron spin density simplified the model by reducing the coordinates to one spin coordinate s_1 and three Cartesian coordinates regardless of the size of the system. Whereas *ab-initio* based systems scale as n^3 or $n^2 \times \ln(n)$, where n is the number of particles.

Instead, an estimate is created by a linear combination of equations known as a basis set. Once calculated, this electron density can then be applied to a modified and simplified version of the Schrödinger equation revealing that the complete ground state energy can be determined from the complete ground state electron density. Therefore that the ground state energy is said to be a functional of the ground state electron density. When the ground state energy is expanded into its components it becomes clear that they too are functionals of the ground state electron density.

$$E_0[\rho_0] = T[\rho_0] + E_{ee}[\rho_0] + E_{Ne}[\rho_0] \quad (4.3)$$

Kohn and Sham use these conclusions to represent the ground state density of an interacting particle system as the ground state density of an auxiliary non-interacting system. They defined an effective external potential which would generate the same electron density as interacting particles. [101]

The total energy of such a system can be expressed as:

$$E[\rho] = T_s[\rho] + \int [V_{ne}\hat{(r)} + \hat{U}_{cl}(r)]\rho(r)dr + E_{xc}[\rho] \quad (4.4)$$

Where T_s is the kinetic energy of a similar system without electron-electron interaction, V_{ne} is the

nuclear potential, and U_{cl} is classical Coulombic electron interaction. E_{xc} is called the exchange-correlation energy. It includes all unaccounted for interactions. Under the assumption that these particles are non-interacting fermions, the Kohn-Sham wavefunction (ψ_i) of a system with energy stated in eq. 4.4 can be found from the solution of:

$$\left(-\frac{\hbar^2}{2m}\nabla^2 + v_{eff}(r) \right) \psi_i(r) = \epsilon_i \psi_i(r) \quad (4.5)$$

Where $v_{eff}(r)$ is the effective external potential and depends on our choice for E_{xc} . The approach is aimed at minimizing the total energy of the system. However, since the exact form of E_{xc} , and therefore v_{eff} , can not be known, an iterative approach must be used. To facilitate the iterative solution, a guess is made for the electronic wavefunction ψ_i . In many approaches, these wavefunctions are localized, but when systems grow beyond the capability of localized basis sets and functionals, another basis set is used. The difficult to calculate Coulombic term is replaced with pseudopotentials, which account for core shell electrons by creating a pseudo nuclear charge. The pseudo nuclear charge behaves as a homogeneous electron gas and the exact eigenfunctions are plane waves which form this extended basis set. These plane wave basis sets allowed Bloch write the single particle Schrödinger equation with a periodic potential as [102]:

$$\psi_k(r) = e^{ikr} u_k(r) \quad (4.6)$$

where k is the wave vector of the plane wave. This can be combined with eq. 4.5 to extend the Kohn-Sham approach to periodic systems, where the infinite number of electronic states has been reduced to finite eigenstates at each k vector (or k-point). There is an infinite number of k-points, so we must choose a specific mesh to accurately sample the Brillouin zone.

In many crystalline calculations, the core electrons play a very small role in the physical and chemical properties. As such, the nuclear potential can be replaced with a pseudopotential. These

can present their own challenges, for example, elements with 2p and 3d valence electrons are difficult to treat with pseudopotentials because their valence electrons are strongly localized in the core region. A new class of pseudopotentials called Vanderbilt ultrasoft pseudopotentials, were introduced to tackle this problem. [103] These reduced the requirement for the full valence wave function to be represented by plane waves. Instead, only a small portion of the wavefunction is represented, reducing computation cost. This approach does present some drawbacks, mostly that new terms must be added and calculated. Even with these additional terms, there is a reduction in computational cost.

DFT methods can only study ground state energies, so in order to extend the calculation to excited state, impose external electric or magnetic fields, or simulate photo-absorption spectra, a time dependent component must be added. Although the mathematics of this approach become more complex, the underlying principles remain intact. This is because TD-DFT uses only the properties of the ground state to describe excited state energies, avoiding the need to apply DFT to excited states. [104]

In practicality, these equations are solved with the variation principle to minimize the energy eigenstates by a self consistent theoretical process. The computation time and accuracy can be optimized with effective choices of basis set, functional, and pseudopotentials. The initial basis set can be easily selected based on the size and geometry of the simulation. In small scale molecular or cluster models a Gaussian style basis set can accurately and effectively model a system. However, when calculating a large scale or bulk model, it is better to use a plane wave basis set. Additionally, periodic boundary conditions can then be applied to effectively extend the calculation in any or all of the three dimensions without sacrificing computational accuracy or time.

4.1.1 Role of Paint Materials

The interactions between the components of paint are difficult to elucidate through experimental means, as isolating a single component or interaction is difficult or impossible. Computation methods, on the other hand, can directly model the interactions of known components and compute the resulting structural and electronic properties. This has been applied previously to model complex interactions of materials used in cultural heritage objects such as indigo/palygorskyte complex, and the organic/inorganic interactions present in lake pigments like Weld lake. [96] Another material, alizarin, deriving from the plant *Rubia tinctorum L.*, commonly known as madder, was used in red dyes and paints. Alizarin is often found in a precipitated form with metal salts known as madder lake. Due to the light absorption properties of alizarin, it has been a popular topic of research in the field of Dye-Sensitized Solar Cells. [105–109] This research can provide assistance for understanding sensitization of pigments in cultural heritage objects.

4.2 Computational Details and Models

We began by modeling a close relative of alizarin, alizarin carmine (also commonly known as Alizarin Red S), shown in Figure 4.2. It has similar in structure to alizarin with the addition of a sulfonic acid (SO_3Na) group on the 2 carbon. The bond angles and bond lengths were optimized with Gaussian09 using DFT and the time dependent extension (TD-DFT) for individual molecular simulations. When the anatase slab was added, Quantum Espresso (QE) was used. For the individual molecular simulations, the Gaussian09 (G09) package was implemented using the B3LYP exchange correlation functional and the 6-31G(d,p) basis set. Solvent effects were investigated using a polarizable continuum model (PCM) in Gaussian09 applied to an already optimized geometry using the eigenvalue-following algorithm inherent to G09. Information about the electronic energy surfaces of the HOMO and LUMO states were taken from single point calculations of an

geometrically optimized structure without solvent effects. The absorption peaks were calculated using time-dependent DFT in the Gaussian09 code using the same functionals and basis set as the time-independent calculations. The absorption spectra was then calculated using in house code using an addition of gaussian curves generated for each absorption peak. For calculations involving TiO_2 , QE was used to take advantage of the periodic boundary conditions in the plane wave pw.x package and Vanderbilt ultrasoft potentials with Perdew-Burke-Ernzerhof exchange correlation functionals. An already created slab of 192 atoms of anatase structure oriented with a +Z facing (101) boundary was optimized using QE's fixed cell structural optimization code. This code uses the Broyden-Fletcher-Goldfarb-Shanno (BFGS) algorithm using only the internal microscopic degrees of freedom as cell dimensions are fixed. Additionally, the z coordinate of the cell dimensions was increased beyond the measurements of the slab to simulate a free surface. Single point, self consistent calculations were performed using the Broyden method sampling the Brillouin zone using only the gamma point ($k=0$). In the case of alizarin carmine attached the TiO_2 the initial structure required the implementation of Gaussian smearing due to the metal like electronic appearance of the initial structure. This process of initial self-consistent field calculation followed by structural optimization was repeated for each dye@ TiO_2 combination. Once the optimized structure was achieved, a final self-consistent field calculation was run to allow for the use of QE's post-processing tools, notably, the use of pp.x to plot the contribution of selected wavefunctions to the charge density. Since the pseudopotentials used were norm-conserving, this correlates to $|\phi^2|$.

The nature of the alizarin carmine's sulfonate group was investigated. The structure was first optimized in vacuum and then solvent effects were introduced for a self-consistent field calculation. Three different possibilities were studied in both solvent, and vacuum conditions. Due to the ionic nature of the sulfonate group, the state of the ionic bond and ionically bonded species is pH dependent. Based on previous literature three possibilities were investigated: (1) the original structure with an ionically bonded sodium ion, (2) a protonated form commonly found in low

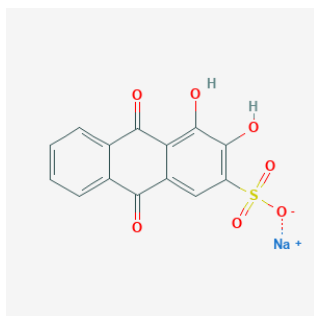


Figure 4.2: Structure of alizarin carmine

pH, or protic solvents, and (3) a de-protonated form found in high pH environments. Due to the differences in chemical composition, it is not useful to compare the formation energy obtained by self-consistent field calculations. Instead, since each form is favorable in certain conditions, the absorption spectra and frontier orbitals were compared for all three variations.

The TiO_2 model was optimized using Quantum Espresso [110] within the generalized gradient approximation (GGA) and the Perdew-Burke-Ernzerhof (PBE) exchange correlation (xc) functional, as reported in Vittadini et al. [111] Electron-ion interactions were modeled using Vanderbilt ultrasoft pseudopotentials. [112] The plane wave basis set cutoff energy was set to 25.0 Ry and the charge density and potential kinetic energy cutoff was set to 200 Ry. Davidson iterative diagonalization with overlap matrix was used with a convergence threshold of 1×10^{-6} and a 0.2 mixing factor. Initial calculations were done on a $(\text{TiO}_2)_{64}$ slab of two TiO_2 (101) layers each with 4 rows of five- and six- coordinated Ti sites. Periodic boundary conditions were applied in the x, y, and z dimensions. To simulate an exposed top surface, the z cell dimension was increased by 10 \AA . Only the Γ -point was considered for all calculations.

The alizarin carmine was attached to the TiO_2 in a bidentate bridging mode similar to that of alizarin using the 3,4 hydroxy groups. The two hydrogens were moved to the surface of the TiO_2 to facilitate the Ti–O–C bond. The resulting complex was modeled using the same computational parameters and procedure as the TiO_2 slab using the GGA functional with the 10 \AA z cell dimension increased from the highest z point with the attached dye. A single point calculation was

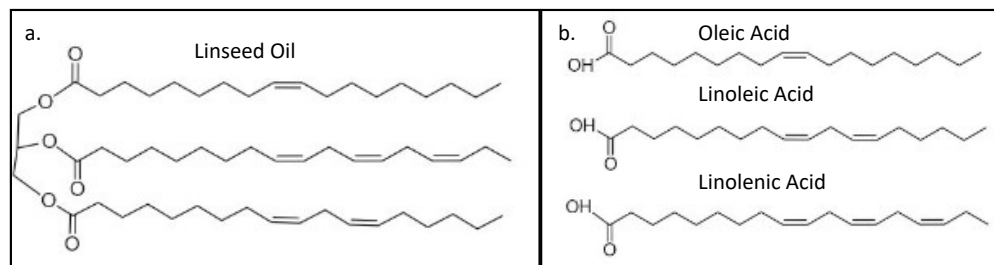


Figure 4.3: Structure of (a) linseed oil and (b) its component fatty acids.

done using Gaussian09 using the same procedure as the component dye without solvent effects. Avogadro software was employed to plot the calculated molecular orbitals by using an iso-density surface cutoff of 0.02. [113] Density of States (DOS) and partial Density of States (pDOS) calculations were performed using Quantum Espresso's DOS.x postprocessing program. A Gaussian broadening of 0.02 Ry and an energy grid step of 0.1 eV were used.

The fatty acids composing linseed oil shown in Figure 4.3 (oleic, linoleic, and linolenic acids) and oleic acid attached to the TiO_2 surface were also modeled computationally. Each component's structure, including bond angles, atomic spacing, and cell dimensions, was optimized and the subsequent electronic properties were analyzed. The oleic, linoleic, and linolenic acids were optimized using Gaussian 09 (G09) [114], the B3LYP [115–117] exchange correlation functional, and the 6-31(d,p) [118] basis set. The electronic structure of the three acids was analyzed in terms of energy and character of the frontier molecular orbitals, to evaluate the possibility of charge transfer between the acid and the TiO_2 (101) slab. Calculations on the oleic acid were repeated using the PBE functional [119] and the 6-31(d,p) [118] basis set to compare with the TiO_2 periodic calculation. The oleic acid was then investigated in a bidentate complex with TiO_2 with the same computational procedure as alizarin carmine.

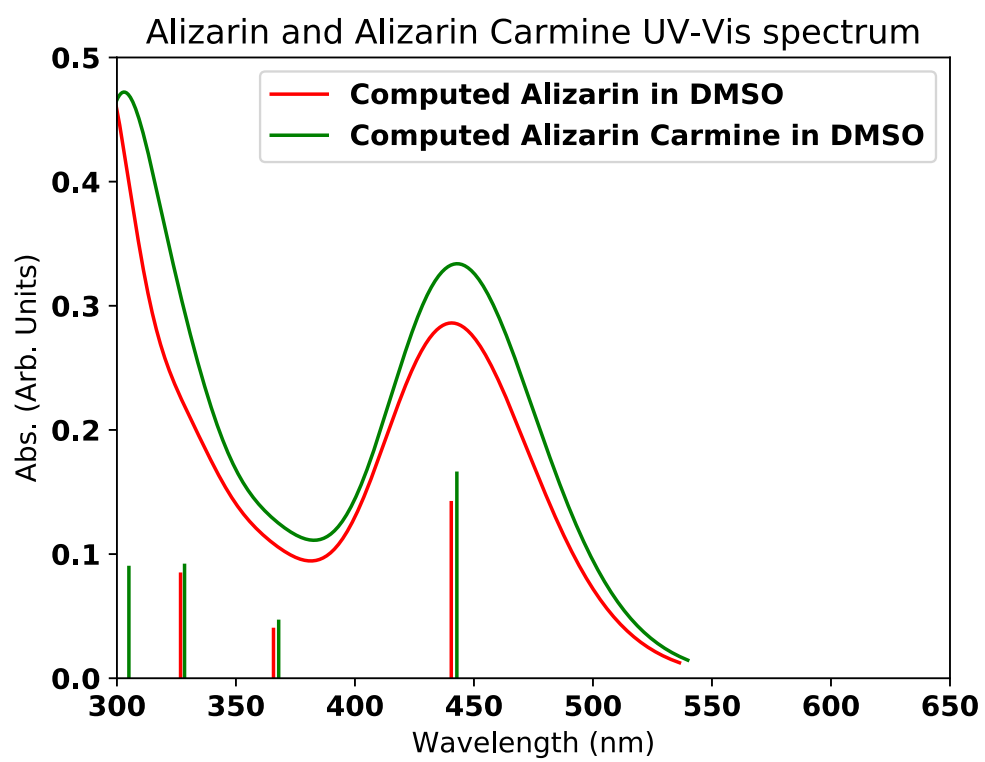


Figure 4.4: Absorption spectra for Alizarin carmine and alizarin

4.3 Computational Results and Discussion

The absorption spectrum was simulated for alizarin carmine in dimethyl sulfoxide (DMSO) and compared with previously calculated results for alizarin as shown in Figure 4.4. The nearly identical absorption spectra suggest that the sulfonate group does not significantly alter the electronic structure compared to base alizarin. The main absorption band is created by a HOMO \rightarrow LUMO transition with an energy of 2.81 eV corresponding to 440 nm. Additionally, the HOMO-1 \rightarrow LUMO transition and HOMO-3 \rightarrow LUMO transitions also contribute to the absorption spectra at the lower wavelengths. These results are in good agreement with experimental results and previously computed results. When the sulfonate group was altered forming protonated and deprotonated forms, the absorption spectra changed significantly. A blue shift was observed for the protonated form, where a red shift was observed for the deprotonated form as can be seen in Figure 4.5.

Next, the frontier orbitals were plotted and shown below. The electron transitions from a more localized state around the OH groups to a completely delocalized state in the excited state. This, although not the most favorable, suggests the possibility for electron transfer if anchored using one or more OH groups. The nature of the sulfonate group, either with a sodium ion, protonated, or di-protonated, does not greatly alter the delocalization, as can be seen in Figure 4.6.

In all cases the electronic delocalization transfers from localized around the sulfonate end of the molecule, to completely delocalized across the entire molecule. This allows for the possibility of electron injection through either a OH group anchoring, similar to alizarin, or a OH group and C=O group anchoring as will be investigated in the future.

Informed by the knowledge from alizarin, the first binding mode tested for alizarin carmine was a bidentate bridging mode again using the hydroxy groups. The resulting structure shown in Figure 4.7 uses the protonated form of the alizarin carmine.

Once this geometry was optimized the resulting electronic energy levels were calculated using self

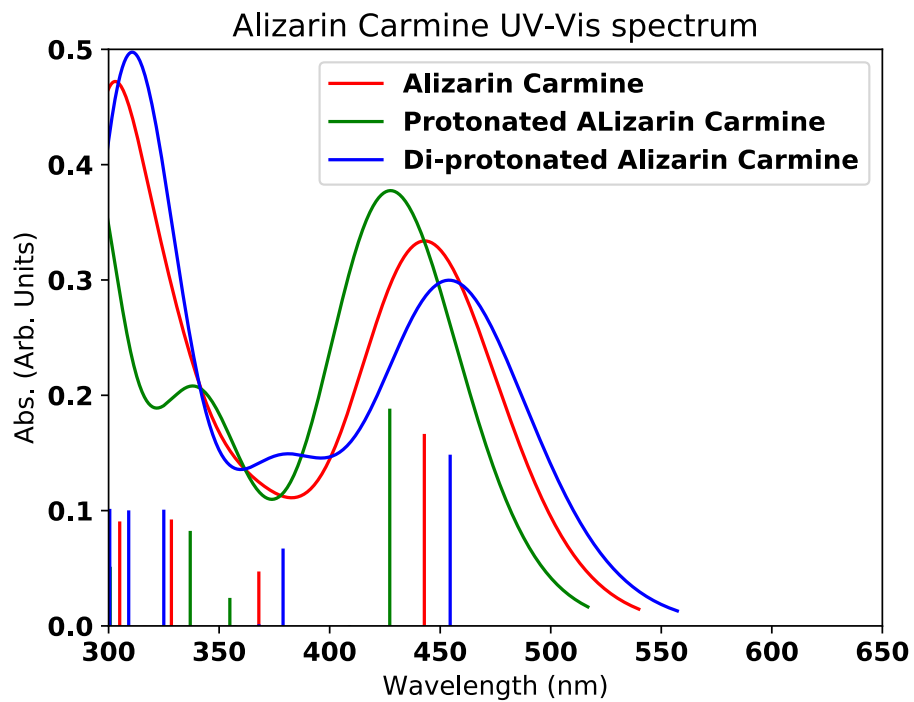


Figure 4.5: Effect of sulfonate composition on absorption spectrum for alizarin carmine

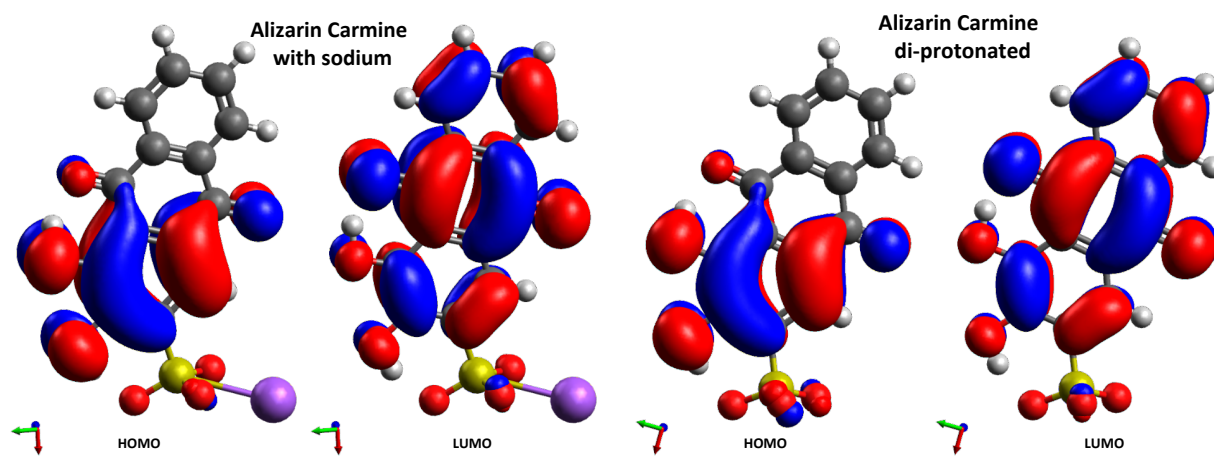


Figure 4.6: Visualization of frontier orbitals for alizarin carmine in different forms.

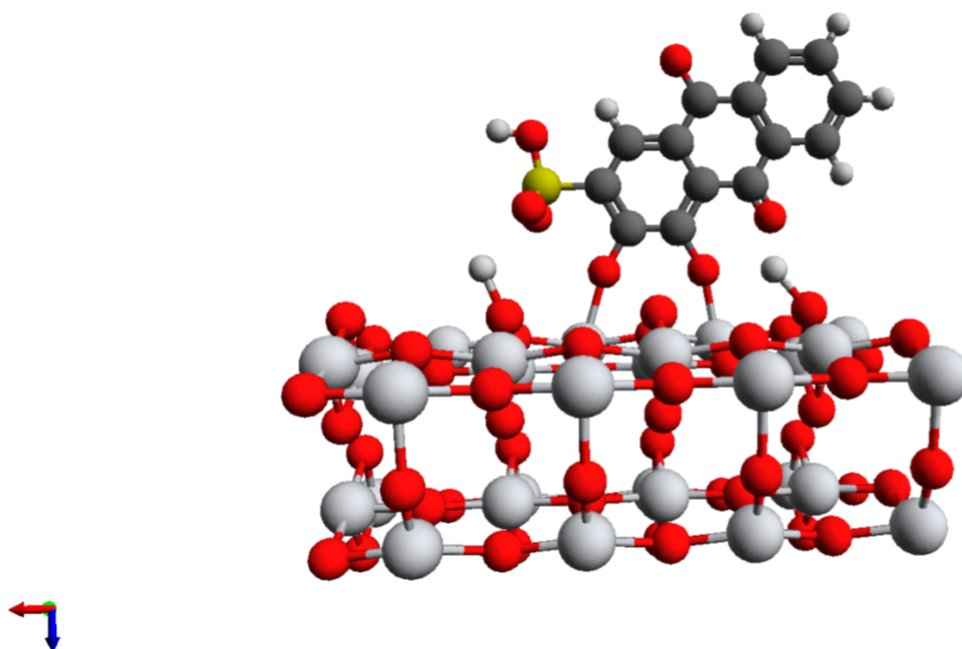


Figure 4.7: Alizarin Carmine attached to TiO_2 slab in a bidentate bridging configuration.

consistent field calculation. The highest occupied level was reported as -1.72 eV and the lowest unoccupied level was reported as -0.51 eV. These levels were then visualized as shown in 4.8. The transfer of electron is clearly from the highest occupied states in the dye to the lowest unoccupied states in the TiO_2 consistent with a charge transfer complex.

The resulting band gap for the bare TiO_2 slab was 1.91 eV. This is underestimated with respect to the experimental value for anatase TiO_2 (3.2 eV), but in line with band gaps computed using GGA exchange-correlation functions. [8, 14] When the alizarin carmine is added, the conduction band of the TiO_2 is shifted by nearly 1.6 eV. This is again in line with a charge transfer complex and would likely result in visible light sensitization.

In Figure 4.10, we report the energies and isodensity plots of the highest occupied molecular orbitals (HOMO) and HOMO-1, and of the lowest unoccupied molecular orbitals (LUMO) and LUMO+1 for oleic, linoleic, and linolenic acids computed with the B3LYP exchange-correlation

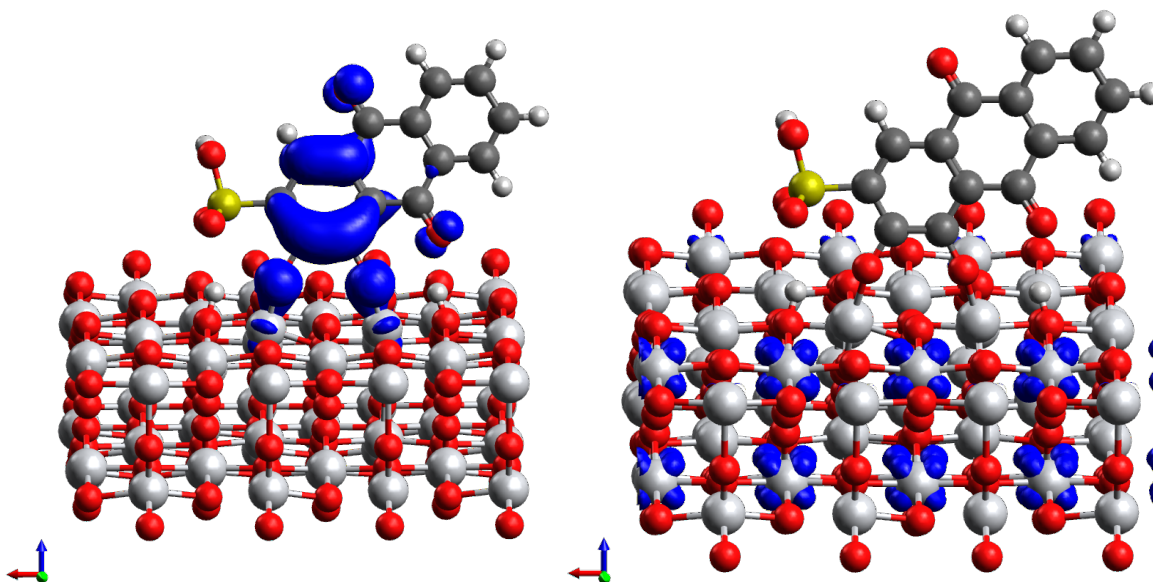


Figure 4.8: Visualized highest occupied electronic states (right) and lowest unoccupied electronic states (left) for the alizarin carmine TiO_2 complex

functional. For all oil fragments, the HOMO is delocalized on the unsaturated bond. For oleic acid, the LUMO is delocalized on the carboxyl group, while for linoleic and linolenic the LUMO is delocalized on the unsaturated bonds. For linoleic and linolenic acids, the LUMO+1 is delocalized around the carboxylic acid group. However, the LUMO energy of the oleic acid is almost isoenergetic with respect to the LUMO+1 energy of linoleic and linolenic acid. In this case, it is more useful to compare the LUMO of oleic acid with the LUMO+1 of the other two component acids. The energy levels of the HOMOs for the three linseed oil components are within ~ 1 eV of each other.

The energy levels of the HOMOs and LUMOs for calculations of both B3LYP and PBE functionals for oleic acid are summarized in Table 4.1. The PBE functional underestimates the HOMO-LUMO energy gap for oleic acid as expected. However, both PBE and B3LYP HOMO-LUMO gaps for all the fatty acids correspond to deep UV light.

Oleic acid was chosen to model the interaction between TiO_2 and the linseed oil as it is a likely

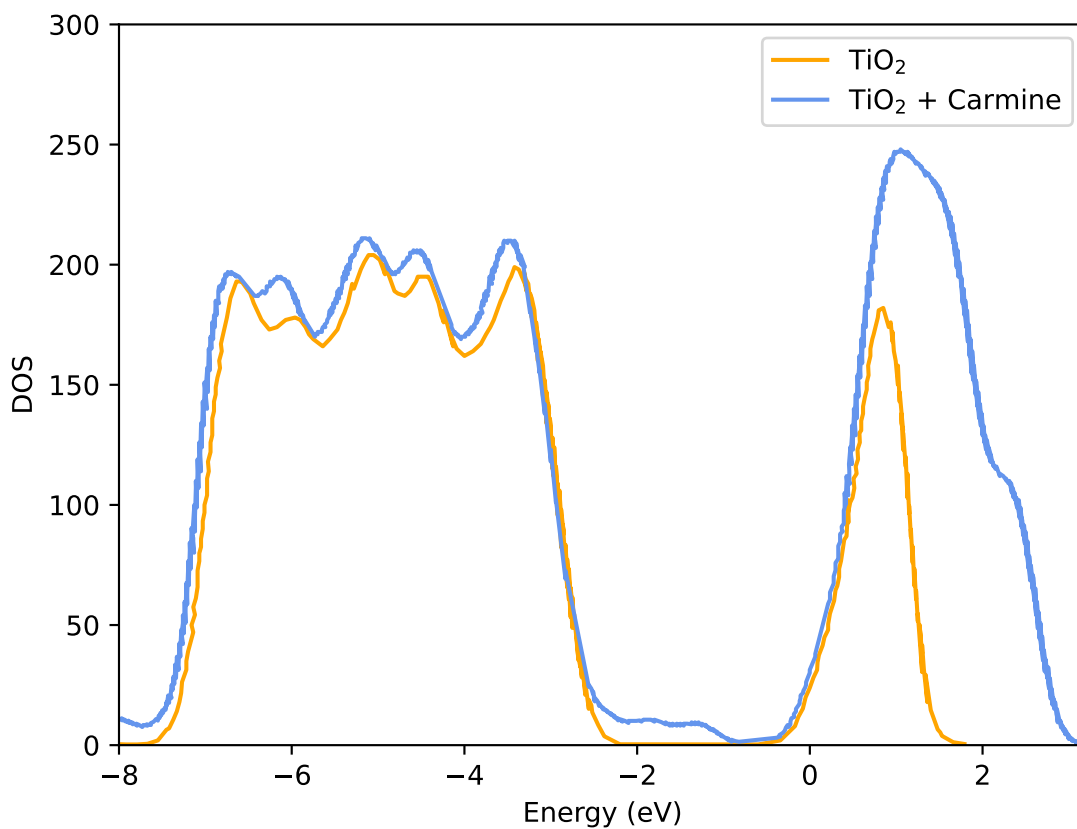


Figure 4.9: Density of States for both bare anatase TiO_2 slab and the same slab with alizarin carmine attached in a bidentate bridging mode

Table 4.1: Frontier energy levels and HOMO-LUMO gap for linseed oil component acids calculated with B3LYP and PBE functionals.

Molecule	Functional	HOMO (eV)	LUMO (eV)	$\Delta E_{\text{H-L}}$
Oleic Acid	B3LYP	-6.37	0.34	6.71
Oleic Acid	PBE	-5.45	-0.64	4.81
Linoleic Acid	B3LYP	-5.67	-0.34	5.33
Linolenic Acid	B3LYP	-5.30	-0.97	4.33

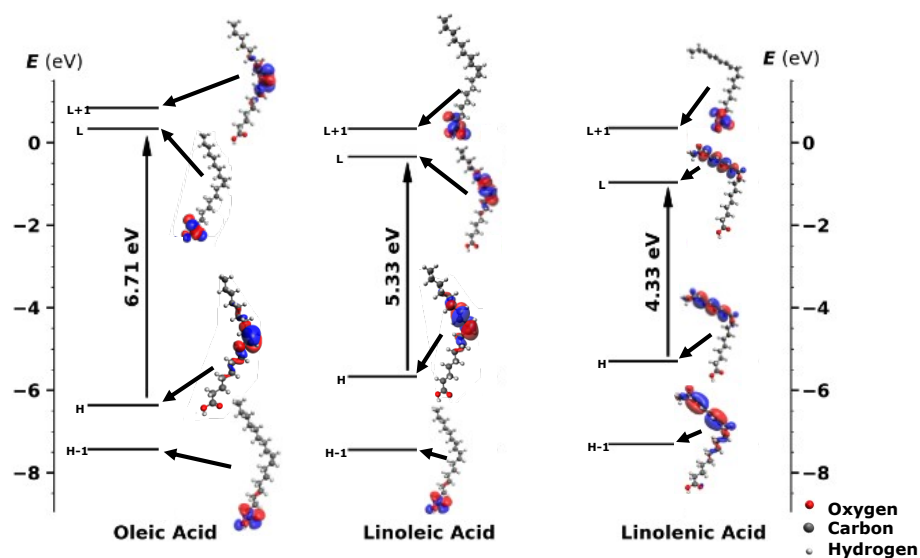


Figure 4.10: Structures and frontier orbitals for the component acids of linseed oil. Positive spin polarization of the frontier orbitals is represented as blue and negative spin polarization is represented as red.

free fatty acid product of the auto-oxidative curing process and because it is monounsaturated. [61, 84, 120] In the oleic acid-TiO₂ complex, the optimized oleic acid was adsorbed to the (101) surface of the TiO₂ slab in either a bidentate bridging mode or monodentate mode as shown in Figure 4.11. For the bidentate mode, the carboxylic proton was dissociated and transferred to the surface of the TiO₂ slab. It was found that the bidentate mode was more energetically favored with respect to the monodentate mode by 3.76 kcal/mol. This form was expected based on other binding modes for carboxylic acids. [121, 122] Therefore, hereafter we discuss only the oleic acid attached to the TiO₂ in bidentate configuration.

The DOS of the oleic acid-TiO₂ system shows the presence of a new energetic state at \sim -2.75 eV. Analysis of the partial/projected DOS (pDOS) shown in Figure 4.12 reveals that this state is derived from the p orbitals of the carbons in the oil molecule. The calculated Fermi level by Quantum Espresso of -2.75 eV signifies that it is occupied under our model conditions, allowing direct injection from the C 2p orbitals of the oleic acid into the conduction band of the TiO₂. This

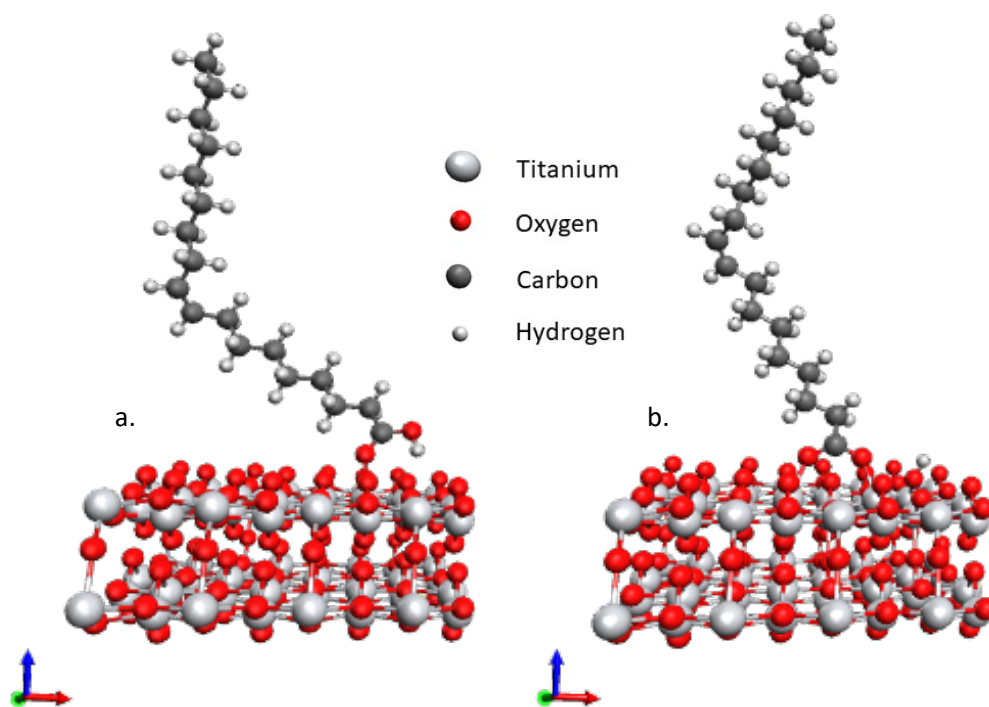


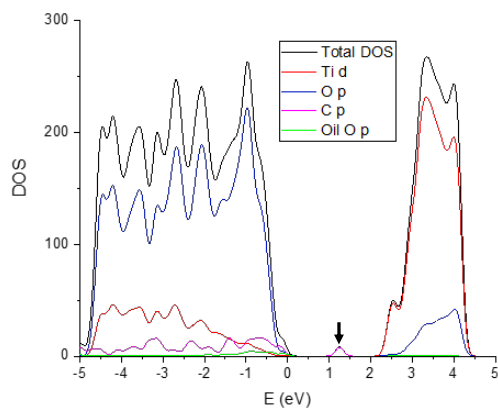
Figure 4.11: Binding modes and optimized geometry for oleic acid on the 101 surface of anatase TiO_2 ; (a) monodentate and (b) bidentate.

transition may have an excitation energy lower than anatase or oleic acid alone and low enough that excitation is possible under visible light. The Fermi level and the occupied status of this state may change in the presence of defects, and should be investigated. The amount of vacuum above the oil and the k-point sampling chosen were found to have no major effect on the DOS as presented in Figure .3.

Second, like TiO_2 , linseed oil shows a $\Delta E_{\text{H} \rightarrow \text{L}}$ much larger than the energy of visible light. It is therefore interesting that two components that are inactive in visible light become active when brought together. This suggests that the presence of linseed oil both enhances the activity of rutile by limiting charge recombination and effectively reduces the band gap of anatase, extending its response to visible light.

Table 4.2: Frontier energy levels and effective band gap for bare TiO₂ and oleic acid-TiO₂ system.

Molecule	Highest Occupied Energy (eV)	Lowest Unoccupied Energy (eV)	Effective Band Gap (eV)
TiO ₂	-3.13	-1.22	1.91
Oleic acid-TiO ₂ system	-2.75	-1.60	1.15

**Figure 4.12:** Density of States of the oleic acid-TiO₂ complex, and the partial density of states separated contributions showing the orbital origin of the intra-band state are reported. The intra-band state is denoted by an arrow.

One possible mechanism of this activity involves the formation of a charge transfer complex as presented computationally in this thesis. This charge transfer complex leads to an occupied orbital within the TiO₂ band gap. This effectively lowers the required ultra-band gap energy and allows visible light ($\lambda > 400$ nm) to excite an electron into the conduction band of the TiO₂. Because the contribution of this state derives from the occupied C p orbital, it can be inferred that a similar state will be created with anatase TiO₂ and linoleic and linolenic acids due to the similar energetic levels of the C p orbital in these fragments.

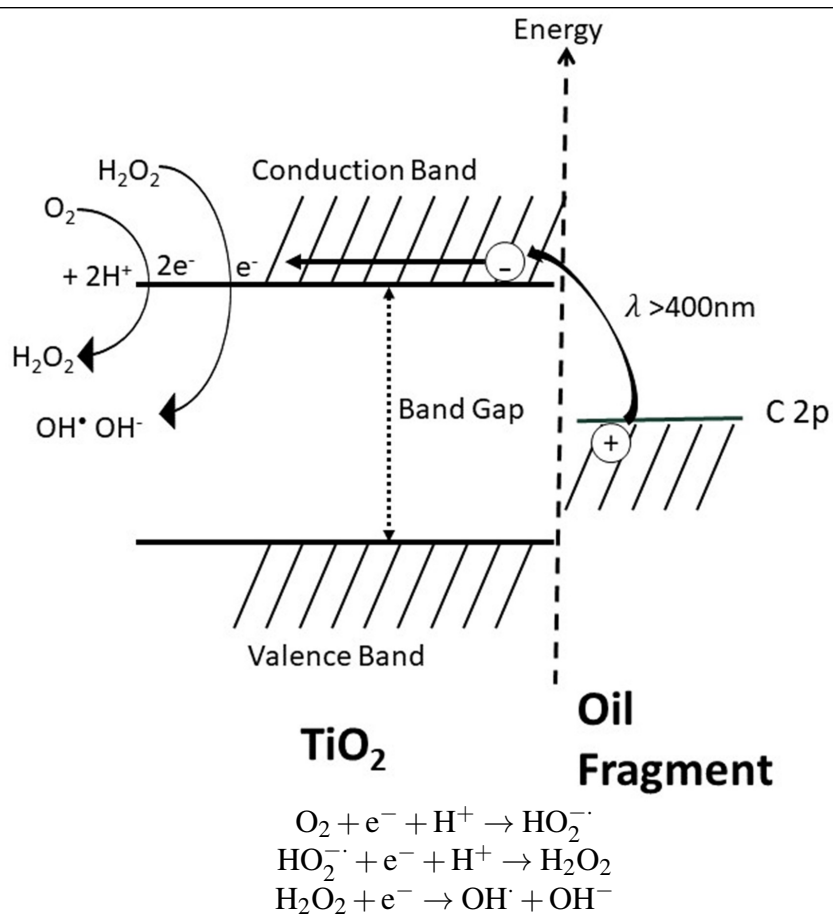
This charge transfer complex between anatase and oleic acid allows for the formation of reactive oxygen species (ROS) needed for the characteristic β -scission reactions, as can be seen in Figure 4.13. It is important to note that due to the lack of a hole in the TiO₂ valence band, electron transfer only occurs at the conduction band where oxygen is reduced. This prevents the formation of hydroxide radicals at the valence band edge since there is no electron vacancy or hole in the TiO₂. However, through sequential charge transfer reactions such as presented in Figure 4.13, hydroxide radicals can be formed via a different route.

The hole in the C p orbital of the oleic acid resulting from the electron transfer into the TiO₂ can lead to yet another mechanism for degradation. After charge injection, the oleic acid forms a cation radical with an unpaired electron located on the previously unsaturated carbon. As shown in Figure 4.14, a reaction with water results in hydroxylation of the oleic acid radical and desorption from the TiO₂ surface. It may also lead to oxidative degradation similar to that outlined by Juita *et al.* [84]

4.4 Conclusions

Through computational calculations, we characterized the electronic and physical structure of a common dye used in cultural heritage, alizarin carmine. We showed that alizarin carmine was a

Figure 4.13: Band alignment diagram for TiO₂ and oleic acid showing a possible pathway and associated reactions for ROS generation.



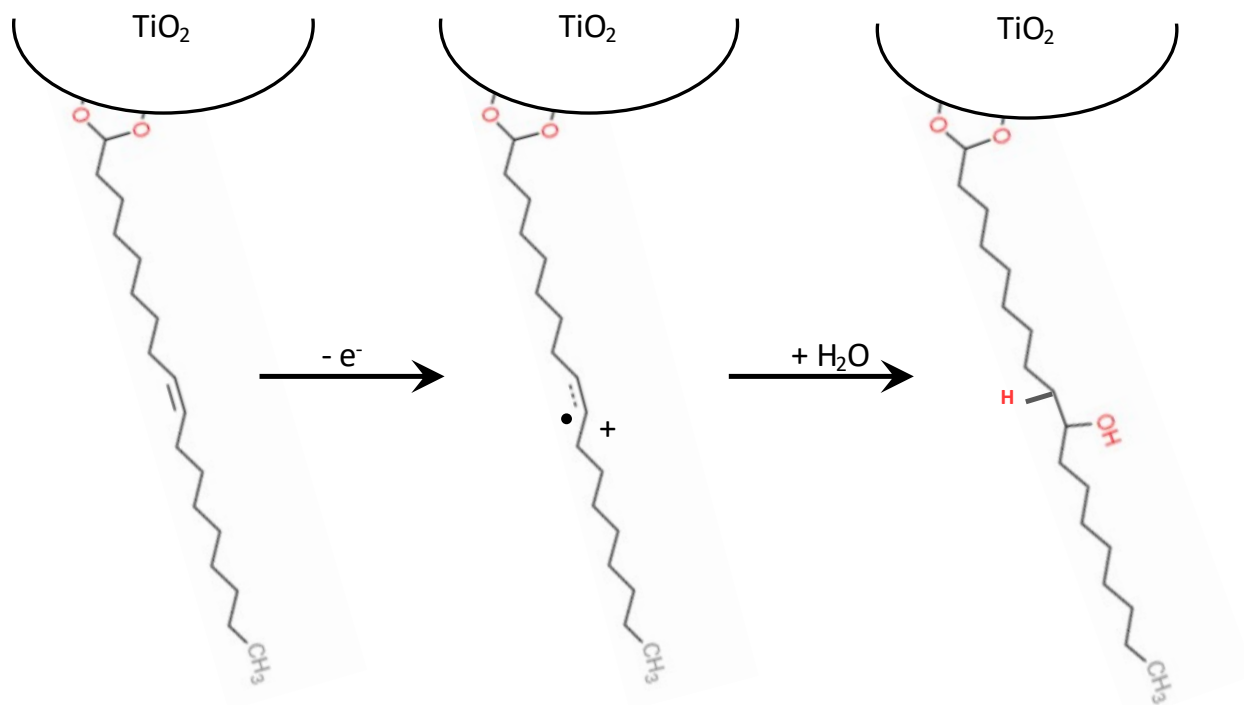


Figure 4.14: Pathway of oleic acid degradation due to electron transfer from the oleic acid to TiO₂.

candidate material for forming a charge transfer complex with TiO₂ to sensitize it to visible light. Such a complex was investigated and the frontier orbitals were visualized and plotted. A similar approach was then applied to the components of linseed oil and a complex was formed by attaching oleic acid to the surface of anatase TiO₂ in a bidentate configuration. The electronic structure of this complex allowed for visible light facilitated electron injection into the TiO₂ conduction band and the subsequent formation of an oleic acid cation radical which can undergo further reaction with water and desorb from the surface. This excited electron can form reactive oxygen species through proton assisted reaction with oxygen and facilitate the degradation of the oil binder.

Chapter 5

Study of Mass and Mechanical Property Changes During TiO₂ Facilitated Degradation Using the Quartz Crystal Microbalance

5.1 Introduction and Background

During the lifetime of a painting, the illumination conditions, humidity, temperature, and presence of other contaminants change greatly. We have shown that visible light under our aging conditions has facilitated degradation of linseed oil, but we have not been able to quantify this degradation. FT-IR methods also do not provide strong distinction between the degradation caused by visible light and UV light or between anatase and rutile based paints. Our understanding of the properties of TiO₂ and other research suggest that these factors should effect the rate and degree of degradation. [5,41] Morphological changes as measured in this thesis by SEM, and in other work measured through AFM, gloss number, and XPS have shown some differences between degradation, but these techniques have drawbacks. [39,42] SEM, AFM, and XPS are destructive methods, preventing in-situ measurement or tracking of a single sample. Gloss Number may provide a good non-invasive measurement of the early degradation, however the change in gloss number quickly stabilizes during chalking. [39] Choi and Cho 2001 have shown through FT-IR head space analysis that illuminated PVC-TiO₂ composite films generate CO₂, increasing with exposure time, suggesting a loss of material from the composite film. They also showed a decrease in the mass of the film with exposure by weighing the sample before and after. [123] This mass information provides important insight into the rate of material loss in the film, a major concern for conservators. It is therefore necessary to develop a quantitative model of the material loss and degradation of a paint film.

Work by Sturdy *et al.* has shown that although often used as a simple dosimeter, the Quartz

Crystal Microbalance (QCM) can be used as a thin film rheometer, collecting mass and mechanical property information simultaneously. [124] She showed that the QCM can be used to quantitatively study the curing behavior of alkyd films. By tracking the modulus-density product at 5 MHz, viscoelastic phase angle at 5 MHz, and density-mass product, specific mechanisms such as water absorption and desorption, incorporation of oxygen in the sample, volatilization of low-molecular weight components of the paint can be observed. [125] In later work, regions of the curing were identified corresponding to initial evaporation of the solvent, early transformation or disappearance of *cis* double bonds, and long term slow mass loss due to formation of volatile products from oxidation reactions. [124] Finally, she was able to probe the acceleration of initial oxidative curing when ZnO pigment was included. [126] There are of course drawbacks to this technique. In the art conservation science field specifically, one major drawback is that the QCM can only be applied to well-defined model systems made for and directly coated on the QCM. This restricts the use of any historical samples as they cannot be coated or may have difficult to measure properties. It is also worthwhile to note that the QCM is a high frequency technique. As such, it cannot be directly compared to other mechanical characterization techniques that operate at much longer time scales. [125] Despite these limitations, the QCM allows us to study the degradation behavior of TiO₂ pigmented oil films through monitoring of mass change in volatilization of the oil binder, and possible stiffening of the film with binder loss.

Operating Principle

The QCM consists of a 2.5 cm diameter quartz disk with gold electrodes patterned on the top and bottom. When a film is deposited on the Quartz crystal and an oscillating voltage is applied across the electrodes, the electrical impedance across the crystal responds to the load impedance. The frequency at which the conductance of the crystal is at a maximum shifts and widens as seen in Figure 5.1. The frequency shift at the *n*th harmonic (Δf_n) and the complex full width half max of

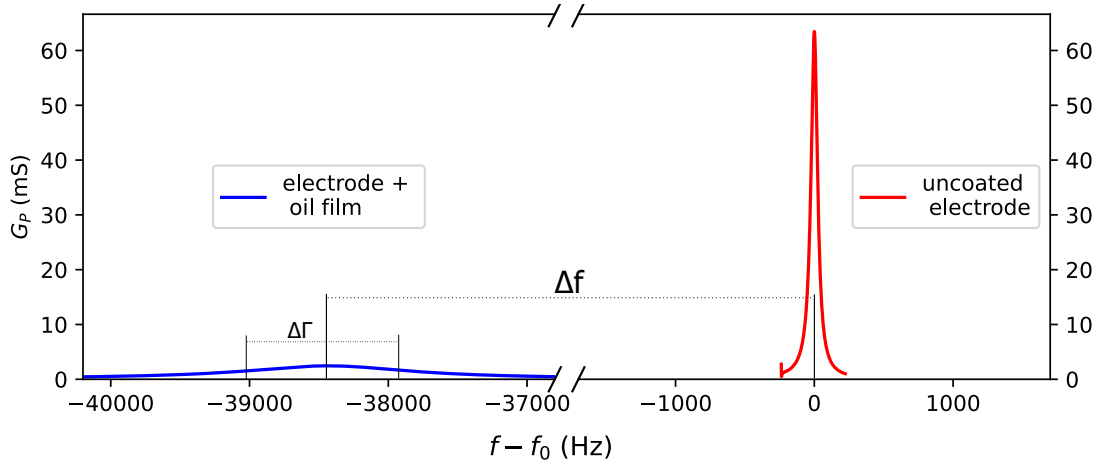


Figure 5.1: Frequency shift resulting from depositing an oil film.

the resonant peak for the n th harmonic ($i\Delta\Gamma_n$) are added to create the complex frequency shift at each harmonic (Δf_n^*). This complex frequency shift is tracked by fitting one or multiple Gaussian curves to the peak as seen in Figure 5.2a. The fit can also be evaluated by plotting the conductance vs susceptance, resulting in a circular fit as seen in Figure 5.2b. Δf_n^* can be related to the acoustic load impedance (Z_n^*) of the film following 5.1.

$$\frac{\Delta f_n^*}{f_1} = \frac{iZ_n^*}{\pi Z_q} \quad (5.1)$$

Where, Z_q is the shear acoustic impedance of the quartz ($8.84 \times 10^6 \text{ kg} \cdot \text{m}^{-2} \text{ s}^{-1}$). The acoustic load impedance (Z_n^*) at each harmonic is related to the propagation rate of the shear wave of $n \cdot 5$ MHz through the deposited film and therefore dependent on certain film properties. For the experiments presented in this thesis the 1st, 3rd, and 5th harmonic are always considered. For samples with sufficiently low thickness, the 7th and 9th harmonic can also be considered.

When the resonance peak bandwidth, or film dissipation ($\Delta\Gamma_n$) is negligible, as in the case of very thin or stiff films, the mass per area ($d\rho$) can be approximated via the Sauerbrey shift, Δf_{sn} . Note that as shown in equation 5.2, the Sauerbrey shift is a real number since the complex component is ignored.

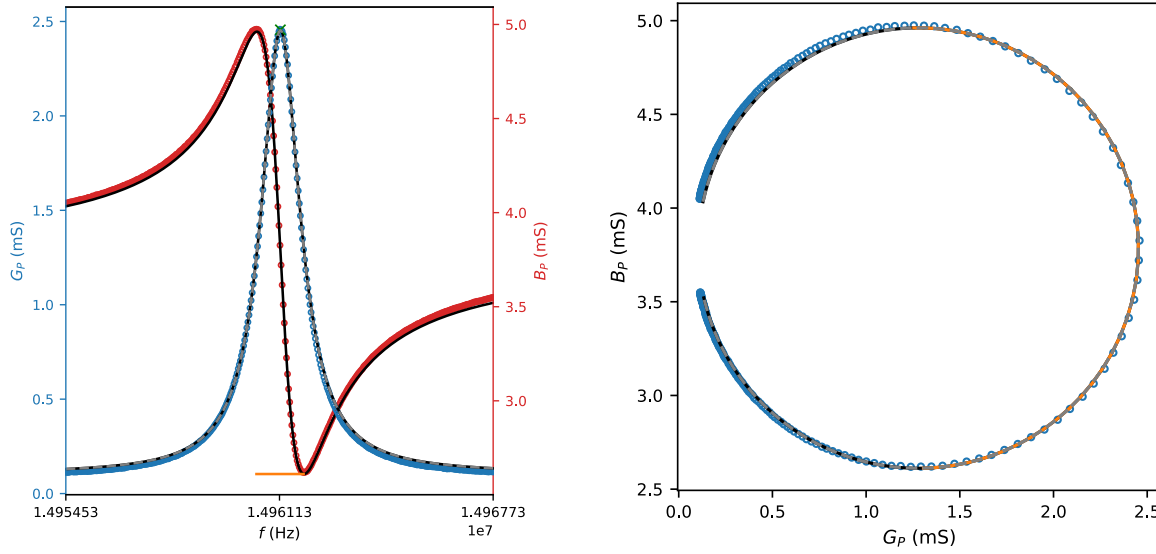


Figure 5.2: (a) Peak fitting of the frequency versus conductance (G_ρ) and susceptance (B_ρ); and (b) the fit and relationship between conductance (G_ρ) and susceptance (B_ρ).

$$\Delta f_{sn} \equiv \frac{2nf_1^2}{Z_q} d\rho \quad (5.2)$$

As the films diverge from ideal elastic behavior and the dissipation term becomes significant, the behavior of the complex frequency shifts begin to depend on two new factors: the viscoelastic phase angle ϕ , and the ratio of the film thickness to the wavelength of the shear wave within the film d/λ_n . To account for these new factors, and the deviation from the Sauerbrey shift, we must use the relationship in equation 5.3 [127, 128]

$$\frac{\Delta f_n^*}{\Delta f_{sn}} = \frac{-\tan\{(2\pi d/\lambda_n)(1 - i \tan(\phi_n/2))\}}{(2\pi d/\lambda_n)(1 - i \tan(\phi_n/2))} \quad (5.3)$$

Previous research has shown that the relationship between λ_n and the viscoelastic properties of $|G_n^*|$ and ϕ is 5.4.

$$\lambda_n = \frac{1}{nf_1} \left(\frac{|G_n^*|}{\rho} \right)^{1/2} \frac{1}{\cos(\phi_n/2)} \quad (5.4)$$

By back substituting we can derive a master equation that depends on measurables of f_1 , Δf_n , and $\Delta\Gamma_n$, and gives film properties d , ρ , $|G_n^*|$, and ϕ_n :

$$\frac{\Delta f_n^* Z_q}{f_1} = \frac{- (|G_n^*| * \rho)^{1/2} * \tan \left\{ \left(\frac{2\pi d n f_1 \rho^{1/2} \cos(\frac{\phi_n}{2})}{|G_n^*|^{1/2}} \right) \left(1 - i \tan(\frac{\phi_n}{2}) \right) \right\}}{\pi \cos(\frac{\phi_n}{2}) \left(1 - i \tan(\frac{\phi_n}{2}) \right)} \quad (5.5)$$

However, each time we measure at a new harmonic we are adding additional unknowns because ϕ and $|G^*|$ have n dependence. We can close the system of equations, by assuming the phase to be harmonic independent, and the relationship in equation 5.6 between the harmonic number and modulus in our analysis:

$$|G_n^*| \propto n^{\phi_n/90} \quad (5.6)$$

With this assumption, data from two harmonics is sufficient to solve the system of equations. Generally, more than two harmonic are measured, so there is a choice of inputs for Δf_n^* . The assumption in equation 5.6 allows us to use the frequency and dissipation shift from one harmonic and only the frequency shift for a second. [129] We represent the choice of $\Delta f_n, \Delta\Gamma_n$ and Δf_m used for a given solution as n.m.n (eg 3.5.5 solves using the data from the 3rd and 5th harmonic frequency shifts and the 3rd harmonic dissipation shift). This allows for the back-calculation of the expected shift for other harmonics. This expected value can be compared to the measured value to gauge the accuracy and validity of the solution.

5.2 Materials and Methods

Coating slurry was created by mixing anatase TiO₂ (J.T. Baker Material No. 4162-01) at 25 wt% and linseed oil (Sigma-Aldrich CAS 8001-26-1) on a glass plate using a palette knife as seen in

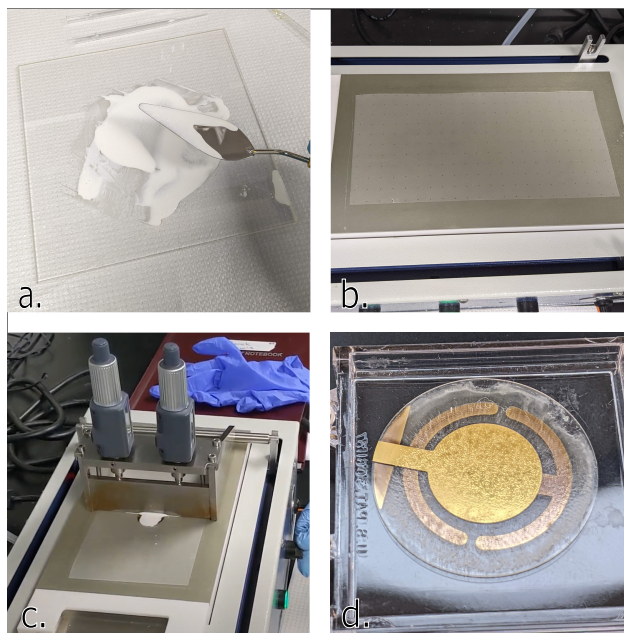


Figure 5.3: Coating Procedure showing (a) mixing the paint on a glass plate with a palette knife, (b) placing the parafilm over the unused vacuum holes, (c) the coating in action, and (d) the finished cured crystal.

Figure 5.3a. The resulting paint was then collected into a vial and diluted to 35% with mineral spirits. The vial was sealed and mechanically stirred using a stir bar on a stir plate until use. Bare QCM crystals were referenced then placed on the Mini Tape Casting Coater (MTI Corporation MSK-AFA-HC100) using parafilm as a buffer layer to seal unused vacuum bed holes with a hole was poked in the parafilm using a needle to hold the crystal as seen in Figure 5.3b. A micrometer adjustable film applicator (MTI Corporation EQ-Se-KTQ-100) was then zeroed to the top of the QCM crystal. The height of the film applicator is then increased by $55\ \mu\text{m}$. Approximately 0.1 mL of the coating slurry is added to the QCM crystal, a delay of 1 second is added to allow for some initial evaporation of the mineral spirits, and the film applicator is drawn across the sample with the speed dial set to 20. The coating and the resulting cured crystal can be seen in Figure 5.3c and d.

After the application, the crystal is removed from the vacuum bed and the back side is cleaned with ethanol. The crystals are then placed in a $60\ ^\circ\text{C}$ oven and after 1 week, an initial QCM measurement

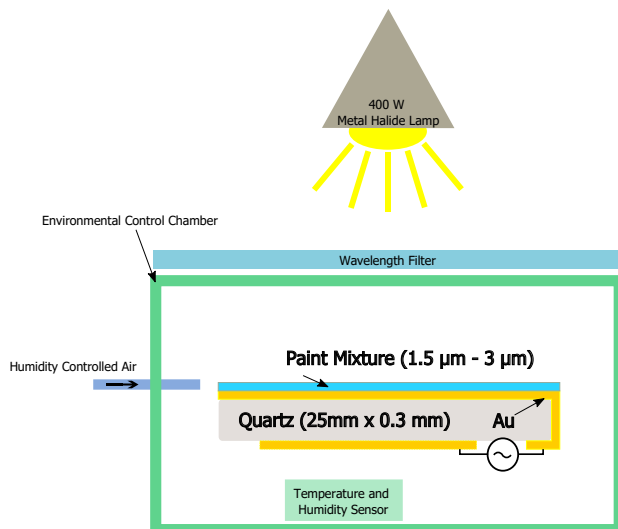


Figure 5.4: Schematic of aging setup showing how humidity and wavelength dependency was achieved and monitored.

is made. Samples are then placed in aging chamber with a specific controlled lighting condition (Vis ($\lambda > 400$ nm) or UV+Vis ($\lambda > 350$ nm)) and either moderate ($\text{RH} = 50 \pm 5\%$) or high ($\text{RH} = 80 \pm 5\%$) humidity as shown schematically in Figure 5.4. The lighting conditions we achieved through a single mounted 400 W metal halide lamp (Sylvania M400/U), with either a Pyrex filter to remove wavelengths below 350 nm for UV-vis light, or a UV blocking filter (Edmund optics UV filter sheet) to remove wavelengths below 400 nm for Vis aging as shown in Figure 5.5.

Sample names and light intensities are reported in Table 5.1. Samples were removed at regular intervals and QCM measurements were made. All measurements were performed at lab temperature and humidity. The QCM sample case was placed over the opening in the holder to obscure the sample surface from light during measurements.

The QCM measurements were performed using an AT-cut quartz disk with gold electrodes patterned on each side from RenLux Crystal (Guangdong, China). Impedance measurements were taken via a N2PK Vector Network Analyzer (Makarov Industries Ontario, Ca). The resonant peaks at each harmonic were determined via Gaussian fitting of the conductance as can be seen in Figure 5.2. In the case of multiple peaks at a single harmonic, the lowest frequency peak was used.

Table 5.1: Sample Names and Conditions

Sample Name	Humidity (% RH)	Lighting Condition	Average Total Light Intensity (μWcm^{-2})	Average UV (350 nm < λ < 400 nm) Light Intensity (μWcm^{-2})	Average Vis (400 nm < λ < 800 nm) Light Intensity (μWcm^{-2})
Ana-Vis-50	50 \pm 5	Vis	11791.9	11164.7	16.6
Ana-Vis-80	80 \pm 5	Vis	11313.2	10682.5	16.9
Ana-UV-50	50 \pm 5	UV+Vis	13519.1	12572.2	379.9
Ana-UV-80	80 \pm 5	UV+Vis	15380.4	14313.6	462.7
Rut-Vis-50	50 \pm 5	Vis	11802.4	11171.7	15.9

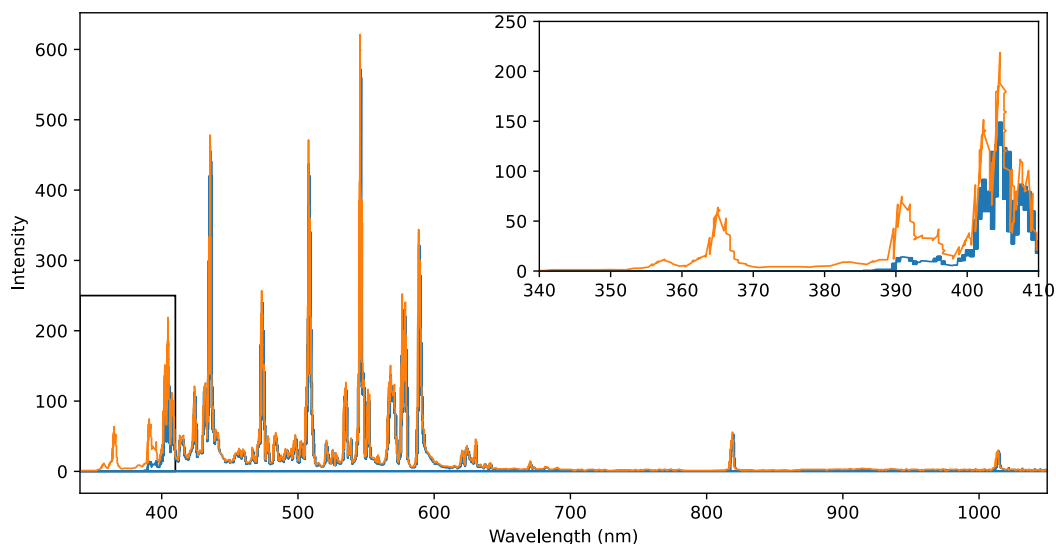


Figure 5.5: Spectra of aging lamp for UV-vis (orange) and vis (blue) aging conditions; the inset shows the zoomed area denoted by the box.

5.3 Results

By measuring the changes in resonant frequency at each harmonic and applying equations 5.2-5.6, we can calculate the modulus-density product at 15 MHz ($|G_3^*|\rho$), the viscoelastic phase angle at 15 MHz (ϕ), and the areal density ($d\rho$), as can be seen in Figure 5.6 for Ana-Vis-50. Changes in each of the calculated properties were plotted versus the total light exposure. It can be observed that the modulus increases by ~ 70 MPa (a 15 % increase) with visible light exposure. This increase could be described by late stage curing of the linseed oil network similar to that observed in oil modified alkyd network in Sturdy *et al.* 2016. [124] The viscoelastic phase angle of the film (ϕ) stays constant at 37 degrees. This angle represents the phase difference between the applied shear wave and the response of the material. An angle of 0 corresponds to a perfectly elastic material, whereas an angle of 90 corresponds to a perfectly inelastic material. The paint film used in this experiment has a greater viscoelastic character (higher phase angle) than the cured alkyd films studied by Sturdy. [124, 126, 130] The mass loss observed in this sample is attributed to degradation of the

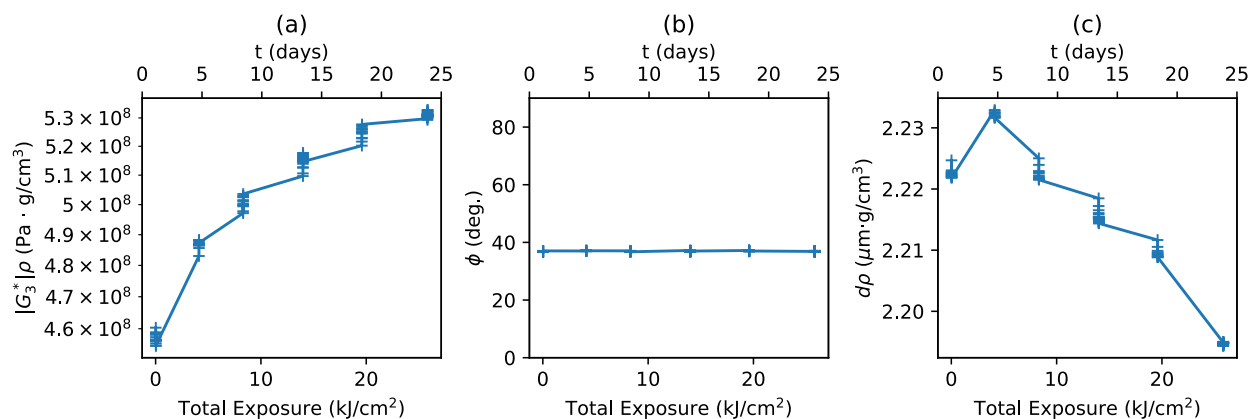


Figure 5.6: Measured properties as a function of the total light exposure dose for the Ana-Vis-50 sample (Anatase TiO_2 , visible light exposure, 55 % relative humidity).

oil binder by TiO_2 . The decrease in mass is observable but small. It is unclear if the mass change is associated with TiO_2 volatilization or normal photo-curing. More control samples will have to be done to compare these mechanisms. I hypothesize that visible light facilitates the formation of larger non-volatile products similar to those presented in Chapter 3 and 4 which are not tracked by the QCM.

To validate our results and to evaluate the error or uncertainty, we can use additional data from unused harmonics to check our solutions. By back-calculating the frequency and dissipation shifts at each point, we can plot the calculated values and the experimental values and visualize the mismatch. As can be seen in Figure 5.7, the back-calculated values for Δf_7 , $\Delta \Gamma_3$ and $\Delta \Gamma_7$ match closely with the experimental values, suggesting that our assumptions of a uniform film thickness and roughness are valid.

We have also extended this investigation into rutile based paints, applying the same visible light aging methodology at 50 % RH as an initial test. Rutile presented different coating behaviors and initial mechanical properties. This requires further process refinement to produce a quality reproducible sample. We were able to successfully measure the frequency and dissipation changes in a rutile TiO_2 based paint film under visible light exposure and $50 \pm 5\%$ RH and calculate the mass and viscoelastic properties using a 3.5.5 calculation as shown in Figure 5.8. We can see that

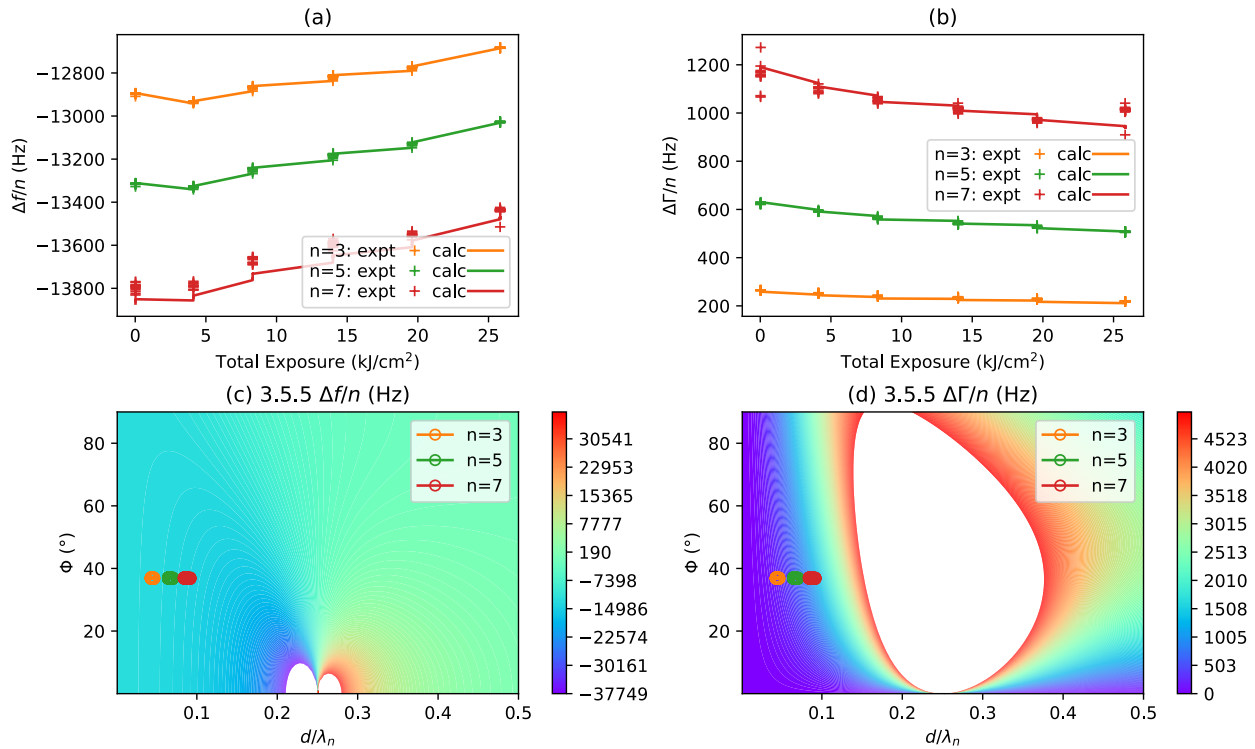


Figure 5.7: Comparison of the experimentally measured values of $\Delta \Gamma_n$ and Δf_n to the values that are calculated from Eqs. 5.2-5.6, using the properties shown in Figure 5.6. These properties were obtained from a 3.5.5 calculation which means that the equations were solved to force agreement of the calculated and measured values of Δf_3 , Δf_5 and $\Delta \Gamma_5$.

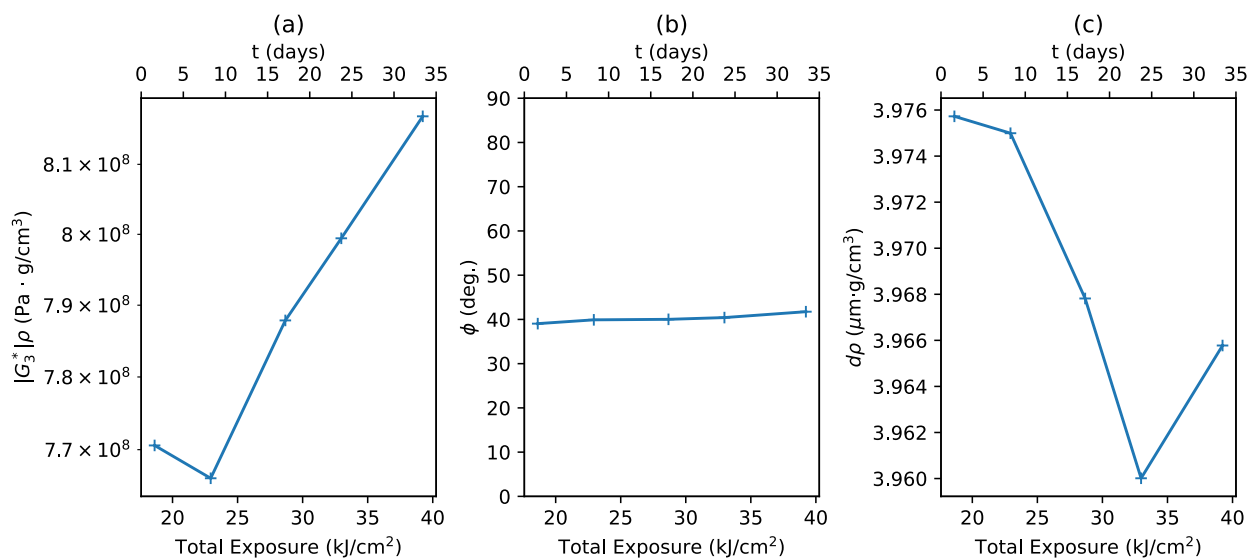


Figure 5.8: Measured properties as a function of the total light exposure dose for the Rut-50-Vis sample as calculated with a 3.5.5 calculation.

there is a slow decrease in $d\rho$ and a slow increase in $|G_3^*|\rho$ with exposure for Rut-Vis-50, similar to the data presented in Figure 5.6 for Ana-Vis-50. The rutile film is has a much larger initial $d\rho$ (3.985 vs. $2.20 \mu\text{m}\cdot\text{g}/\text{cm}^3$) and a larger initial $|G_3^*|\rho$ (7.4×10^8 vs $4.6 \times 10^8 \text{Pa}\cdot\text{g}/\text{cm}^3$). We can observe that rutile's shear modulus increased by only 8.43 %. In order to more directly compare the rates of degradation, more similar samples will need to be created. Additionally, the effect of visible light on both samples is small, with only $0.026 \mu\text{m}\cdot\text{g}/\text{cm}^3$ of change over $40 \text{kJ}/\text{cm}^2$ (0.8 %) of exposure for Rut-Vis-50 and only $0.03 \mu\text{m}\cdot\text{g}/\text{cm}^3$ of change over $27 \text{kJ}/\text{cm}^2$ of exposure (1.3 %) for Ana-Vis-50.

We explored the effect of UV light and high ($80 \pm 5\%$ RH) humidity on anatase based samples and applied the same mult-harmonic analysis to calculate $|G_3^*|\rho$, ϕ and $d\rho$ as can be seen in Figure 5.10. It can be seen that a very strong decrease in modulus is observed under UV lighting and high relative humidity. This suggests that there is significant oil loss and porosity forming. When we compare $|G_3^*|\rho$ and ϕ for the other anatase based samples, we can see that there is not this strong effect of humidity under visible light. All samples visible and 50% RH samples behave similarly, with a slow increase in modulus over exposure and no change in viscoelastic phase angle as can

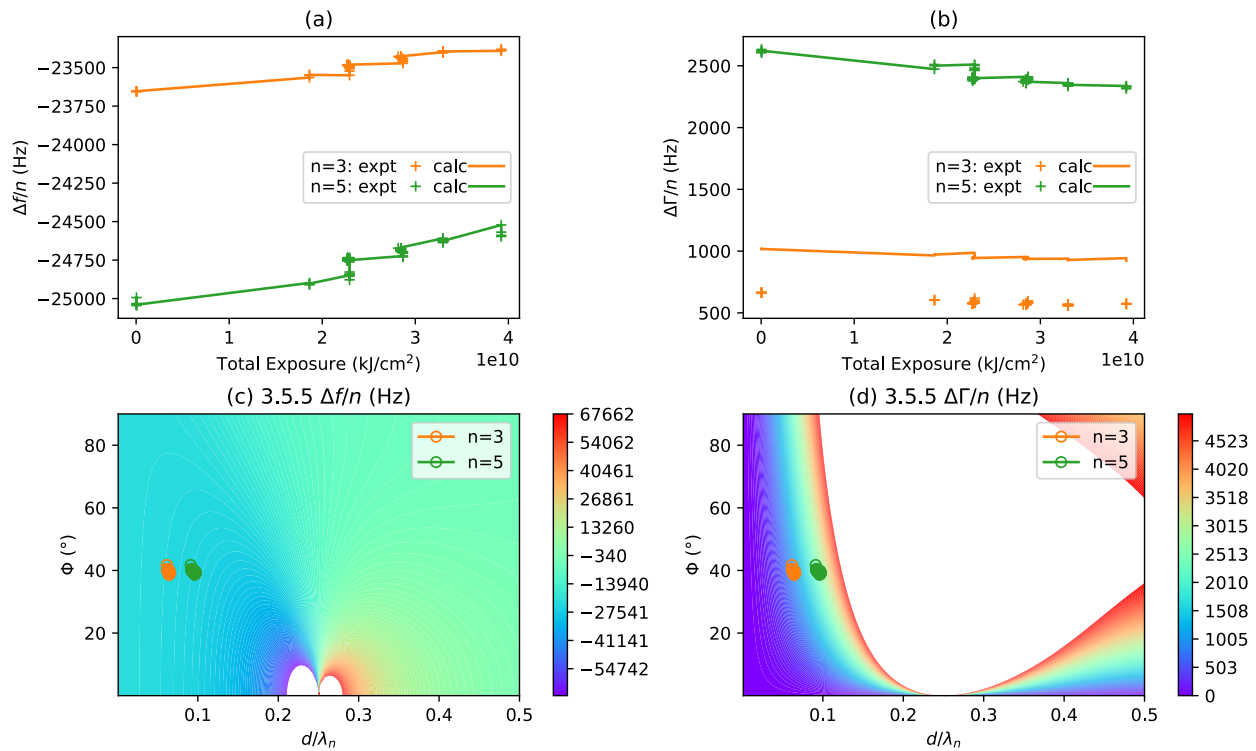


Figure 5.9: Comparison of the experimentally measured values of $\Delta \Gamma_n$ and Δf_n to the values that are calculated from Eqs. 5.2-5.6, using the properties shown in Figure 5.8. These properties were obtained from a 3.5.5 calculation which means that the equations were solved to force agreement of the calculated and measured values of Δf_3 , Δf_5 and $\Delta \Gamma_5$.

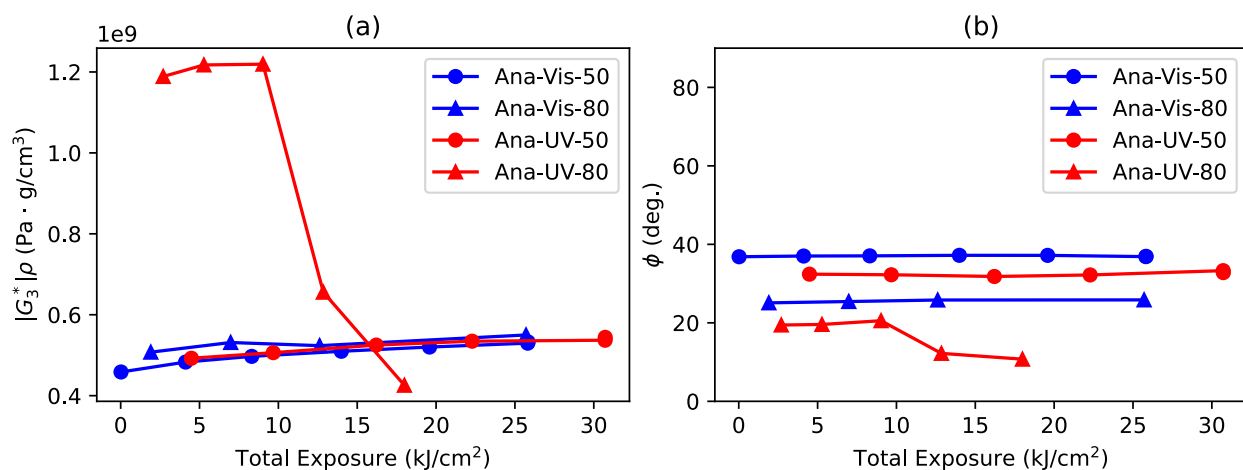


Figure 5.10: Measured values of the modulus-density product and phase angle as a function of the total light exposure dose for four different anatase samples.

be seen more closely in Figure 5.11. The solution check for each of these samples can be found in the Appendix Figures .4- .6. All samples shown are aged over similar exposure conditions and similar time. Therefore, we can look at the x axis as either time or exposure. We can then suggest that this may be a time based stiffening rather than light mediated. In order to test this we need to explore the effects of dark conditions.

When the mass change is plotted for each exposure we can clearly see the effect of TiO₂. The decrease in mass may be driven by scission of fatty acids leading to the formation of low molecular weight volatile products, although other reaction mechanisms may become important in the presence of relatively large concentrations of hydroxyl radicals. The increase in water present in high humidity environments allows for rapid generation of reactive oxygen species and degradation of the oil binder. When the humidity is reduced, UV irradiation still drives degradation and loss of mass. As mentioned above, the mass loss for visibly aged samples in both moderate and high humidity environments is small suggesting limited degradation. The FT-IR results presented in Chapter 3 suggest that visible light does degrade the oil binder, seemingly contradicting the QCM results. However, the chemical products observed in the FT-IR results were non-volatile. As such, the QCM is not sensitive to the formation of these compounds. Instead the QCM is de-

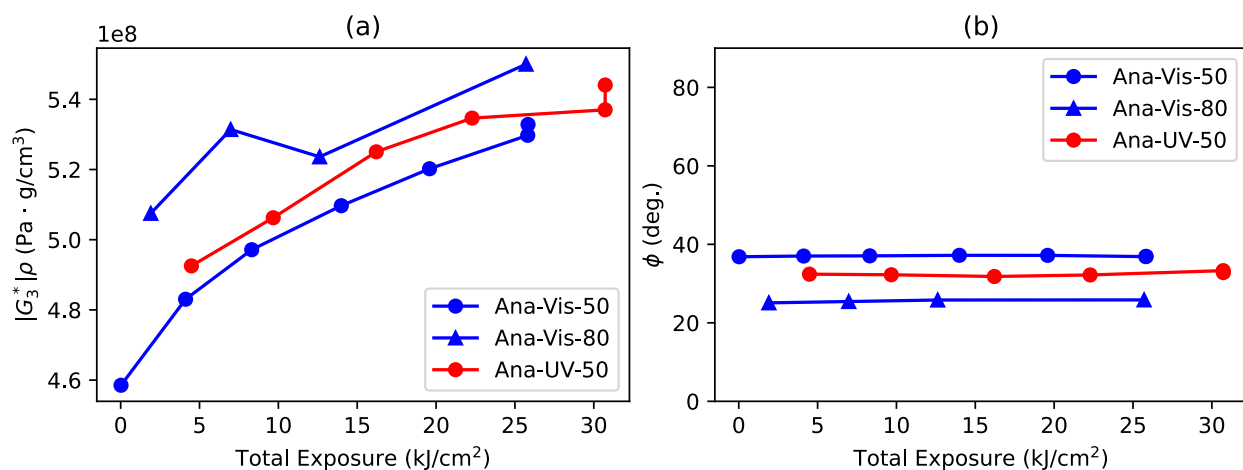


Figure 5.11: Measured values of the modulus-density product and phase angle as a function of the total light exposure dose for similarly behaving anatase samples.

tecting the generation of (but not identifying!) lower molecular weight non-volatile compounds. Additionally, especially with respect to the mechanical properties, the QCM measures an average of the properties of the film. Under low exposure times, the degradation layer is small compared to the thickness of the film, this limits the sensitivity of these properties to surface level changes. However, since mass is calculated as total, even small losses at the surface are seen. This can be evident in Ana-UV-80 where a third of mass is lost during degradation leading to clear changes in mechanical properties. With this understanding, using these two techniques together may provide a picture of both the chemistry present in the remaining film, and the material lost during degradation.

The QCM provides clear evidence of the effect of UV light. In FT-IR spectra, the difference between UV exposed samples and visibly exposed samples was not clear as both sets showed significant signs of degradation products. By combining the results we can suggest a more complete mechanism of the degradation of oil binder under multiple environmental conditions. Visible light facilitates the formation of higher molecular weight products very rapidly and under moderate illumination. However, the further degradation to volatile products and loss of material is much slower and not as sensitive to humidity. As a contrast, under UV illumination both volatile and

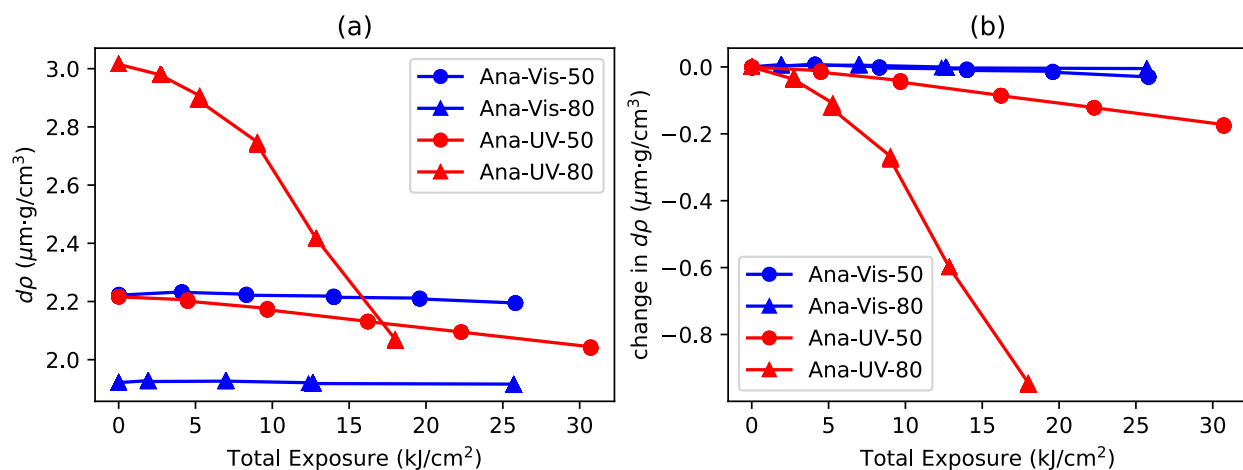


Figure 5.12: Film mass as a function of light exposure dose for films containing anatase TiO_2 .

non-volatile degradation products form rapidly and the humidity has a major effect on the rate.

5.4 Conclusions

We have presented a novel use of the QCM as a high frequency rheometer. By measuring mass change with exposure, we have been able to track the TiO_2 facilitated degradation of linseed oil under UV light. We have quantitatively shown the difference in mass loss between TiO_2 based paint under UV light at 50 % RH and 80 % RH, showing another application of this technique. Finally, we have shown that the complex shear modulus and the viscoelastic phase angle can be tracked with exposure, but they are less sensitive to surface changes. We believe that this shows that the QCM is a powerful tool to investigate the changes in a titanium white paint film during different aging conditions.

Chapter 6

Outlook, Future Work, and Summary

The first section discusses the major findings of this work and the impacts on the field. The second section discusses work that will bring immediate impact to the understanding of TiO₂ facilitated degradation. The third section summarizes the work and major findings of each chapter.

6.1 Outlook

6.1.1 Identification of TiO₂ Based Paints in Jackson Pollock Paintings

It is fairly accepted that TiO₂ based paints were widely used throughout the 20th century, but more work is needed to investigate the properties of historical TiO₂ pigments. Work published by Van Driel *et al.* was the one of first to investigate the crystal structure present in TiO₂ based paints on a wide scale. With the inclusion of the work in this thesis, TiO₂ based paints have been identified in primarily Dutch and Pollock paintings. Because these works have shown anatase TiO₂ in artwork painted after 1950, the community is beginning to focus more research on this topic. I expect that the outlook of non-invasive investigation of 20th century paintings will focus on identifying signs of degradation with more attention paid to the exposure conditions and the phase of TiO₂ present.

6.1.2 New Insights into TiO₂ Facilitated Degradation Under Visible Light

The main goal of this work was to convince the field of cultural heritage science that TiO₂ based paints with either rutile or anatase formulations may cause degradation in modern oil paintings. The visible light degradation challenges the current belief of TiO₂ activity. I expect there will be doubt about the activity of rutile based paints and both TiO₂ formulations under low levels of

visible light exposure. I do note that this work does not prove visible light activity in museums or real paintings. It presents a set of conditions under which degradation products formed under visible illumination and validates the formation of degradation products and mass loss under UV light. There will need to be more research done to extend these findings to real paintings and better characterize the degradation under visible light. It is better to prevent a problem than attempt to fix the damage, and we have the opportunity to more thoroughly investigate our materials for stability, safety, and environmental harm. The better we understand the conditions that accelerate and limit degradation, the better we can preserve our paintings. Additionally, if this information is then provided to artists, they can make more informed decisions about the materials they choose, and the conditions under which they want their work to be displayed, stored, or preserved.

6.1.3 Computational Modeling of Interactions in Art Materials

The of cultural heritage science field is beginning to study the effects of mixtures and recognize that model systems are not simply scaled down versions of a real system. Computational methods can help us narrow that gap between our model system and the real system. We can specifically probe the effect of certain parameters using first-principles knowledge. This can allow for a more intelligent building of a model system that behaves closer to our real system. The computational methods that have been studied and developed for other fields can fairly easily be applied to cultural heritage materials, which should help the adaptation of the technique in the cultural heritage field. The cultural heritage field is rapidly adopting these computation methods and applying them to more and more systems. The current state of research is a mix of applying well defined methods to materials for cultural heritage, and developing methods specifically made for cultural heritage applications. This work is an example of the first. The Broadbelt group at Northwestern is developing a micro-kinetic model for the curing of linseed oil. This could provide an incredibly powerful tool for probing reactions possible in certain paint systems. Like much of material science, there

is a lot of work to be done in computational modeling.

6.1.4 Study of Mass and Mechanical Property Changes during TiO₂ facilitated degradation using the QCM

The QCM as a solid state rheometer for paint materials was first pioneered by Lauren Sturdy. Since then, the QCM has been used as a tool for monitoring processes relevant for cultural heritage such as early curing of alkyds and oil paints, and degradation of cellulose acetate systems. The QCM presents an incredibly powerful tool for the art conservation science community if used properly. Our goal was to provide a model for the art conservation community of the validity of TiO₂ facilitated degradation especially under UV light by showing the clear loss of mass associated with relatively little exposure. We were able to show the role of water and UV light in the loss of mass facilitated by TiO₂ pigments.

For other mechanisms where cracking, or material loss is a major degradation process, the QCM may provide immense value in quantifying that degradation. There are some significant hurdles to widespread use of the QCM by the art conservation field. First, the difference in properties of different art materials can make coating procedures and ideal sample parameters wildly different. Second, it is difficult to produce reliable samples with pure oil. As oil cures, the properties change rapidly, it is difficult to prepare a film which will remain smooth and intact throughout curing. Adding pigment helps stabilize the films and results in more successful samples, but this limits the comparisons and controls that can be used. A lot of work is being done by Gwen dePolo to work around many of these issues. Third, the analysis of the data, and validation of the results is not trivial. A lot of work has been done by Qifeng Wang and Ken Shull to develop a robust analysis program. Despite these hurdles, other groups have begun to use the QCM to study materials relevant to art conservation science, and I expect more will adopt it in the next few years.

6.2 Future Work

6.2.1 Identification of TiO₂ based paints in Jackson Pollock Paintings

Future work could be done to further analyze the paints used in these paintings, such as the areas containing both colored pigment and titanium white in *The Moon Woman*. Due to possible interactions between these colored pigments and titanium dioxide, the identification of these pigments, especially if they are organic, could motivate future computational and experimental work. A more invasive characterization of the surface and chemistry of titanium white paint could provide more details on the state of degradation. This could help guide long term accelerated aging studies and provide a better picture of long term stability under different conditions. Finally, to probe if paintings containing titanium white are actively degrading under current conditions, an aging study of model samples or small samples of the painting in the Peggy Guggenheim Collection could be undertaken. This would allow for real time tracking of surface conditions such as roughness or gloss, and chemical information through ATR-FTIR such as presented in Chapter 3. Finally, more robust chemical analysis of the degradation products could be done especially if performed *in-situ*. These could help identify the chemical species formed during TiO₂ facilitated degradation leading to a better understanding of the reactions taking place. Methods such as NMR and certain chromatographic techniques may provide such information.

6.2.2 New Insights into TiO₂ Facilitated Degradation Under Visible Light

This work aimed to characterize the material left in the paint film. However, this is only half the story. Head space FT-IR could be employed with *in-situ* ATR-FT-IR to analyze gas and solid products formed during degradation. This information could be fed into a micro-kinetic model of TiO₂ facilitated degradation and perhaps determine pathways and rates of reaction. In addition to IR methods, other techniques such as mass spectroscopy or chromatographic techniques

may provide better characterization of the organic compounds found in the degradation paint film. However, these techniques have their drawbacks including difficulty with sample preparation and signal analysis.

The FT-IR techniques used in this thesis focused on the top surface layer ($<1 \mu\text{m}$). In order to quantify the thickness of the degradation layer and probe the rate of degradation, cross section FT-IR mapping can be done. The mounting and polishing of the samples must be done with care, as smearing of degraded oil products could artificially inflate the degradation layer thickness. Additionally, the cross section sample should be taken under cold conditions to prevent bending and smearing when the sample is taken. This cross section analysis could also provide a model for conservators to compare for historical cross sections.

Because the effect of interactions of pigments with other compounds was shown to have such a large effect on the activity of TiO_2 based paint, future work should investigate mixtures of materials that are commonly present in 20th century paintings. Two clear early contenders could be a heterostructured anatase-rutile composite which may have been made early in the TiO_2 pigment production process, or an anatase- BaSO_4 composite which were available for much of the 1920s-1930s.

6.2.3 Computational Modeling of Interactions in Art Materials

We showed how alizarin carmine and oleic acid may interact with anatase TiO_2 slabs to form new states. One obvious extrapolation of this work would be to model linoleic and linolenic acid with the anatase already studied. This would provide information on the effect of the degree of saturation on the creation or levels of the intra-band state and could inform the type of curing oil used when making paint.

The model we investigated was fairly simple in that we studied only one face with no surface features such as hydration. Multiple levels of complexity could be added to the simulation to more

closely model real life. This would be useful to the extent that emission spectra could be calculated and compared with experimental results. If the model more closely resembles real conditions, it may match experimental results better and provide stronger support for the interaction.

Finally, the other TiO_2 crystal structure: rutile will also likely form a similar complex and should be investigated. An investigation into band bending and recombination rates in the presence of linseed oil component acids may provide insight into the activity of rutile based paint observed in Chapter 3.

6.2.4 Study of Mass and Mechanical Property Changes during TiO_2 facilitated degradation using the QCM

The work we completed for this thesis investigated the effect of visible and UV light on anatase based films. It is clear the film conditions and sample preparation plays a major role in the reliability of the sample. As such, some more refinement to the sample preparation procedure could be done. With more time, the rutile based samples and controls of either BaSO_4 pigmented films or pure linseed oil films could be aged under dark, visible, and UV light and under low, moderate, and high RH. The apparent disagreement between the degradation shown in visible light exposed samples in Chapter 3 and the low change in mass presented in Chapter 5 bring up many questions to the visible light degradation. I propose that visible light degradation forms higher molecular weight products which do not volatilize, but are observable through FT-IR. As mentioned before, other techniques could confirm the presence of these products. Because the degradation layer is thin compared to the thickness of our sample, the complex shear modulus is primarily responding to the bulk properties. If a sufficiently thin film were to be prepared or the degradation were to be significant, the stiffening of a paint film under visible light may be observed.

Finally, an extrapolation and improvement to the multi-modal approach used in this thesis could be designed which would perform FT-IR of the QCM film, QCM analysis, and head space mass

spectroscopy. This would allow for characterization of the chemistry, mass, and shear modulus of the paint film, and the analysis of volatile degradation products during photo-aging.

6.3 Summary

Chapter 1 of this thesis gives background into the history of development and use of TiO_2 as an artist's pigment. Two different crystallographic phases were produced; anatase, first around 1920 and rutile, later around 1950. Anatase and rutile have similar crystal structures with rutile having a small distortion. This leads to similar band structures with anatase having a slightly larger at (3.2 eV vs 3.0 eV for rutile). Anatase shows much higher photocatalytic activity than rutile, often attributed to rutile's increase rate of recombination due to band bending. Paintings were introduced which have been found to use TiO_2 based white paints including many works by Jackson Pollock. TiO_2 has also been found in paints with ZnO and BaSO_4 which may interact with TiO_2 creating unintended compounds.

The mechanism of TiO_2 photocatalytic activity was presented discussing the formation of Reactive Oxygen Species (ROS) species following the excitation of an electron from the valence band into the conduction band. Oil, in TiO_2 based paints degrades by scission reactions facilitated by ROS. We discussed that smaller particle size has a decrease in calculated band structure until a critical size when the band gap increases. Smaller particles also exhibit higher generation of ROS measured via methylene blue degradation. We discussed how adsorbents of small molecules can extend the response of TiO_2 into the visible spectrum and/or reduce the recombination rate. We also presented an example of an interaction between anatase and rutile crystal phases in one particle which may exist in TiO_2 based paint films. These composites show drastically increased photocatalytic activity, showing how interactions can often amplify the response of photocatalytically active materials.

We presented a model for the proposed degradation of TiO₂ based oil paints informed by previously published research. We proposed that TiO₂ pigments in oil films absorb light and generate reactive oxygen species (ROS) inside the paint film. These ROS attack the linseed oil binder, breaking the fatty acid chains, and generating volatile species such as CO₂. The loss of this material over time leads to the formation of craters on the surface of the paint film visible under SEM and at long exposures, a chalky texture visible to the naked eye. This process is distinct from other pigments which may be photo-unstable, such as ZnO. These pigments interact with the oil binder and form a complex which remains in the paint film. These complexes can change the color of the pigment or become mobile and migrate to the surface of the film. Because TiO₂ facilitated degradation is not as visible to the naked eye as color change degradation, it has received less attention and research. We present a multi-modal approach using a combination of experimental and computational methods to add to the field of research on TiO₂ based paint.

Chapter 2 of this thesis adds to the survey of 20th century paintings which may contain TiO₂ based paints. We investigated 11 Jackson Pollock paintings currently displayed at the Peggy Guggenheim Collection all painted between 1942 and 1946. We used a combination of portable Raman, portable reflection FT-IR, portable XRF, and reference sample data, to identify some of the pigments used in each painting and the binders used in the painting *Eyes in the Heat* ('46). All four paintings contained anatase TiO₂ based paint, but the later two paintings also contained areas with rutile. *The Moon Woman* showed areas of anatase TiO₂ in areas which were blue and pink. When investigated with fluorescence and UV-Vis spectroscopy, the presence of organic dyes spectroscopically similar to phalo blue and alizarin were found. These dyes may interact with TiO₂ to create a more photocatalytically active material. *Eyes in the Heat* ('46) was analyzed with reflection FT-IR spectroscopy which, together with Raman and XRF, revealed the presence of anatase/barium sulfate and rutile/zinc oxide based paints in the upper layers and lead white based paints in the lower and ground layers. The anatase based paints in *Eyes in the Heat* showed significant signs of yellowing, cracking, chalking, and delamination. Areas containing rutile did not have significant

yellowing, chalking or delamination. There was some small cracks that were visible in these areas however.

Chapter 3 investigates the effect of lower intensity light and visible light on the degradation of rutile and anatase based paints. This challenges the previous understanding that anatase is only active under UV illumination and that rutile is inactive under all light. We compared FT-IR spectra of anatase and rutile based paints, to controls of BaSO₄ and unpigmented linseed oil during photo aging under visible ($\lambda > 400$ nm) and UV+vis ($\lambda > 350$ nm) light. We showed that both TiO₂ based sets of samples showed significant formation of degradation products under both visible and UV light. TiO₂ pigmented samples showed significant increases in the spectral region 1670 – 1610 cm⁻¹ associated with $\nu(\text{C}=\text{C})$ of conjugated dienes and in the tri-glyceride ester linkage region centered at 1168 cm⁻¹. Control samples showed no change in the spectral region 1670 – 1610 cm⁻¹ and an increase over exposure of the tri-glyceride ester linkage region centered at 1168 cm⁻¹. This is counter to the current beliefs that both formulations are not active in visible light, and rutile is much less active than anatase under all lighting conditions. We suggest that interactions between the linseed oil and TiO₂ may sensitize it to visible light and allow for visible light degradation. We do note that there may be a difference between the photocatalytic activity of anatase and rutile based paints, but our analysis of degradation products with FT-IR was not sensitive to it.

Chapter 4 presents a computational model of some common molecules present in paint films with TiO₂, and investigates the interactions between one of these molecules, oleic acid, and anatase TiO₂. It also presents a study of a common red dye, alizarin carmin, and a possible interaction with anatase TiO₂. We used computation programs Gaussian 09 and Quantum Espresso to optimize the geometry of each molecule, the TiO₂ slab, and the molecule-TiO₂ complex. We then visualized the molecular orbitals of the molecule and molecule-TiO₂ complex finding that alizarin carmine may inject an electron into the TiO₂ in the excited state. This is also represented in the DOS which show the formation of a intra-band state, narrowing the band gap. We visualized the molecular

orbitals of the component acids of linseed oil (oleic, linoleic and linolenic acids) and compared the frontier orbitals. Oleic acid was then selected for study in a bidentate complex with anatase TiO_2 . The DOS of the resulting complex showed an occupied intra-band state possibly allowing the visible light sensitization of anatase TiO_2 . We proposed two pathways for degradation arising from this complex.

Chapter 5 introduces a novel method for characterizing the degradation of TiO_2 based paints. Using the Quartz Crystal Microbalance (QCM), we probed the mass per area, modulus-density product, and viscoelastic phase angle of TiO_2 pigmented films under various aging conditions. We showed the ability to track mass loss associated with UV degradation at moderate (50% RH) and high (80% RH) humidity. Under visible illumination, we showed small but noticeable decrease in mass over exposure. In most films, we were able to monitor the complex shear modulus and viscoelastic phase angle. These properties increased over time for all samples which suggests that TiO_2 facilitated degradation does not significantly alter the mechanical properties of the films at the amount of exposure achieved in our experiments. After longer times and exposures, TiO_2 facilitated degradation may cause significant stiffening in the paint film, and should be further investigated.

References

- [1] M. Pelaez, N. T. Nolan, S. C. Pillai, M. K. Seery, P. Falaras, A. G. Kontos, P. S. Dunlop, J. W. Hamilton, J. Byrne, K. O'Shea, M. H. Entezari, D. D. Dionysiou, A review on the visible light active titanium dioxide photocatalysts for environmental applications, *Applied Catalysis B: Environmental* 125 (2012) 331–349. doi:10.1016/j.apcatb.2012.05.036.
- [2] E. W. Fitzhugh, *Artists' Pigments: A Handbook of Their History and Characteristics*, National gallery of art, Washington, 1997.
- [3] A. L. Linsebigler, G. Lu, J. T. Yates, Photocatalysis on TiO₂ Surfaces: Principles, Mechanisms, and Selected Results, *Chemical Reviews* 95 (3) (1995) 735–758. doi:10.1021/cr00035a013.
- [4] M. Reyes-Estebanez, B. O. Ortega-Morales, M. Chan-Bacab, C. Granados-Echegoyen, J. C. Camacho-Chab, J. E. Pereañez-Sacarias, C. Gaylarde, Antimicrobial engineered nanoparticles in the built cultural heritage context and their ecotoxicological impact on animals and plants: A brief review, *Heritage Science* 6 (1). doi:10.1186/s40494-018-0219-9.
- [5] S. Morsch, B. A. van Driel, K. J. van den Berg, J. Dik, Investigating the Photocatalytic Degradation of Oil Paint using ATR-IR and AFM-IR, *ACS Applied Materials & Interfaces* 9 (11) (2017) 10169–10179. doi:10.1021/acsami.7b00638.
- [6] F. De Angelis, C. Di Valentin, S. Fantacci, A. Vittadini, A. Selloni, Theoretical Studies on Anatase and Less Common TiO₂ Phases: Bulk, Surfaces, and Nanomaterials, *Chemical Reviews* 114 (19) (2014) 9708–9753. doi:10.1021/cr500055q.
- [7] M. Bacci, M. Picollo, G. Trumpy, M. Tsukada, D. Kunzelman, Non-Invasive Identification of White Pigments on 20Th-Century Oil Paintings by Using Fiber Optic Reflectance Spectroscopy, *Journal of the American Institute for Conservation* 46 (1) (2007) 27–37. doi:10.1179/019713607806112413.
- [8] V. Etacheri, C. Di Valentin, J. Schneider, D. Bahnemann, S. C. Pillai, Visible-light activation of TiO₂ photocatalysts: Advances in theory and experiments, *Journal of Photochemistry and Photobiology C: Photochemistry Reviews* 25 (2015) 1–29. doi:10.1016/j.jphotochemrev.2015.08.003.
- [9] F. Rosi, C. Grazia, R. Fontana, F. Gabrieli, L. Pensabene Buemi, E. Pampaloni, A. Romani, C. Stringari, C. Miliani, Disclosing Jackson Pollock's palette in *Alchemy* (1947) by non-invasive spectroscopies, *Heritage Science* 4 (1). doi:10.1186/s40494-016-0089-y.
- [10] A. Martins, J. Coddington, G. Van der Snickt, B. van Driel, C. McGlinchey, D. Dahlberg, K. Janssens, J. Dik, Jackson Pollock's Number 1A, 1948: A non-invasive study using macro-x-ray fluorescence mapping (MA-XRF) and multivariate curve resolution-

- alternating least squares (MCR-ALS) analysis, *Heritage Science* 4 (1). doi:10.1186/s40494-016-0105-2.
- [11] B. A. van Driel, K. J. van den Berg, J. Gerretzen, J. Dik, The white of the 20th century: An explorative survey into Dutch modern art collections, *Herit Sci* 6 (1) (2018) 16. doi:10.1186/s40494-018-0183-4.
- [12] B. van Driel, Titanium Dioxide Friend or Foe, Ph.D. thesis, Delft University of Technology (May 2019).
- [13] A. Martins, C. Albertson, C. McGlinchey, J. Dik, Piet Mondrian's Broadway Boogie Woogie: Non invasive analysis using macro X-ray fluorescence mapping (MA-XRF) and multivariate curve resolution-alternating least square (MCR-ALS), *Heritage Science* 4 (1) (2016) 22. doi:10.1186/s40494-016-0091-4.
- [14] Á. Morales-García, R. Valero, F. Illas, An Empirical, yet Practical Way To Predict the Band Gap in Solids by Using Density Functional Band Structure Calculations, *The Journal of Physical Chemistry C* 121 (34) (2017) 18862–18866. doi:10.1021/acs.jpcc.7b07421.
- [15] F. De Angelis, S. Fantacci, A. Selloni, M. K. Nazeeruddin, M. Grätzel, First-Principles Modeling of the Adsorption Geometry and Electronic Structure of Ru(II) Dyes on Extended TiO₂ Substrates for Dye-Sensitized Solar Cell Applications, *The Journal of Physical Chemistry C* 114 (13) (2010) 6054–6061. doi:10.1021/jp911663k.
- [16] K. E. Engates, H. J. Shipley, Adsorption of Pb, Cd, Cu, Zn, and Ni to titanium dioxide nanoparticles: Effect of particle size, solid concentration, and exhaustion, *Environmental Science and Pollution Research* 18 (3) (2011) 386–395. doi:10.1007/s11356-010-0382-3.
- [17] M. Setvin, J. Hulva, H. Wang, T. Simschitz, M. Schmid, G. S. Parkinson, C. Di Valentin, A. Selloni, U. Diebold, Formaldehyde Adsorption on the Anatase TiO₂ (101) Surface: Experimental and Theoretical Investigation, *The Journal of Physical Chemistry C* 121 (16) (2017) 8914–8922. doi:10.1021/acs.jpcc.7b01434.
- [18] M. Setvin, X. Shi, J. Hulva, T. Simschitz, G. S. Parkinson, M. Schmid, C. Di Valentin, A. Selloni, U. Diebold, Methanol on Anatase TiO₂ (101): Mechanistic Insights into Photocatalysis, *ACS Catalysis* 7 (10) (2017) 7081–7091. doi:10.1021/acscatal.7b02003.
- [19] P. Prajongtatt, S. Suramitr, S. Nokbin, K. Nakajima, K. Mitsuke, S. Hannongbua, Density functional theory study of adsorption geometries and electronic structures of azo-dye-based molecules on anatase TiO₂ surface for dye-sensitized solar cell applications, *Journal of Molecular Graphics and Modelling* 76 (2017) 551–561. doi:10.1016/j.jmgm.2017.06.002.

- [20] M. Nilsing, P. Persson, L. Ojamäe, Anchor group influence on molecule–metal oxide interfaces: Periodic hybrid DFT study of pyridine bound to TiO₂ via carboxylic and phosphonic acid, *Chemical Physics Letters* 415 (4-6) (2005) 375–380. doi:10.1016/j.cplett.2005.08.154.
- [21] A. Mattsson, L. Österlund, Adsorption and Photoinduced Decomposition of Acetone and Acetic Acid on Anatase, Brookite, and Rutile TiO₂ Nanoparticles, *The Journal of Physical Chemistry C* 114 (33) (2010) 14121–14132. doi:10.1021/jp103263n.
- [22] V. Etacheri, M. K. Seery, S. J. Hinder, S. C. Pillai, Oxygen Rich Titania: A Dopant Free, High Temperature Stable, and Visible-Light Active Anatase Photocatalyst, *Adv. Funct. Mater.* 21 (19) (2011) 3744–3752. doi:10.1002/adfm.201100301.
- [23] Z. Zhang, J. T. Yates, Band Bending in Semiconductors: Chemical and Physical Consequences at Surfaces and Interfaces, *Chemical Reviews* 112 (10) (2012) 5520–5551. doi:10.1021/cr3000626.
- [24] J. Schneider, M. Matsuoka, M. Takeuchi, J. Zhang, Y. Horiuchi, M. Anpo, D. W. Bahnemann, Understanding TiO₂ Photocatalysis: Mechanisms and Materials, *Chemical Reviews* 114 (19) (2014) 9919–9986. doi:10.1021/cr5001892.
- [25] S. Auvinen, M. Alatalo, H. Haario, J.-P. Jalava, R.-J. Lamminmäki, Size and Shape Dependence of the Electronic and Spectral Properties in TiO₂ Nanoparticles, *The Journal of Physical Chemistry C* 115 (17) (2011) 8484–8493. doi:10.1021/jp112114p.
- [26] C. B. Almquist, P. Biswas, Role of Synthesis Method and Particle Size of Nanostructured TiO₂ on Its Photoactivity, *Journal of Catalysis* 212 (2) (2002) 145–156. doi:10.1006/jcat.2002.3783.
- [27] H. Gerischer, Photocatalysis in aqueous solution with small TiO₂ particles and the dependence of the quantum yield on particle size and light intensity, *Electrochimica Acta* 40 (10) (1995) 1277–1281. doi:10.1016/0013-4686(95)00058-M.
- [28] N. Xu, Z. Shi, Y. Fan, J. Dong, J. Shi, M. Z.-C. Hu, Effects of Particle Size of TiO₂ on Photocatalytic Degradation of Methylene Blue in Aqueous Suspensions, *Ind. Eng. Chem. Res.* 38 (2) (1999) 373–379. doi:10.1021/ie980378u.
- [29] G. Li, K. A. Gray, The solid–solid interface: Explaining the high and unique photocatalytic reactivity of TiO₂-based nanocomposite materials, *Chemical Physics* 339 (1-3) (2007) 173–187. doi:10.1016/j.chemphys.2007.05.023.
- [30] M. Nolan, N. A. Deskins, K. C. Schwartzberg, K. A. Gray, Local Interfacial Structure Influences Charge Localization in Titania Composites: Beyond the Band Alignment Paradigm, *The Journal of Physical Chemistry C* 120 (3) (2016) 1808–1815. doi:10.1021/acs.jpcc.5b12326.

- [31] Y. Won, K. Schwartzberg, K. A. Gray, TiO₂-based transparent coatings create self-cleaning surfaces, *Chemosphere* 208 (2018) 899–906. doi:10.1016/j.chemosphere.2018.06.014.
- [32] G. Li, N. M. Dimitrijevic, L. Chen, J. M. Nichols, T. Rajh, K. A. Gray, The Important Role of Tetrahedral Ti⁴⁺ Sites in the Phase Transformation and Photocatalytic Activity of TiO₂ Nanocomposites, *Journal of the American Chemical Society* 130 (16) (2008) 5402–5403. doi:10.1021/ja711118u.
- [33] C. Wu, Y. Yue, X. Deng, W. Hua, Z. Gao, Investigation on the synergetic effect between anatase and rutile nanoparticles in gas-phase photocatalytic oxidations, *Catalysis Today* 93–95 (2004) 863–869. doi:10.1016/j.cattod.2004.06.087.
- [34] A. G. Agrios, K. A. Gray, E. Weitz, Photocatalytic Transformation of 2,4,5-Trichlorophenol on TiO₂ under Sub-Band-Gap Illumination, *Langmuir* 19 (4) (2003) 1402–1409. doi:10.1021/1a026397x.
- [35] M. Lazzari, O. Chiantore, Drying and oxidative degradation of linseed oil, *Polymer Degradation and Stability* 65 (2) (1999) 303–313. doi:10.1016/S0141-3910(99)00020-8.
- [36] M. R. Hoffmann, S. T. Martin, W. Choi, D. W. Bahnemann, Environmental Applications of Semiconductor Photocatalysis, *Chem. Rev.* 95 (1) (1995) 69–96. doi:10.1021/cr00033a004.
- [37] C. Anastasescu, C. Negrila, D. G. Angelescu, I. Atkinson, M. Anastasescu, N. Spataru, M. Zaharescu, I. Balint, Particularities of photocatalysis and formation of reactive oxygen species on insulators and semiconductors: Cases of SiO₂, TiO₂ and their composite SiO₂-TiO₂, *Catal. Sci. Technol.* 8 (21) (2018) 5657–5668. doi:10.1039/C8CY00991K.
- [38] P. P. Fu, Q. Xia, H.-M. Hwang, P. C. Ray, H. Yu, Mechanisms of nanotoxicity: Generation of reactive oxygen species, *Journal of Food and Drug Analysis* 22 (1) (2014) 64–75. doi:10.1016/j.jfda.2014.01.005.
- [39] B. van Driel, T. Wezendonk, K. van den Berg, P. Kooyman, J. Gascon, J. Dik, Determination of early warning signs for photocatalytic degradation of titanium white oil paints by means of surface analysis, *Spectrochimica Acta Part A: Molecular and Biomolecular Spectroscopy* 172 (2017) 100–108. doi:10.1016/j.saa.2016.04.026.
- [40] W. Anaf, O. Schalm, K. Janssens, K. De Wael, Understanding the (in)stability of semiconductor pigments by a thermodynamic approach, *Dyes and Pigments* 113 (2015) 409–415. doi:10.1016/j.dyepig.2014.09.015.
- [41] B. A. van Driel, K. J. van den Berg, M. Smout, N. Dekker, P. J. Kooyman, J. Dik, Investigating the effect of artists' paint formulation on degradation rates of TiO₂-based oil paints, *Heritage Science* 6 (1) (2018) 21. doi:10.1186/s40494-018-0185-2.

- [42] B. van Driel, P. Kooyman, K. van den Berg, A. Schmidt-Ott, J. Dik, A quick assessment of the photocatalytic activity of TiO₂ pigments — From lab to conservation studio!, *Microchemical Journal* 126 (2016) 162–171. doi:10.1016/j.microc.2015.11.048.
- [43] M. Franquelo, A. Duran, J. Castaing, D. Arquillo, J. Perez-Rodriguez, XRF, μ -XRD and μ -spectroscopic techniques for revealing the composition and structure of paint layers on polychrome sculptures after multiple restorations, *Talanta* 89 (2012) 462–469. doi:10.1016/j.talanta.2011.12.063.
- [44] M. Garrote, M. Robador, J. Perez-Rodriguez, Analytical investigation of Mudéjar polychrome on the carpentry in the Casa de Pilatos palace in Seville using non-destructive XRF and complementary techniques, *Spectrochimica Acta Part A: Molecular and Biomolecular Spectroscopy* 173 (2017) 279–291. doi:10.1016/j.saa.2016.09.027.
- [45] C. Miliani, F. Rosi, B. G. Brunetti, A. Sgamellotti, In Situ Noninvasive Study of Artworks: The MOLAB Multitechnique Approach, *Acc. Chem. Res.* 43 (6) (2010) 728–738. doi:10.1021/ar100010t.
- [46] C. Ricci, C. Miliani, B. G. Brunetti, A. Sgamellotti, Non-invasive identification of surface materials on marble artifacts with fiber optic mid-FTIR reflectance spectroscopy, *Talanta* 69 (5) (2006) 1221–1226. doi:10.1016/j.talanta.2005.12.054.
- [47] F. Rosi, A. Daveri, P. Moretti, B. G. Brunetti, C. Miliani, Interpretation of mid and near-infrared reflection properties of synthetic polymer paints for the non-invasive assessment of binding media in twentieth-century pictorial artworks, *Microchemical Journal* 124 (2016) 898–908. doi:10.1016/j.microc.2015.08.019.
- [48] P. Brouwer, *Theory of XEF: Getting Acquainted with the Principles.*, PANalytical BV, Almelo, 2003.
- [49] P. Larkin, *Infrared and Raman Spectroscopy: Principles and Spectral Interpretation*, Elsevier, 2017.
- [50] D. Lin-Vien, N. B. Colthup, W. G. Fateley, J. G. Grasselli, *The Handbook of Infrared and Raman Characteristic Frequencies of Organic Molecules*, Elsevier, 1991.
- [51] R. Mastrangelo, D. Chelazzi, G. Poggi, E. Fratini, L. Pensabene Buemi, M. L. Petruzzellis, P. Baglioni, Twin-chain polymer hydrogels based on poly(vinyl alcohol) as new advanced tool for the cleaning of modern and contemporary art, *Proc. Natl. Acad. Sci. U.S.A.* 117 (13) (2020) 7011–7020. doi:10.1073/pnas.1911811117.
- [52] L. Pensabene Buemi, M. L. Petruzzellis, D. Chelazzi, M. Baglioni, R. Mastrangelo, R. Giorgi, P. Baglioni, Twin-chain polymer networks loaded with nanostructured fluids for the selective removal of a non-original varnish from Picasso's "L'Atelier" at

- the Peggy Guggenheim Collection, Venice, *Herit Sci* 8 (1) (2020) 77. doi:10.1186/s40494-020-00420-0.
- [53] R. Mazzeo, S. Prati, M. Quaranta, E. Joseph, E. Kendix, M. Galeotti, Attenuated total reflection micro FTIR characterisation of pigment–binder interaction in reconstructed paint films, *Analytical and Bioanalytical Chemistry* 392 (1-2) (2008) 65–76. doi:10.1007/s00216-008-2126-5.
- [54] M. P. Sáez-Pérez, J. Rodríguez-Gordillo, J. A. Durán-Suárez, Synthetic white pigments (white titanium and white zinc) in different binding media. Influence of environmental agents, *Construction and Building Materials* 114 (2016) 151–161. doi:10.1016/j.conbuildmat.2016.03.140.
- [55] K. Helwig, J. Poulin, M.-C. Corbeil, E. Moffatt, D. Duguay, Conservation Issues in Several Twentieth-Century Canadian Oil Paintings: The Role of Zinc Carboxylate Reaction Products, in: *Issues in Contemporary Oil Paint*, Springer, Cham, 2014, pp. 167–184. doi:10.1007/978-3-319-10100-2_11.
- [56] G. Osmond, Zinc White and the Influence of Paint Composition for Stability in Oil Based Media, in: *Issues in Contemporary Oil Paint*, Springer, Cham, 2014, pp. 263–281. doi:10.1007/978-3-319-10100-2_18.
- [57] F. Casadio, K. Keune, P. Noble, A. Van Loon, E. Hendriks, S. A. Centeno, G. Osmond (Eds.), *Metal Soaps in Art: Conservation and Research*, Cultural Heritage Science, Springer International Publishing, Cham, 2019. doi:10.1007/978-3-319-90617-1.
- [58] F. Gabrieli, F. Rosi, A. Vichi, L. Cartechini, L. Pensabene Buemi, S. G. Kazarian, C. Miliani, Revealing the Nature and Distribution of Metal Carboxylates in Jackson Pollock's *Alchemy* (1947) by Micro-Attenuated Total Reflection FT-IR Spectroscopic Imaging, *Analytical Chemistry* 89 (2) (2017) 1283–1289. doi:10.1021/acs.analchem.6b04065.
- [59] A. Artesani, Zinc oxide instability in drying oil paint, *Materials Chemistry and Physics* 255 (2020) 123640. doi:10.1016/j.matchemphys.2020.123640.
- [60] T. Tong, K. Fang, S. A. Thomas, J. J. Kelly, K. A. Gray, J.-F. Gaillard, Chemical Interactions between Nano-ZnO and Nano-TiO₂ in a Natural Aqueous Medium, *Environmental Science & Technology* 48 (14) (2014) 7924–7932. doi:10.1021/es501168p.
- [61] L. Baij, L. Chassouant, J. J. Hermans, K. Keune, P. D. Iedema, The concentration and origins of carboxylic acid groups in oil paint, *RSC Advances* 9 (61) (2019) 35559–35564. doi:10.1039/C9RA06776K.
- [62] J. J. Hermans, K. Keune, A. van Loon, P. D. Iedema, The crystallization of metal soaps and fatty acids in oil paint model systems, *Physical Chemistry Chemical Physics* 18 (16) (2016) 10896–10905. doi:10.1039/C6CP00487C.

- [63] C. Sessa, R. Jiménez de Garnica, F. Rosi, R. Fontana, J. F. Garcia, A Study of Picasso's Painting Materials and Techniques in Six of His Early Portraits, *Journal of the American Institute for Conservation* 55 (4) (2016) 198–216. doi:10.1080/01971360.2016.1235438.
- [64] F. Rosi, C. Miliani, C. Clementi, K. Kahrim, F. Presciutti, M. Vagnini, V. Manuali, A. Daveri, L. Cartechini, B. G. Brunetti, A. Sgamellotti, An integrated spectroscopic approach for the non-invasive study of modern art materials and techniques, *Applied Physics A* 100 (3) (2010) 613–624. doi:10.1007/s00339-010-5744-7.
- [65] C. Di Valentin, A. Tilocca, A. Selloni, T. J. Beck, A. Klust, M. Batzill, Y. Losovyj, U. Diebold, Adsorption of Water on Reconstructed Rutile TiO₂ (011)-(2×1): TiO Double Bonds and Surface Reactivity, *Journal of the American Chemical Society* 127 (27) (2005) 9895–9903. doi:10.1021/ja0511624.
- [66] X. Zhang, Photocatalytical effect of TiO₂ pigments on the surface of paint films.
- [67] T. Luttrell, S. Halpegamage, J. Tao, A. Kramer, E. Sutter, M. Batzill, Why is anatase a better photocatalyst than rutile? - Model studies on epitaxial TiO₂ films, *Scientific Reports* 4 (1). doi:10.1038/srep04043.
- [68] University of Pitesti, E. M. Modan, Review on the titanium oxide for catalytic applications, University of Pitesti. *Scientific Bulletin - Automotive Series* 29 (1) (2019) 1–10. doi:10.26825/bup.ar.2019.007.
- [69] X.-Q. Gong, A. Selloni, A. Vittadini, Density Functional Theory Study of Formic Acid Adsorption on Anatase TiO₂ (001): Geometries, Energetics, and Effects of Coverage, Hydration, and Reconstruction, *The Journal of Physical Chemistry B* 110 (6) (2006) 2804–2811. doi:10.1021/jp056572t.
- [70] Y. Gurdal, M. Iannuzzi, DFT-based Theoretical Simulations for Photocatalytic Applications Using TiO₂, in: M. Janus (Ed.), *Titanium Dioxide*, InTech, 2017. doi:10.5772/intechopen.68976.
- [71] M. Nilsing, S. Lunell, P. Persson, L. Ojamäe, Phosphonic acid adsorption at the TiO₂ anatase (101) surface investigated by periodic hybrid HF-DFT computations, *Surface Science* 582 (1-3) (2005) 49–60. doi:10.1016/j.susc.2005.02.044.
- [72] M. Yao, Y. Ji, H. Wang, Z. Ao, G. Li, T. An, Adsorption Mechanisms of Typical Carbonyl-Containing Volatile Organic Compounds on Anatase TiO₂ (001) Surface: A DFT Investigation, *The Journal of Physical Chemistry C* 121 (25) (2017) 13717–13722. doi:10.1021/acs.jpcc.7b02964.
- [73] A. Amat, C. Miliani, A. Romani, S. Fantacci, DFT/TDDFT investigation on the UV-vis absorption and fluorescence properties of alizarin dye, *Physical Chemistry Chemical Physics* 17 (9) (2015) 6374–6382. doi:10.1039/C4CP04728A.

- [74] L. de Viguierie, P. Payard, E. Portero, P. Walter, M. Cotte, The drying of linseed oil investigated by Fourier transform infrared spectroscopy: Historical recipes and influence of lead compounds, *Progress in Organic Coatings* 93 (2016) 46–60. doi:10.1016/j.porgcoat.2015.12.010.
- [75] R. J. Meilunas, J. G. Bentsen, A. Steinb, Analysis of Aged Paint Binders by FTIR Spectroscopy (2021) 20.
- [76] J. van den Berg, K. van den Berg, J. Boon, Determination of the degree of hydrolysis of oil paint samples using a two-step derivatisation method and on-column GC/MS, *Progress in Organic Coatings* 41 (1-3) (2001) 143–155. doi:10.1016/S0300-9440(01)00140-0.
- [77] E. P. van Dam, K. J. van den Berg, A. N. Proaño Gaibor, M. van Bommel, Analysis of triglyceride degradation products in drying oils and oil paints using LC–ESI-MS, *International Journal of Mass Spectrometry* 413 (2017) 33–42. doi:10.1016/j.ijms.2016.09.004.
- [78] P. Fjällström, B. Andersson, C. Nilsson, K. Andersson, Drying of linseed oil paints: A laboratory study of aldehyde emissions, *Industrial Crops and Products* 16 (3) (2002) 173–184. doi:10.1016/S0926-6690(02)00035-3.
- [79] S. Zumbühl, N. C. Scherrer, U. Eggenberger, Derivatization Technique to Increase the Spectral Selectivity of Two-Dimensional Fourier Transform Infrared Focal Plane Array Imaging: Analysis of Binder Composition in Aged Oil and Tempera Paint, *Applied Spectroscopy* 68 (4) (2014) 458–465. doi:10.1366/13-07280.
- [80] I. Bonaduce, L. Carlyle, M. P. Colombini, C. Duce, C. Ferrari, E. Ribechini, P. Selleri, M. R. Tiné, New Insights into the Ageing of Linseed Oil Paint Binder: A Qualitative and Quantitative Analytical Study, *PLoS ONE* 7 (11) (2012) e49333. doi:10.1371/journal.pone.0049333.
- [81] B. M. Berto, R. K. Garcia, G. D. Fernandes, D. Barrera-Arellano, G. G. Pereira, Linseed oil: Characterization and study of its oxidative degradation, *Grasas y Aceites* 71 (1) (2020) 337. doi:10.3989/gya.1059182.
- [82] I. N. Hayati, Y. B. C. Man, C. P. Tan, I. N. Aini, Monitoring peroxide value in oxidized emulsions by Fourier transform infrared spectroscopy, *Eur. J. Lipid Sci. Technol.* 107 (12) (2005) 886–895. doi:10.1002/ejlt.200500241.
- [83] E. Ioakimoglou, S. Boyatzis, P. Argitis, A. Fostiridou, K. Papapanagiotou, N. Yannovits, Thin-Film Study on the Oxidation of Linseed Oil in the Presence of Selected Copper Pigments, *Chemistry of Materials* 11 (8) (1999) 2013–2022. doi:10.1021/cm9806578.
- [84] Juita, B. Z. Dlugogorski, E. M. Kennedy, J. C. Mackie, Low temperature oxidation of linseed oil: A review, *Fire Science Reviews* 1 (1) (2012) 3. doi:10.1186/2193-0414-1-3.

- [85] S. Boyatzis, E. Ioakimoglou, P. Argitis, UV exposure and temperature effects on curing mechanisms in thin linseed oil films: Spectroscopic and chromatographic studies, *Journal of Applied Polymer Science* 84 (5) (2002) 936–949. doi:10.1002/app.10117.
- [86] A. Dupuis, F.-X. Perrin, A. Ulloa Torres, J.-P. Habas, L. Belec, J.-F. Chailan, Photo-oxidative degradation behavior of linseed oil based epoxy resin, *Polymer Degradation and Stability* 135 (2017) 73–84. doi:10.1016/j.polymdegradstab.2016.11.021.
- [87] O. Carp, Photoinduced reactivity of titanium dioxide, *Progress in Solid State Chemistry* 32 (1-2) (2004) 33–177. doi:10.1016/j.progsolidstchem.2004.08.001.
- [88] C. B. Lauridsen, J. Sanyova, K. P. Simonsen, Analytical study of modern paint layers on metal knight shields: The use and effect of Titanium white, *Spectrochimica Acta Part A: Molecular and Biomolecular Spectroscopy* 124 (2014) 638–645. doi:10.1016/j.saa.2014.01.077.
- [89] G. Irick, G. C. Newland, R. H. S. Wang, Effect of Metal Salts on the Photoactivity of Titanium Dioxide: Stabilization and Sensitization Processes, in: S. P. Pappas, F. H. Winslow (Eds.), *Photodegradation and Photostabilization of Coatings*, Vol. 151, AMERICAN CHEMICAL SOCIETY, WASHINGTON, D. C., 1981, pp. 147–162. doi:10.1021/bk-1981-0151.ch011.
- [90] M. Buchholz, M. Xu, H. Noei, P. Weidler, A. Nefedov, K. Fink, Y. Wang, C. Wöll, Interaction of carboxylic acids with rutile TiO₂(110): IR-investigations of terephthalic and benzoic acid adsorbed on a single crystal substrate, *Surface Science* 643 (2016) 117–123. doi:10.1016/j.susc.2015.08.006.
- [91] S. A. Haque, Y. Tachibana, R. L. Willis, J. E. Moser, M. Grätzel, D. R. Klug, J. R. Durrant, Parameters Influencing Charge Recombination Kinetics in Dye-Sensitized Nanocrystalline Titanium Dioxide Films, *The Journal of Physical Chemistry B* 104 (3) (2000) 538–547. doi:10.1021/jp991085x.
- [92] P. Christopher, H. Xin, A. Marimuthu, S. Linic, Singular characteristics and unique chemical bond activation mechanisms of photocatalytic reactions on plasmonic nanostructures, *Nature Materials* 11 (12) (2012) 1044–1050. doi:10.1038/nmat3454.
- [93] A. E. Jacobsen, Titanium Dioxide Pigments: Correlation between Photochemical Reactivity and Chalking., *Industrial & Engineering Chemistry* 41 (3) (1949) 523–526. doi:10.1021/ie50471a018.
- [94] H. G. Voltz, G. Kaempfer, H. G. Fitzky, A. Klaeren, The Chemical Nature of Chalking in the Presence of Titanium Dioxide Pigments, *Photodegradation and Photostabilization of Coatings* 151 (Chapter 12) (1981) 163–182.

- [95] J. Gong, J. Liang, K. Sumathy, Review on dye-sensitized solar cells (DSSCs): Fundamental concepts and novel materials, *Renewable and Sustainable Energy Reviews* 16 (8) (2012) 5848–5860. doi:10.1016/j.rser.2012.04.044.
- [96] S. Fantacci, A. Amat, A. Sgamellotti, Computational Chemistry Meets Cultural Heritage: Challenges and Perspectives, *Accounts of Chemical Research* 43 (6) (2010) 802–813. doi:10.1021/ar100012b.
- [97] A. Hagfeldt, G. Boschloo, L. Sun, L. Kloo, H. Pettersson, Dye-Sensitized Solar Cells, *Chemical Reviews* 110 (11) (2010) 6595–6663. doi:10.1021/cr900356p.
- [98] F. De Angelis, S. Fantacci, E. Mosconi, M. K. Nazeeruddin, M. Grätzel, Absorption Spectra and Excited State Energy Levels of the N719 Dye on TiO₂ in Dye-Sensitized Solar Cell Models, *The Journal of Physical Chemistry C* 115 (17) (2011) 8825–8831. doi:10.1021/jp111949a.
- [99] M. Pastore, S. Fantacci, F. De Angelis, Ab Initio Determination of Ground and Excited State Oxidation Potentials of Organic Chromophores for Dye-Sensitized Solar Cells, *The Journal of Physical Chemistry C* 114 (51) (2010) 22742–22750. doi:10.1021/jp1088965.
- [100] P. Hohenberg, W. Kohn, Inhomogeneous Electron Gas, *Physical Review* 136 (3B) (1964) B864–B871. doi:10.1103/PhysRev.136.B864.
- [101] W. Kohn, L. J. Sham, Self-Consistent Equations Including Exchange and Correlation Effects, *Physical Review* 140 (4A) (1965) A1133–A1138. doi:10.1103/PhysRev.140.A1133.
- [102] A. Amat, Materials of Interest in the Cultural Heritage field: Theoretical Investigations, Ph.D. thesis, Università degli Studi di Perugia (2009).
- [103] D. Vanderbilt, Soft self-consistent pseudopotentials in a generalized eigenvalue formalism, *Physical Review B* 41 (11) (1990) 7892–7895. doi:10.1103/PhysRevB.41.7892.
- [104] W. Koch, *A Chemist's Guide to Density Functional Theory*, 2nd Edition, Wiley-VCH, Weinheim ; New York, 2001.
- [105] W. R. Duncan, W. M. Stier, O. V. Prezhdo, Ab Initio Nonadiabatic Molecular Dynamics of the Ultrafast Electron Injection across the Alizarin-TiO₂ Interface, *Journal of the American Chemical Society* 127 (21) (2005) 7941–7951. doi:10.1021/ja042156v.
- [106] W. R. Duncan, O. V. Prezhdo, Electronic Structure and Spectra of Catechol and Alizarin in the Gas Phase and Attached to Titanium, *The Journal of Physical Chemistry B* 109 (1) (2005) 365–373. doi:10.1021/jp046342z.

- [107] W. R. Duncan, C. F. Craig, O. V. Prezhdo, Time-Domain *ab Initio* Study of Charge Relaxation and Recombination in Dye-Sensitized TiO₂, *J. Am. Chem. Soc.* 129 (27) (2007) 8528–8543. doi:10.1021/ja0707198.
- [108] R. Sánchez-de-Armas, J. Oviedo López, M. A. San-Miguel, J. F. Sanz, P. Ordejón, M. Pruneda, Real-Time TD-DFT Simulations in Dye Sensitized Solar Cells: The Electronic Absorption Spectrum of Alizarin Supported on TiO₂ Nanoclusters, *J. Chem. Theory Comput.* 6 (9) (2010) 2856–2865. doi:10.1021/ct100289t.
- [109] R. Sánchez-de-Armas, M. San-Miguel, J. Oviedo, J. F. Sanz, Direct vs. indirect mechanisms for electron injection in DSSC: Catechol and alizarin, *Computational and Theoretical Chemistry* 975 (1-3) (2011) 99–105. doi:10.1016/j.comptc.2011.01.010.
- [110] P. Giannozzi, S. Baroni, N. Bonini, M. Calandra, R. Car, C. Cavazzoni, D. Ceresoli, G. L. Chiarotti, M. Cococcioni, I. Dabo, A. D. Corso, S. de Gironcoli, S. Fabris, G. Fratesi, R. Gebauer, U. Gerstmann, C. Gougoussis, A. Kokalj, M. Lazzeri, L. Martin-Samos, N. Marzari, F. Mauri, R. Mazzarello, S. Paolini, A. Pasquarello, L. Paulatto, C. Sbraccia, S. Scandolo, G. Sclauzero, A. P. Seitsonen, A. Smogunov, P. Umari, R. M. Wentzcovitch, QUANTUM ESPRESSO: A modular and open-source software project for quantum simulations of materials, *Journal of Physics: Condensed Matter* 21 (39) (2009) 395502 (19pp).
- [111] A. Vittadini, A. Selloni, F. P. Rotzinger, M. Grätzel, Structure and Energetics of Water Adsorbed at TiO₂ Anatase (101) and (001) Surfaces, *Physical Review Letters* 81 (14) (1998) 2954–2957. doi:10.1103/PhysRevLett.81.2954.
- [112] A. Dal Corso, Pseudopotentials periodic table: From H to Pu, *Computational Materials Science* 95 (2014) 337–350. doi:10.1016/j.commatsci.2014.07.043.
- [113] M. D. Hanwell, D. E. Curtis, D. C. Lonie, T. Vandermeersch, E. Zurek, G. R. Hutchison, Avogadro: An advanced semantic chemical editor, visualization, and analysis platform, *Journal of Cheminformatics* 4 (1) (2012) 17. doi:10.1186/1758-2946-4-17.
- [114] M. J. Frisch, G. W. Trucks, H. B. Schlegel, G. E. Scuseria, M. A. Robb, J. R. Cheeseman, G. Scalmani, V. Barone, G. A. Petersson, H. Nakatsuji, X. Li, M. Caricato, A. V. Marenich, J. Bloino, B. G. Janesko, R. Gomperts, B. Mennucci, H. P. Hratchian, J. V. Ortiz, A. F. Izmaylov, J. L. Sonnenberg, Williams, F. Ding, F. Lipparini, F. Egidi, J. Goings, B. Peng, A. Petrone, T. Henderson, D. Ranasinghe, V. G. Zakrzewski, J. Gao, N. Rega, G. Zheng, W. Liang, M. Hada, M. Ehara, K. Toyota, R. Fukuda, J. Hasegawa, M. Ishida, T. Nakajima, Y. Honda, O. Kitao, H. Nakai, T. Vreven, K. Throssell, J. A. Montgomery Jr., J. E. Peralta, F. Ogliaro, M. J. Bearpark, J. J. Heyd, E. N. Brothers, K. N. Kudin, V. N. Staroverov, T. A. Keith, R. Kobayashi, J. Normand, K. Raghavachari, A. P. Rendell, J. C. Burant, S. S. Iyengar, J. Tomasi, M. Cossi, J. M. Millam, M. Klene, C. Adamo, R. Cammi, J. W. Ochterski, R. L. Martin, K. Morokuma, O. Farkas, J. B. Foresman, D. J. Fox, *Gaussian 16 Rev. B.01* (2016).

- [115] A. D. Becke, Density-functional thermochemistry. III. The role of exact exchange, *The Journal of Chemical Physics* 98 (7) (1993) 5648–5652. doi:10.1063/1.464913.
- [116] S. H. Vosko, L. Wilk, M. Nusair, Accurate spin-dependent electron liquid correlation energies for local spin density calculations: A critical analysis, *Canadian Journal of Physics* 58 (8) (1980) 1200–1211. doi:10.1139/p80-159.
- [117] P. J. Stephens, F. J. Devlin, C. F. Chabalowski, M. J. Frisch, Ab Initio Calculation of Vibrational Absorption and Circular Dichroism Spectra Using Density Functional Force Fields, *The Journal of Physical Chemistry* 98 (45) (1994) 11623–11627. doi:10.1021/j100096a001.
- [118] G. A. Petersson, M. A. Al-Laham, A complete basis set model chemistry. II. Open-shell systems and the total energies of the first-row atoms, *The Journal of Chemical Physics* 94 (9) (1991) 6081–6090. doi:10.1063/1.460447.
- [119] J. P. Perdew, K. Burke, M. Ernzerhof, Generalized Gradient Approximation Made Simple, *Physical Review Letters* 77 (18) (1996) 3865–3868. doi:10.1103/PhysRevLett.77.3865.
- [120] Y. Orlova, R. E. Harmon, L. J. Broadbelt, P. D. Iedema, Review of the kinetics and simulations of linseed oil autoxidation, *Progress in Organic Coatings* 151 (2021) 106041. doi:10.1016/j.porgcoat.2020.106041.
- [121] P. McGill, H. Idriss, DFT study of carboxylic acids modes of adsorption on rutile TiO₂(011) surfaces, *Surface Science* 602 (24) (2008) 3688–3695. doi:10.1016/j.susc.2008.10.010.
- [122] A. V. Ignatchenko, Density Functional Theory Study of Carboxylic Acids Adsorption and Enolization on Monoclinic Zirconia Surfaces, *The Journal of Physical Chemistry C* 115 (32) (2011) 16012–16018. doi:10.1021/jp203381h.
- [123] S. Cho, W. Choi, Solid-phase photocatalytic degradation of PVC–TiO₂ polymer composites, *Journal of Photochemistry and Photobiology A: Chemistry* 143 (2-3) (2001) 221–228. doi:10.1016/S1010-6030(01)00499-3.
- [124] L. F. Sturdy, A. Yee, F. Casadio, K. R. Shull, Quantitative characterization of alkyd cure kinetics with the quartz crystal microbalance, *Polymer* 103 (2016) 387–396. doi:10.1016/j.polymer.2016.09.063.
- [125] L. Sturdy, F. Casadio, M. Kokkori, K. Muir, K. R. Shull, Quartz crystal rheometry: A quantitative technique for studying curing and aging in artists' paints, *Polymer Degradation and Stability* 107 (2014) 348–355. doi:10.1016/j.polymdegradstab.2014.02.009.

- [126] L. F. Sturdy, M. S. Wright, A. Yee, F. Casadio, K. T. Faber, K. R. Shull, Effects of zinc oxide filler on the curing and mechanical response of alkyd coatings, *Polymer* 191 (2020) 122222. doi:10.1016/j.polymer.2020.122222.
- [127] D. A. Brass, K. R. Shull, Membrane-enhanced surface acoustic wave analysis of grafted polymer brushes, *Journal of Applied Physics* 103 (7) (2008) 073517. doi:10.1063/1.2903880.
- [128] D. Johannsmann, Viscoelastic, mechanical, and dielectric measurements on complex samples with the quartz crystal microbalance, *Physical Chemistry Chemical Physics* 10 (31) (2008) 4516. doi:10.1039/b803960g.
- [129] K. R. Shull, M. Taghon, Q. Wang, Investigations of the high-frequency dynamic properties of polymeric systems with quartz crystal resonators, *Biointerphases* 15 (2) (2020) 021012. doi:10.1116/1.5142762.
- [130] G. Hedley, M. Odlyha, A. Burnstock, J. Tillinghast, C. Husband, A study of the mechanical and surface properties of oil paint films treated with organic solvents and water, *Journal of Thermal Analysis* 37 (9) (1991) 2067–2088. doi:10.1007/BF01905579.

Appendix

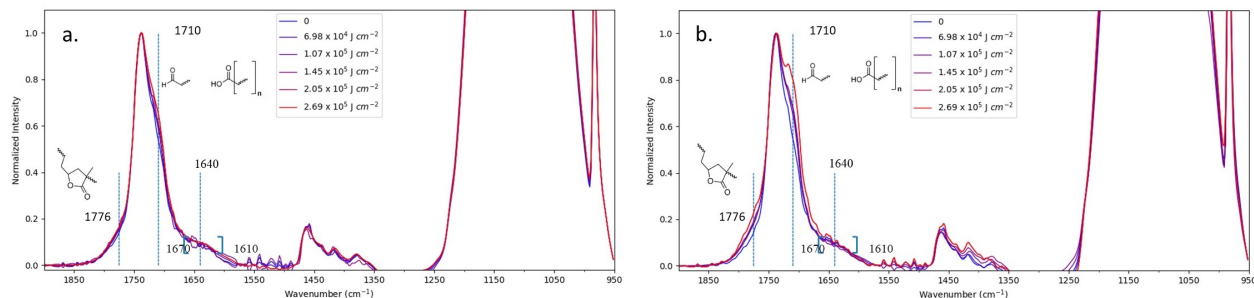


Figure .1: (a)Vis and (b) UV-vis aging of BaSO₄ based paints

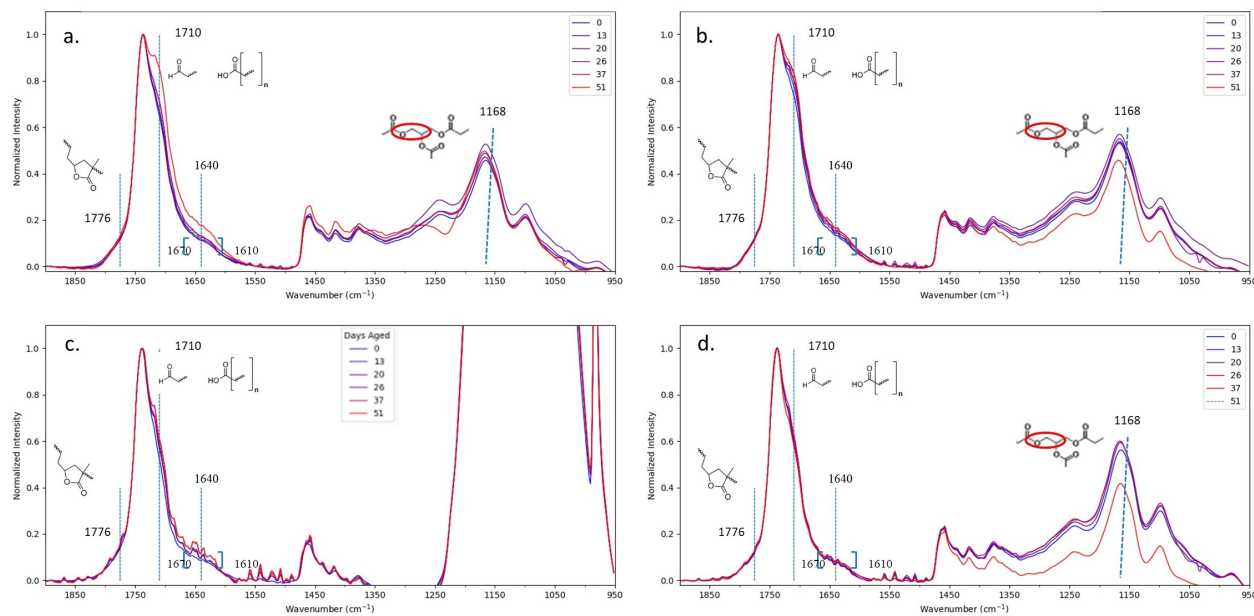


Figure .2: Dark aged (a) anatase, (b) rutile, (c) BaSO₄, and (d) linseed oil films

To further check the reliability of the employed model we tested the convergence by performing i) single point using a k-point grid of $2 \times 2 \times 1$ and ii) single point using 20 \AA of vacuum along the z non-periodic direction and we reported the respective DOS compared with the calculation carried out at Γ with 10 \AA of vacuum, see Figure .3. The final energies obtained from both single-point calculations are essentially the same (within 0.01 eV) of the energy evaluated at Γ with 10 \AA

of vacuum indicating that the employed approach is at convergence. Moreover, as we can see in Figure .3, using a higher value of vacuum or higher k-point sampling does not introduce significant changes in the DOS confirming the reliability of the employed model.

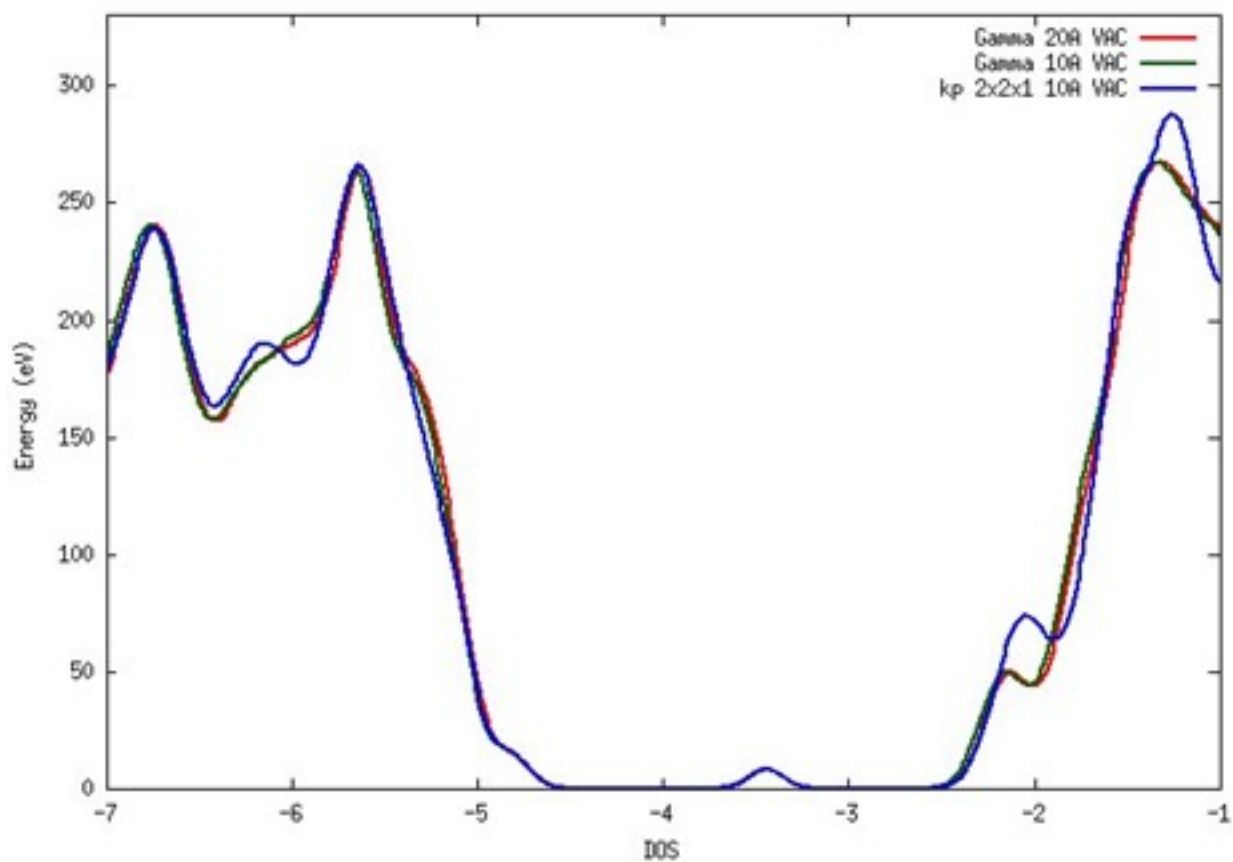


Figure .3: DOS comparison between the calculation carried out at Γ point with 10A of vacuum, with 20A of vacuum and with a k-point grid of 2x2x1 and 10A of vacuum

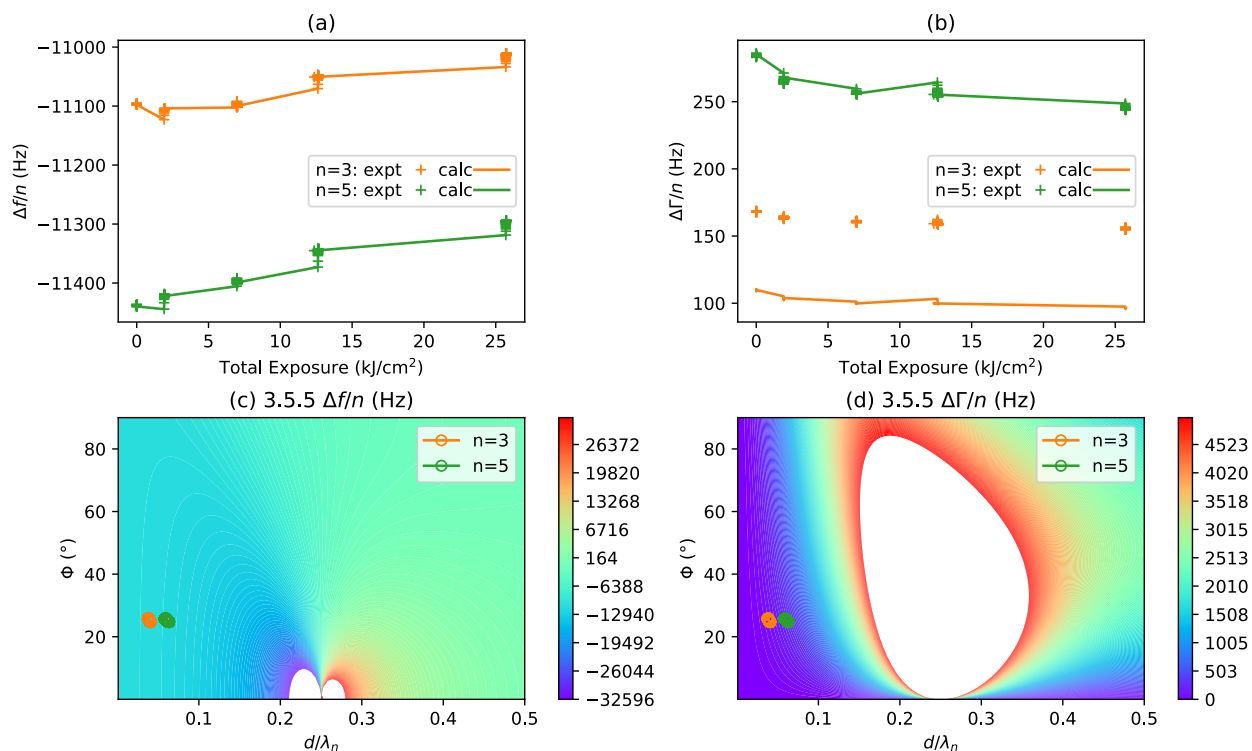


Figure .4: Comparison of the experimentally measured values of $\Delta \Gamma_n$ and Δf_n to the values that are calculated from Eqs. 5.2-5.6, using the properties for Ana-Vis-80 shown in Figure 5.10. These properties were obtained from a 3.5.5 calculation which means that the equations were solved for agreement of the calculated and measured values of Δf_3 , Δf_5 and $\Delta \Gamma_5$.

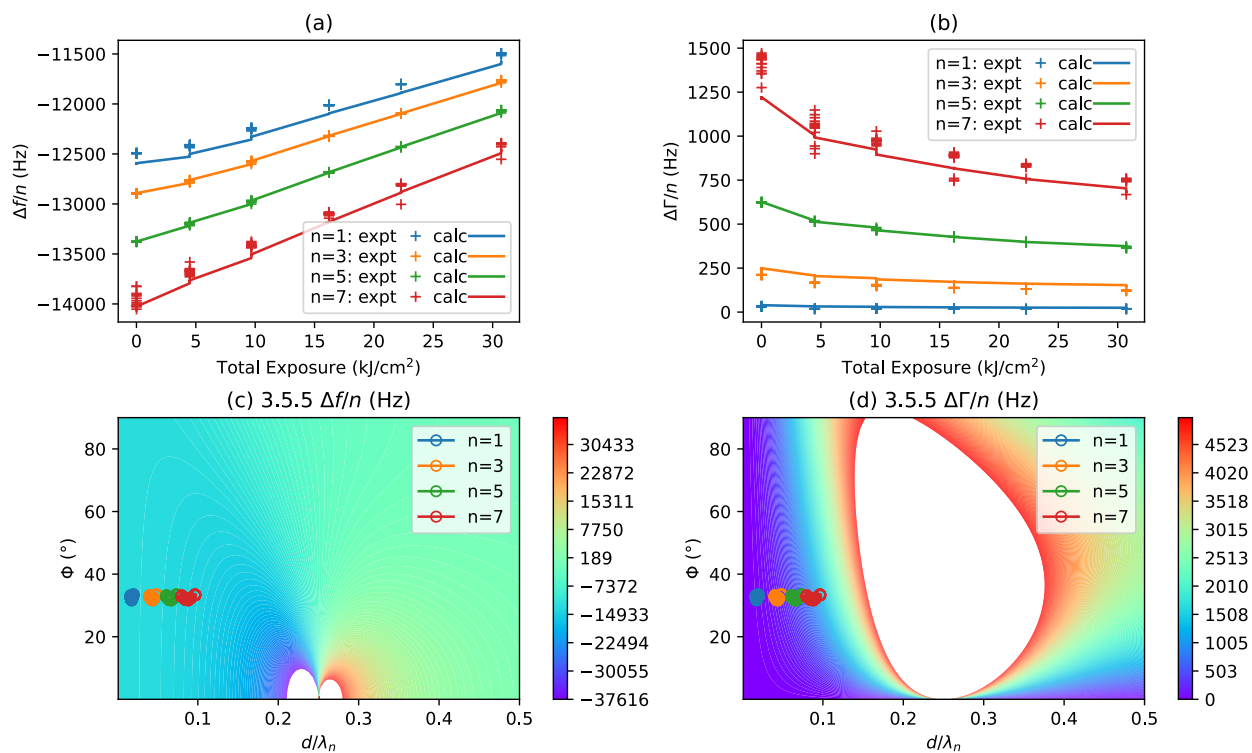


Figure .5: Comparison of the experimentally measured values of $\Delta \Gamma_n$ and Δf_n to the values that are calculated from Eqs. 5.2-5.6, using the properties for Ana-UV-50 shown in Figure 5.10. These properties were obtained from a 3.5.5 calculation which means that the equations were solved to force agreement of the calculated and measured values of Δf_3 , Δf_5 and $\Delta \Gamma_5$.

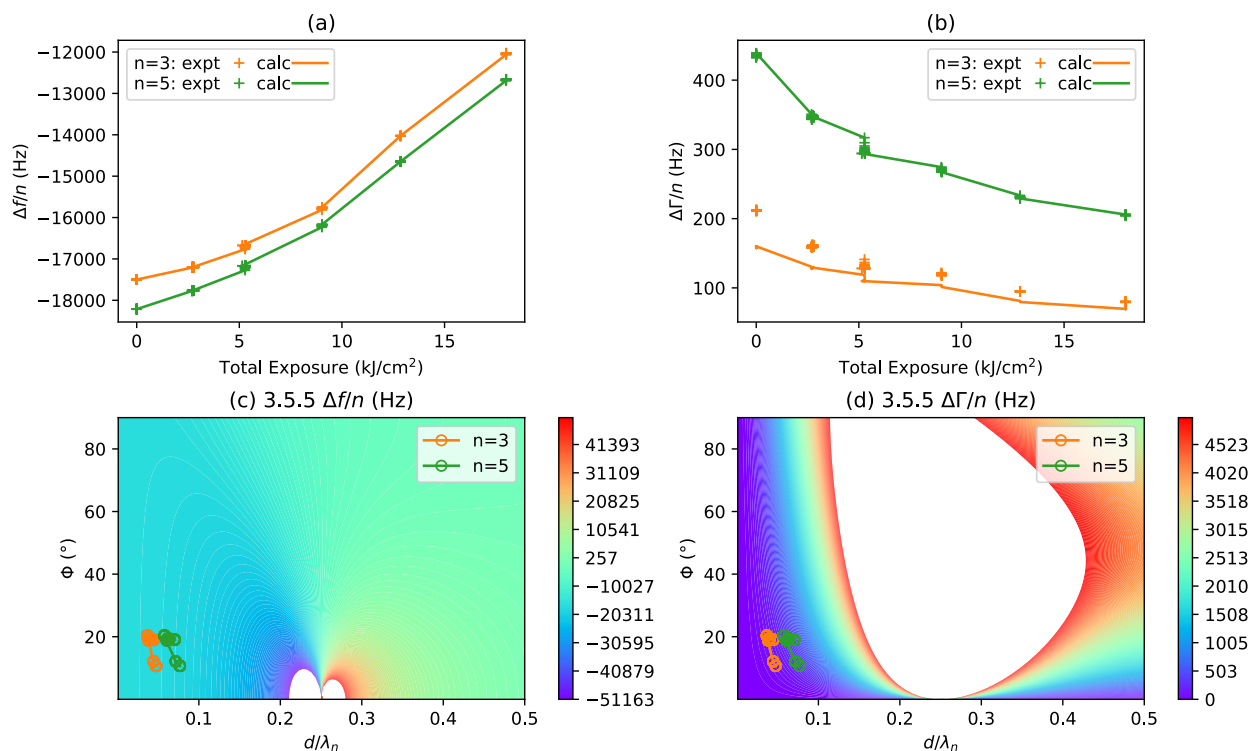


Figure .6: Comparison of the experimentally measured values of $\Delta\Gamma_n$ and Δf_n to the values that are calculated from Eqs. 5.2-5.6, using the properties for Ana-UV-80 shown in Figure 5.10. These properties were obtained from a 3.5.5 calculation which means that the equations were solved to force agreement of the calculated and measured values of Δf_3 , Δf_5 and $\Delta\Gamma_5$.